Report of Investigation 2021-6

TSUNAMI INUNDATION MAPS FOR AKHIOK, CHINIAK, OLD HARBOR, OUZINKIE, AND PORT LIONS ON KODIAK ISLAND, ALASKA

E.N. Suleimani, J.B. Salisbury, and D.J. Nicolsky

Ouzinkie, Alaska.

Published by
STATE OF ALASKA
DEPARTMENT OF NATURAL RESOURCES
DIVISION OF GEOLOGICAL & GEOPHYSICAL SURVEYS
2021

TSUNAMI INUNDATION MAPS FOR AKHIOK, CHINIAK, OLD HARBOR, OUZINKIE, AND PORT LIONS ON KODIAK ISLAND, ALASKA

E.N. Suleimani, J.B. Salisbury, and D.J. Nicolsky

Report of Investigation 2021-6

State of Alaska
Department of Natural Resources
Division of Geological & Geophysical Surveys

STATE OF ALASKA
Mike Dunleavy, Governor

DEPARTMENT OF NATURAL RESOURCES
Corri A. Feige, Commissioner

DIVISION OF GEOLOGICAL & GEOPHYSICAL SURVEYS
Steve Masterman, State Geologist and Director

Publications produced by the Division of Geological & Geophysical Surveys (DGGS) are available for free download from the DGGS website (dggs.alaska.gov). Publications on hard-copy or digital media can be examined or purchased in the Fairbanks office:

Alaska Division of Geological & Geophysical Surveys
3354 College Rd., Fairbanks, Alaska 99709-3707
Phone: (907) 451-5010 Fax (907) 451-5050
dggspubs@alaska.gov | dggs.alaska.gov

DGGS publications are also available at:
Alaska State Library,
Historical Collections & Talking Book Center
395 Whittier Street
Juneau, Alaska 99811

Alaska Resource Library and Information Services (ARLIS)
3150 C Street, Suite 100
Anchorage, Alaska 99503

Suggested citation:
Suleimani, E.N., Salisbury, J.B., and Nicolsky, D.J., 2021, Tsunami inundation maps for Akhiok, Chiniak, Old Harbor, Ouzinkie, and Port Lions on Kodiak Island, Alaska: Alaska Division of Geological & Geophysical Surveys Report of Investigation 2021-6, 72 p. https://doi.org/10.14509/30760

Contents

Figures

Tables

Appendix

Map Sheets

TSUNAMI INUNDATION MAPS FOR AKHIOK, CHINIAK, OLD HARBOR, OUZINKIE, AND PORT LIONS ON KODIAK ISLAND, ALASKA

E.N. Suleimani[1], J.B. Salisbury[2], and D.J. Nicolsky[1]

Abstract

We evaluate potential tsunami hazards for the Kodiak Island communities of Akhiok, Chiniak, Old Harbor, Ouzinkie, and Port Lions, Alaska, by numerically modeling the extent of inundation from tsunami waves generated by hypothetical earthquakes. Worst-case inundation scenarios are defined by analyzing the tsunami dynamics related to various plausible earthquake slip distributions along the Alaska–Aleutian megathrust. Potential worst-case tsunami sources include megathrust earthquakes in the Kodiak Island region. A hypothetical earthquake near Kodiak Island with maximum slip distributed at depths between 10 and 20 km (6.2–12.4 mi) with a splay fault dipping 60° in the Albatross fault zone results in "worst case" tsunami inundation for Akhiok, and an earthquake with maximum slip distributed at depths between 0 and 10 km (0–6.2 mi) with a splay fault dipping 30° in the backstop splay zone is the "worst case" scenario for the remaining communities. The maximum predicted overland flow depths in the communities ranges from 10 to 25 m (33 to 82 ft), and the currents in community harbors could be as strong as 8.4 m/sec (16.3 knots). Dangerous wave activity is expected to last for at least 12 hours after the hypothetical worst-case earthquakes. Results presented here are intended to provide guidance to local emergency management agencies for tsunami inundation assessment, evacuation planning, and public education to mitigate future tsunami damage.

INTRODUCTION

Subduction of the Pacific plate under the North American plate has resulted in numerous great (M > 8) earthquakes and is the source of locally generated tsunamis in Alaska (Dunbar and Weaver, 2008). During the 20th century, several tsunamis generated during Alaska–Aleutian subduction zone earthquakes have resulted in widespread damage and loss of life in exposed coastal communities throughout the Pacific (Lander, 1996). However, tsunamis originating in the vicinity of the Alaska Peninsula, Aleutian Islands, and Gulf of Alaska are considered near-field hazards and could reach Alaska's coastal communities within minutes of an earthquake.

On March 27, 1964, the largest earthquake ever recorded in North America struck Southcentral Alaska. This moment magnitude (M_W) 9.2 megathrust earthquake, known as the Great Alaska Earthquake (fig. 1), generated the most destructive tsunami in Alaska history and, farther south, impacted the west coast of Canada and the United States (Plafker and others, 1969; Kanamori, 1970; Johnson and others, 1996; Lander, 1996; Fine and others, 2018a, 2018b; Rabinovich and others, 2019). Kodiak, the largest community on Kodiak Island, suffered great losses from the earthquake and the ensuing tsunami. Damage was primarily caused by 1.7 m (5.6 ft) of tectonic subsidence and

[1]Alaska Earthquake Center, Geophysical Institute, University of Alaska, P.O. Box 757320, Fairbanks, Alaska 99775-7320; ensuleimani@alaska.edu
[2]Alaska Division of Geological & Geophysical Surveys, 3354 College Rd., Fairbanks, Alaska 99709-3707.

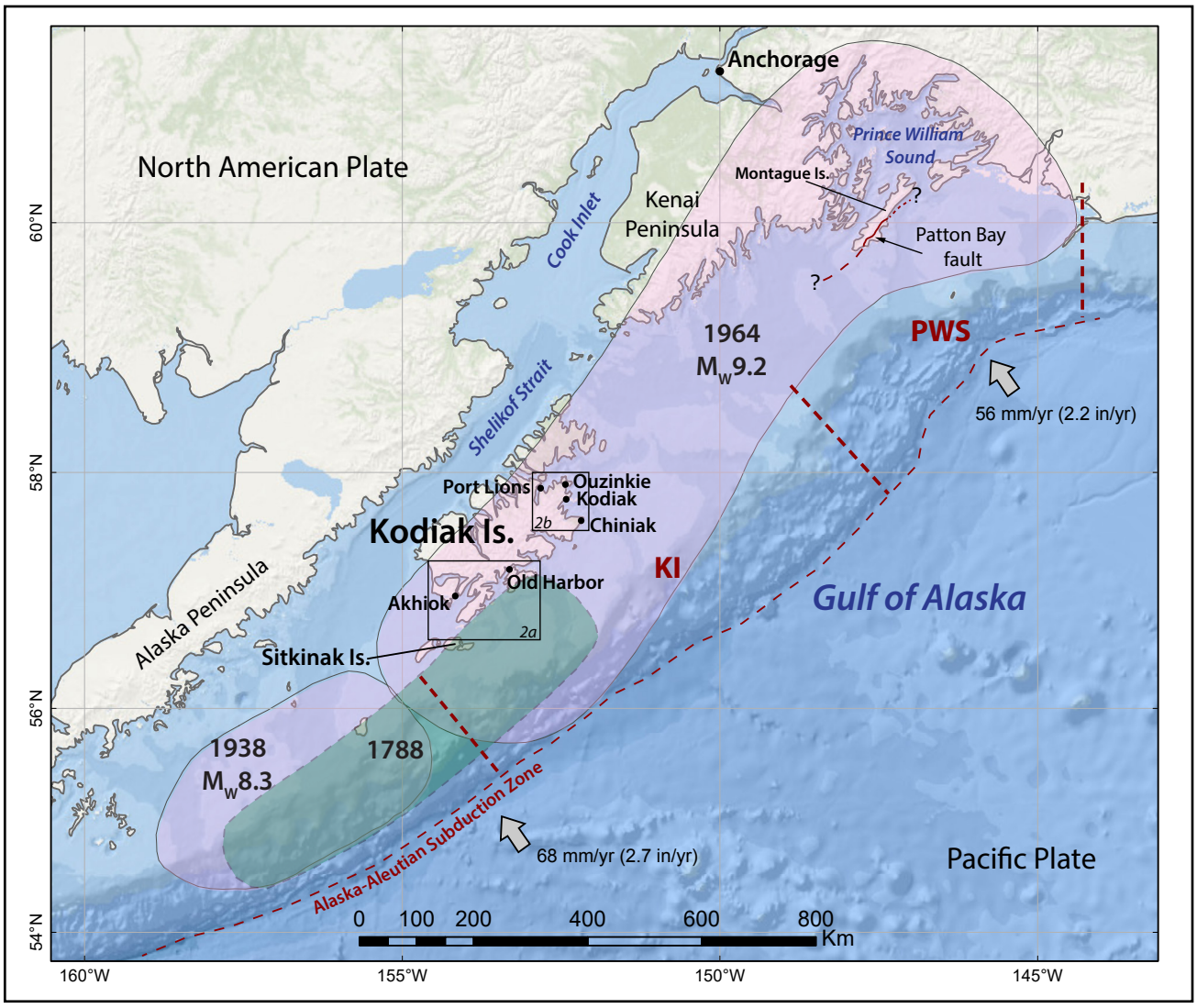

Figure 1. Map of southcentral Alaska, showing the location of Kodiak Island and the rupture zones of the 1788, 1938 and 1964 Alaska-Aleutian megathrust earthquakes (shaded areas). KI = Kodiak Island asperity; PWS = Prince William Sound asperity. The Patton Bay fault is shown by solid, dashed, and dotted lines where it is mapped, approximated, and inferred, respectively.

a train of waves that inundated the low-elevation areas of town (Kachadoorian and Plafker, 1967). In addition to the major tectonic tsunami generated by ocean-floor displacement in the Gulf of Alaska, numerous local tsunamis were generated by landslides in coastal Alaska during the Great Alaska Earthquake (Lander, 1996). Landslide-generated tsunamis arrived almost immediately after the earthquake shaking, leaving no time for warning or evacuation. Of the 131 fatalities associated with this earthquake, 122 were caused by tsunami waves (Lander, 1996). Despite this relatively recent M_w 9.2 earthquake, the region still has high potential for future large earthquakes and it is only a matter of time before another devastating tsunami occurs. Thus, estimating the potential flooding of the coastal zone in the next local or distant tsunami is an essential component of the preparedness process.

The tsunami inundation maps for the Kodiak Island communities described in this report represent the results of a continuous, combined effort of state and federal agencies to mitigate tsunami damage in coastal Alaska. The intended audience of this report consists of scientists, engineers, and community planners interested in an applied approach to developing tsunami inundation and

evacuation maps. Digital data and documentation provided with the report enable technical users to explore the range of possible tsunami inundation for potential events. We use a deterministic approach for our earthquake and tsunami hazard modeling, which is distinctly different from the probabilistic tsunami hazard analysis used in projects with different objectives, such as land-use planning or insurance estimates (Geist and Parsons, 2006). We are less concerned about the probability that an earthquake of a certain magnitude will occur in a given amount of time and are more focused on the community-specific tsunami inundation that might result from the largest hypothetical, yet scientifically plausible earthquake scenarios. The methodologies used to develop tsunami inundation maps are described in detail in multiple publications and are not reviewed in this report. Refer to Suleimani and others (2016) for a complete description of the process.

PROJECT BACKGROUND: REGIONAL AND HISTORICAL CONTEXT

Setting

Kodiak Island is the largest island in Alaska and the second largest island in the United States (fig. 1). The following information about coastal communities on the coast of Kodiak Island is extracted from the Alaska Community Database maintained by the State of Alaska Division of Community and Regional Affairs of the Department of Commerce, Community, and Economic Development (DCCED/DCRA, 2015).

Kodiak Island has been inhabited for the past 8,000 years. The first non-Native contacts were in 1763 by Russian Stephen Glotov and in 1792 by Alexander Baranov, a Russian fur trapper. Sea otter pelts were the primary incentive for Russian exploration, and a settlement was established at Chiniak Bay, the site of present-day Kodiak (fig. 1). At that time the island was called "Kikhtak," and later was known as "Kadiak," the Inuit word for island. In 1882 a fish cannery opened at the Karluk spit, sparking the development of commercial fishing in the area. Currently, there are several communities on Kodiak Island. Below we provide a short description of the communities for which tsunami inundation maps are included in this report.

Akhiok is located at the southern end of Kodiak Island at Alitak Bay. It lies 128.7 km (80 mi) southwest of the City of Kodiak and 340 miles southwest of Anchorage (figs. 1 and 2A). Akhiok is an Alutiiq village with a fishing and subsistence lifestyle. The community was originally a sea otter hunting settlement, located at Humpy Cove. The name Akhiok was reported in the 1880 Census. In 1881, residents relocated to the present site at Alitak Bay. The community's Russian Orthodox church, Protection of the Theotokos Chapel, was built around 1900 at the site of an earlier structure. A post office was established in 1933. Residents of nearby Kaguyak relocated to Akhiok after the 1964 earthquake and tsunami destroyed their village. The city was incorporated in 1972.

The community of Chiniak is located 45 miles southeast of the City of Kodiak on the easternmost point of Kodiak Island (figs. 1 and 2B). Chiniak is an Alutiiq (Russian-Aleut) name first reported in 1888 by Lt. Comdr. Tanner of the US Navy steamer *Albatross*. It had previously been named Cape Greville by Captain Cook in 1778. During the mid-1950s, an Air Force White Alice Radar Tracking Station was constructed in Chiniak. In 1964, Cape Chiniak observed the first tsunami wave about 30 minutes after the earthquake. A technician at the Air Force station used ham radio to report the arriving waves (Lander, 1996).

Old Harbor is located on the southeast coast of Kodiak Island, 70 miles southwest of the City of Kodiak and 322 miles southwest of Anchorage (figs. 1 and 2A). Old Harbor practices its traditional Alutiiq culture and subsistence lifestyle. Fishing provides income to the community. Residents of Kaguyak, a summer fish camp, also live in Old Harbor. The area around Old Harbor is thought to have been inhabited for nearly 2,000 years by

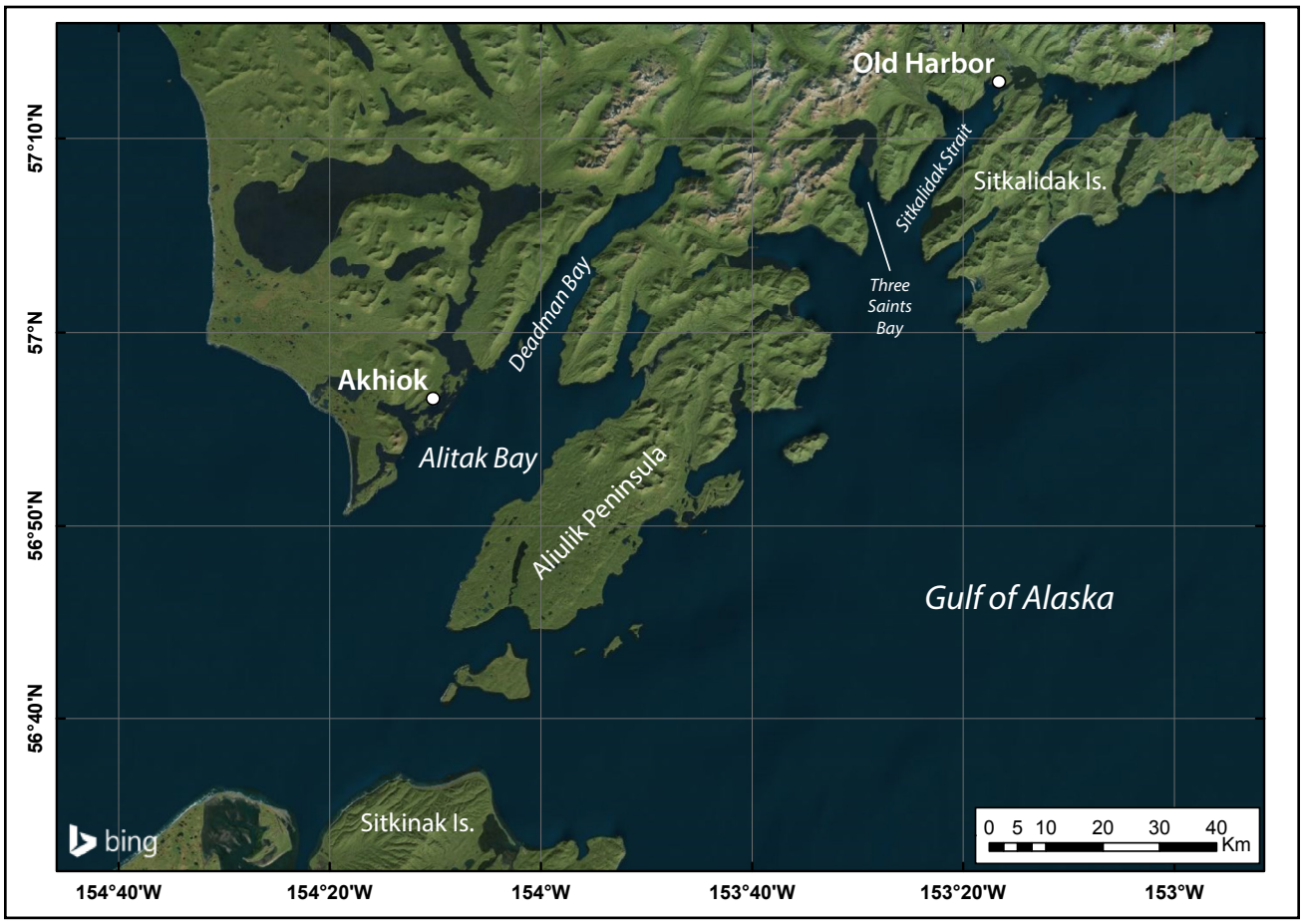

Figure 2A. Map of southeastern shore of Kodiak Island and communities of Akhiok and Old Harbor.

the Alutiiq. The area was visited by the Russian Grigori Shelikov and his "*Three Saints*" flagship in 1784. Three Saints Bay became the first Russian colony in Alaska (fig. 2A). In 1788, a tsunami destroyed the settlement. Two more earthquakes struck before 1792. In 1793, the town relocated from the northeast coast to "Saint Paul's," now known as Kodiak. A settlement was reestablished at Three Saints Harbor in 1884. The town was recorded as "Staruigavan," meaning "old harbor" in Russian. The Old Harbor post office was opened in 1931. In 1964, the Great Alaska Earthquake and resulting tsunami destroyed the community; only two homes and the church remained standing. The community was rebuilt in the same location. The city was incorporated in 1966.

Ouzinkie is an Alutiiq village located on the west coast of Spruce Island, adjacent to Kodiak Island. It lies northwest of the City of Kodiak and 247 air miles southwest of Anchorage (figs. 1 and 2B). Commercial fishing and subsistence activities support the community. Ouzinkie started as a retirement community for the Russian American Company. In 1889, the Royal Packing Company constructed a cannery at Ouzinkie. Shortly afterward, the American Packing Company built another. In 1890 a Russian Orthodox church was built, and in 1927 a post office was established. Cattle ranching was popular in the early 1900s. In 1964, the Great Alaska Earthquake and resulting tsunami destroyed the Ouzinkie Packing Company cannery. Following the disaster, Columbia Ward bought the remains and rebuilt the store and dock but not the cannery. The city was incorporated in 1967. In the late 1960s, the Ouzinkie Seafoods cannery was constructed. The operation was sold

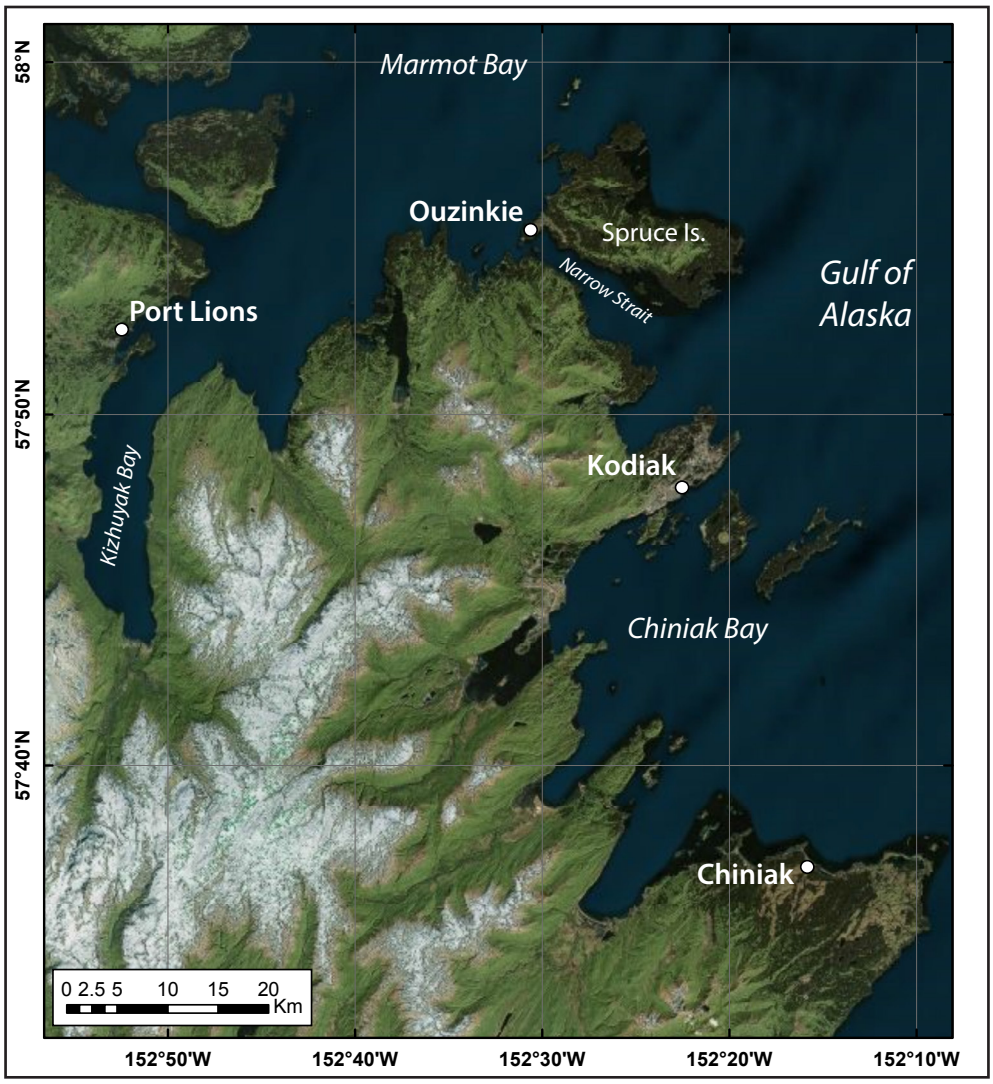

Figure 2B. Map of Chiniak and Kizhuyak Bays and communities of Chiniak, Ouzinkie, and Port Lions.

to Glacier Bay and burned down in 1976 shortly after the sale. No canneries have operated since.

Port Lions is located in Kizhuyak Bay on the north coast of Kodiak Island, 247 air miles southwest of Anchorage (figs. 1 and 2B). The majority of the population in Port Lions is Alutiiq. Most residents lead a fishing and subsistence lifestyle. Port Lions was founded in 1964 by the displaced inhabitants of Afognak, an Afognak Island community that was destroyed by a tsunami after the Great Alaska Earthquake. The community was named in honor of the Lions Club for their support in rebuilding and relocating the village. The city was incorporated in 1966. For many years, Port Lions was the site of the large Wakefield Cannery on Peregrebni Point. The cannery burned down in March 1975. Soon thereafter, the village corporation purchased a 149-foot floating processor, *the Smokwa*. Although sold in 1978, *the Smokwa* processed crab in the area intermittently between 1975 and 1980. A small sawmill, located south of town, operated until 1976.

Seismic and tsunami history

Kodiak Island is located at the eastern end of the Alaska–Aleutian subduction zone, the boundary along which the Pacific and North American tectonic plates converge (fig. 1). The rate of plate convergence near the island is approximately 60

mm (2.4 in) per year (DeMets and others, 1990), and the eastern end of the megathrust has produced significant tsunamigenic earthquakes. On March 28, 1964, Southcentral Alaska was struck by the largest earthquake ever recorded in North America and the second largest ever recorded in the world after the 1960 M_W 9.5 earthquake off the coast of Chile. The 1964 M_W 9.2 megathrust earthquake (fig. 1) generated a destructive tsunami that caused fatalities and great damage in Alaska, Hawaii, and the west coast of the United States and Canada. The earthquake ruptured an 800-km-long (~500-mi-long) section of the Aleutian megathrust, producing vertical displacements over an area of about 285,000 km^2 (110,039 mi^2) in Southcentral Alaska (Plafker, 1969). The area of coseismic subsidence included Kodiak Island (KI), Kenai Peninsula, Cook Inlet, and part of northern Prince William Sound (PWS) (fig. 1). The major zone of uplift in the Gulf of Alaska was seaward of the subsidence zone (Plafker, 1969). Several communities on Kodiak Island suffered greatly from the resulting tsunami waves. The penultimate significant tsunami event near Kodiak Island occurred on July 21, 1788, when a strong earthquake near Sitkinak Island caused a 3–10 m tsunami that forced relocation of the first Russian settlement at Three Saints Bay on southwestern Kodiak Island (Soloviev, 1990; Lander, 1996) (fig. 1). Briggs and others (2014) present stratigraphic evidence of land level change and 137Cs and 210Pb bracketing ages of a sand deposit that can be traced 1.5 km inland on Sitkinak Island—suggesting that the 1788 earthquake was a large megathrust rupture that generated the tsunami.

Analysis of historical earthquake data in the PWS and KI regions (Nishenko and Jacob, 1990) showed that significant megathrust earthquakes have occurred more frequently in the KI region, which has also ruptured independently of the PWS region. For example, paleoseismic data show that the KI region ruptured independently in a large earthquake about 500 years ago—about 360 years more recently than the penultimate great earthquake that ruptured both the KI and PWS regions (Carver and Plafker, 2008). The PWS and KI regions have different recurrence intervals, with estimates of the recurrence interval for M 7.5–8 earthquakes in the KI segment being as low as 60 years (Nishenko, 1991).

Using seismic waveform data, Christensen and Beck (1994) showed that there were two areas of high-moment (i.e., energy) release during the 1964 Great Alaska Earthquake. The two major asperities, or areas of maximum defined slip, form the overall 1964 rupture zone: the Prince William Sound asperity with an average slip of 18 m (59 ft), and the Kodiak Island asperity with an average slip of 10 m (33 ft) (fig. 1). The results of joint inversion of tsunami and geodetic data from the 1964 event (Johnson and others, 1996) also corroborate two areas of high moment release. Subsequent studies have shown that the PWS asperity is on the Yakutat–North American megathrust whereas the KI asperity is on the Pacific–North American megathrust (Ferris and others, 2003; Eberhart-Phillips and others, 2006; Worthington and others, 2010, 2012; Gulick and others, 2013).

The most recent deformation model of the 1964 earthquake incorporated updated fault geometries and the postseismic deformation that followed the earthquake (Suito and Freymueller, 2009). This model was developed as a 3-D viscoelastic model in combination with afterslip for a shallow-dipping elastic slab. Suito and Freymueller (2009) used the inversion-based model by Johnson and others (1996) as a basis for their coseismic slip model, adjusting it to the new geometry and critically reinterpreting the coseismic data. One important change was the extension of the Montague Island high-angle splay, the Patton Bay fault (fig.1), from its subaerial outcrop to a longer length along the southern Kenai Peninsula coast to explain the pattern of subsidence in this area. The authors preferred forward finite-element modeling for calculation of coseismic slip due to inconsistency and systematic errors in coseismic displacement data. At the same time, their resulting slip distribution resembles that derived from inversion

models of Holdahl and Sauber (1994) and Ichinose and others (2007).

On the basis of all published paleoseismic data for the region, Carver and Plafker (2008) calculate that the median interval between the past eight great (M > 8) earthquakes in the PWS segment of the eastern Aleutian seismic zone ranges from 333 to 875 years, with an average of 589 years. Shennan, Bruhn, and others (2014) revised the recurrence intervals of great earthquakes in the PWS segment based on the new paleoseismic field data from three sites in the PWS segment. Their results suggest that the intervals range from ~420 to ~610 years, with a mean of ~535 years. Their calculations exclude the ~833 year interval between the 1964 earthquake and the penultimate PWS event.

Recently, Shennan, Barlow, and others (2014) presented new paleoseismic data from Kodiak Island which suggest that the intervals between ruptures of the Kodiak segments are shorter than previously assumed, and that the KI segment ruptured more frequently than the PWS segment. The authors tested the hypothesis of the Kodiak single-segment ruptures of 1788 and of ca. A.D. 1440–1620, both of which occurred between the multi-segment ruptures of the 1964 earthquake and the earthquake of ca. A.D. 1020–1150 when the PWS and KI segments ruptured together (Carver and Plafker, 2008; Shennan, Bruhn, and others, 2014). Shennan, Barlow, and others (2014) also analyzed the patterns of uplift and subsidence for the three most recent events on the KI segment—the 1964, the 1788, and the ca. A.D. 1440–1620 earthquakes—and found that the location of the hinge line, or the contour of zero vertical deformation between regions of uplift and subsidence, was different for all three events.

Briggs and others (2014) presented stratigraphic evidence of land-level change and tsunami inundation during prehistoric and historical earthquakes west of Kodiak Island. They reported mixed uplift and subsidence records for Sitkinak Island (fig. 1), which suggests that it is located above a nonpersistent boundary near the edge of the 1964 rupture. This island experienced either uplift or subsidence depending on where the ruptures stopped along strike.

Akhiok, Chiniak, Old Harbor, and Ouzinkie have been impacted by tsunamis in the past, as documented by the National Centers for Environmental Information/World Data Centers (NCEI/WDS) Global Historical Tsunami Database (in progress) and Lander (1996). Table 1 summarizes all historically recorded tsunami events that were experienced by the Kodiak Island communities considered in this report. Port Lions has no record of past tsunamis.

Landslide-generated tsunami hazards

Tsunamis caused by submarine and subaerial slope failures are a significant hazard in the fjords of coastal Alaska and other high-latitude fjord coastlines (Lee and others, 2006). Kulikov and others (1998) analyzed tsunami catalog data for the northern Pacific coast and showed that this region has a long record of tsunami waves generated by submarine and subaerial landslides, avalanches, and rockfalls. For example, as a result of the 1964 earthquake, numerous local submarine and subaerial landslide tsunamis were generated in Alaska, which accounted for 76 percent of the tsunami fatalities (Lander, 1996). Long-duration ground shaking of the 1964 earthquake triggered numerous rockslides, rockfalls, rotational slumps, and debris avalanches on the slopes of Kodiak Island. Plafker and Kachadoorian (1966) documented and classified the observed landslides and provided a map of the distribution of the larger landslides and slope failures on Kodiak Island. In 1964, most ground failures were located along the southeastern shore of the island. The concentration of slides along the southeast coast of Kodiak Island and their scarcity elsewhere appeared to be controlled by local lithology; slope steepness was not found to be an important factor that controlled the distribution of slides around the island (Plafker and Kachadoo-

rian, 1966). The authors showed a strong correlation between the maximum concentration of slides and outcrops of bedded Tertiary rock, the physical properties of which likely contributed to slide initiation. The map of ground shaking intensity suggests that ground accelerations in areas underlain by Tertiary rock were greater than in areas underlain by pre-Tertiary rock (Plafker and Kachadoorian, 1966). Another factor that probably contributed to the slide concentration along the southeastern shore was that large aftershocks were also located closer to that shore, and therefore caused higher-intensity ground motion.

There were no observations or documented evidence of landslides reaching the water and generating waves in Kodiak communities during the 1964 earthquake. Even though slide material could hypothetically reach water and generate a wave during the next large earthquake, there are insufficient data to appropriately constrain landslide tsunami sources. Therefore, in this report we do not model tsunamis generated by landslides.

METHODOLOGY AND DATA

Grid development and data sources

We use a series of nested computational grids in the Kodiak Island area to generate detailed maps of potential tsunami inundation triggered by local and distant earthquakes. The coarsest grid, with 2-arc-minute (approximately 2 km [~1.2 mi]) resolution, spans the central and northern Pacific Ocean. We used three intermediate grids between the coarsest- and highest-resolution grids (table 2; fig. 3). The highest-resolution (level 4) grids (shaded rectangles in fig. 3) cover the five Kodiak Island communities. The spatial resolution of the level 4 grids, with cell dimensions of about 15 × 16 m (49.2 × 52.5 ft), satisfies National Oceanic and

Table 1. Tsunami effects at the Kodiak Island communities; data from the National Geophysical Data Center Global Historical Tsunami Database and comments from Lander (1996).

Date	Magnitude (M_w)	Origin	Maximum water height ft (m)	Comments
Akhiok				
03/28/1964	9.2	Gulf of Alaska	49 (15)	Homes and boats destroyed.
Chiniak				
03/28/1964	9.2	Gulf of Alaska	30 (9.1)	Cape Chiniak observed the first tsunami wave about 30 minutes after the earthquake. A technician at the Air Force satellite-tracking station used ham radio to report the arriving waves.
Old Harbor				
07/21/1788	8.0 (?)	Gulf of Alaska	10–33 (3–10)	Ship cast on shore; several huts destroyed in Three Saints Bay.
1792	?	Alaska Peninsula		Agitated and anomalous waves in Three Saints Bay following strong earthquake. Ship damaged.
03/28/1964	9.2	Gulf of Alaska	24 (7.3)	Village nearly destroyed, $150,000 damage, 1 death on Sitkalidak Island.
08/15/2007	8.0	Peru	0.3 (0.1)	
09/29/2009	8.1	Samoa Islands	0.2 (0.06)	
02/27/2010	8.8	Chile	1.7 (0.51)	
03/11/2011	9.1	Japan	1.2 (0.38)	
10/28/2012	7.7	Canada	0.5 (0.14)	
01/23/2018	7.9	Gulf of Alaska	0.5 (0.15)	
Ouzinkie				
03/28/1964	9.2	Gulf of Alaska	30 (9.1)	3 deaths, $500,000 damage.

Atmospheric Administration (NOAA) minimum recommended requirements for computation of tsunami inundation (National Tsunami Hazard Mapping Program [NTHMP], 2010).

To develop the high-resolution level 4 grids, bathymetric, topographic, and shoreline digital datasets were obtained from various agencies as described in Carignan and others (2013). The bathymetric datasets include National Ocean Service (NOS) hydrographic surveys, NOAA Electronic Navigational Chart (ENC) soundings, a U.S. Army Corps of Engineers (USACE) harbor survey, and multibeam swath sonar surveys. The topographic datasets include the city of Kodiak bare-earth lidar DEM and IFSAR DEM, the USGS National Elevation Dataset (NED) topographic DEM, and the USACE topographic points. More detailed information on grid development is contained in Lim and others (2009) and Carignan and others (2013).

The map sheets of potential tsunami inundation included in this report show the maximum composite extent of inundation for all considered tsunami scenarios, and the maximum composite flow depths over dry land. The composite values are calculated as follows: for each tsunami scenario, the tsunami flow depth is computed at each grid point and at every time step during the tsunami propagation time the maximum value is kept; then we compute the composite maximum flow depth from all considered scenarios by choosing the maximum value for each grid point among all scenarios. The same methodology is used to calculate the composite extent of tsunami inundation. The calculated extent of inundation accounts for coseismic deformation in the communities.

Numerical model of tsunami propagation and runup

To estimate tsunami propagation and runup in the Kodiak area, we used the same numerical modeling techniques as previous Alaska tsunami inundation studies (for example, Suleimani and others, 2010, 2013, 2015, 2016; Nicolsky, Sulei-

Table 2. Nested grids used to compute propagation of tsunami waves generated in the Pacific Ocean to the Kodiak Island communities. The high-resolution grid is used to compute the inundation. Note that the grid resolution in meters is not uniform: the first dimension is the longitudinal grid resolution and the second is the latitudinal resolution.

Grid name	Resolution		West–East boundaries	South–North boundaries
	arc-seconds	ft (m)		
Level 0, Northern Pacific	120 × 120	≈6,611 x 12,139 (2,015 × 3,700)	120°00'00" E–100°00'00" W	10°00'00" N–65°00'00" N
Level 1, Southcentral Alaska	24 × 24	≈1,322 x 2,428 (403 × 740)	156°00'00" W–145°00'00" W	55°00'00" N–62°00'00" N
Level 2, Coarse resolution, Kodiak Island	8 × 8	≈443 x 810 (135 × 247)	155°38'36" W–149°50'33" W	56°01'45" N–59°02'06" N
Level 3, Fine resolution, Kodiak Island	8/3 × 8/3	≈148 x 269 (45 × 82)	153°38'48" W–151°51'31" W	57°32'22" N–58°04'09" N
Level 4, High resolution, Akhiok	8/9 × 1/2	≈49 × 52 (15 × 16)	154°16'12" W–154°5'24" W	56°53'24" N–56°58'48" N
Level 4, High resolution, Chiniak	8/9 × 1/2	≈49 × 52 (15 × 16)	152°22'48" W–152°10'48" W	57°36'00" N–57°39'01" N
Level 4, High resolution, Old Harbor	8/9 × 1/2	≈49 × 52 (15 × 16)	153°19'48" W–153°9'00" W	57°15'36" N–57°10'12" N
Level 4, High resolution, Ouzinkie	8/9 × 1/2	≈49 × 52 (15 × 16)	152°31'48" W–152°28'12" W	57°54'01" N–57°55'48" N
Level 4, High resolution, Port Lions	8/9 × 1/2	≈49 × 52 (15 × 16)	152°54'36" W–152°49'12" W	57°50'24" N–57°53'24" N

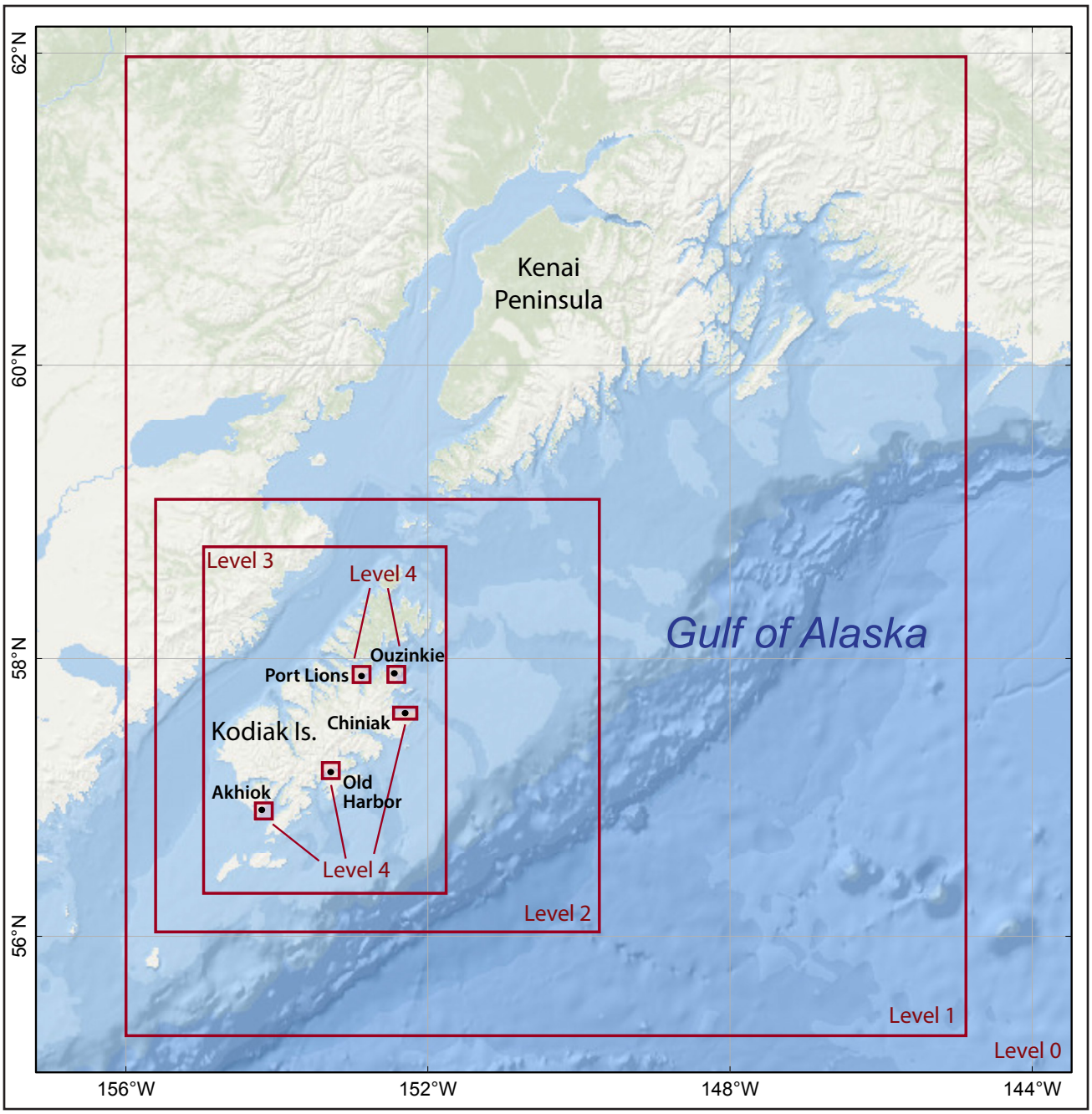

Figure 3. Nesting of the levels 0–4 bathymetry/topography grids for numerical modeling of tsunami propagation and runup in the Kodiak Island area. Each embedded grid is outlined by a red rectangle.

mani, Combellick, and others, 2011; Nicolsky and others, 2013, 2014, 2015). All hypothetical tsunami simulations were conducted using the bathymetric/topographic data corresponding to the Mean Higher High Water (MHHW) tide level in the Kodiak communities. Because the numerical model of tsunami propagation and runup does not dynamically simulate interaction of tides and tsunami waves, we use a conservative approach and assume that all simulated tsunamis arrive during high tides. To test the accuracy of the grid nesting around the Kodiak communities and verify our approach, we modeled the Tohoku tsunami of March 11, 2011, which is described in detail in Suleimani and others (2017).

The numerical modeling results presented in this report are relevant for existing sea level conditions and do not account for changes in water levels caused by global sea level rise, regional tectonic processes, and isostatic rebound. Even though the report on global sea level changes for 2050 and 2100 by the Intergovernmental Panel on Climate Change (Oppenheimer and others, 2019) predicts global sea level rise, rapid regional uplift in southern Alaska caused by ice loss contributes to negative sea level changes in the region (Larsen and others, 2004; Shirzaei and others, 2021).

TSUNAMI SOURCES

In general, all the great historic earthquakes along the Alaska–Aleutian subduction zone occurred on the megathrust—the fault, or contact surface, between the subducting Pacific plate and the overriding North American plate (fig. 1). Friction between the two converging plates generally keeps them stuck, or "locked" together at the edges, but as the rest of the tectonic plates continue to move, shear stress causes a build up of elastic strain energy. The shear strain eventually overcomes the friction and strength of the rocks, and the energy is released during an earthquake, propagating through the ground and causing the strong shaking associated with earthquakes. It is theorized that the shear strain primarily accumulates in the locked, or coupled, regions of the megathrust where friction on the fault is greatest.

Zweck and others (2002) used a three-dimensional elastic dislocation model to demonstrate that the GPS data in southern Alaska can be satisfied by the presence of locked areas near southwest Prince William Sound and southwest Kodiak Island. They found that locked areas correspond to the Prince William Sound and Kodiak Island asperities that ruptured in 1964, and that the locked regions repeat from one earthquake cycle to another. The authors showed that the site velocities on Kodiak Island are consistent with a model of plate locking near Kodiak Island, and that elastic strain is accumulating in the area.

Recent paleoseismological findings indicate that prehistoric and historical earthquakes that occurred on the Kodiak segment of the Alaska-Aleutian megathrust have different spatial patterns of coseismic deformation in both the along-strike and downdip directions (Briggs and others, 2014; Shennan Barlow, and others, 2014). The varying patterns of coseismic deformation mean that earthquakes, even though all within the Kodiak segment, rupture different lateral/vertical extents and result in energy release at different specific locations on the plate interface. The role of downgoing plate topography in fault segmentation and strain release is debated, with high relief topography thought to potentially be both barriers to and triggers for rupture. Increases in mechanical coupling may strengthen the plate boundary, but changes in fault zone physical properties (e.g., fracturing and fluid content) may limit strain accumulation. The geologic history and recent seismic imaging of the Alaska-Aleutian subduction zone suggest the interface is complex and warrants further study, as it may exert controls on rupture behavior. Because the width of the plate interface around Kodiak Island is quite large (measured in the down-dip direction, e.g., fig. 4), earthquakes in this area do not necessarily rupture the whole interface every time. Our goal is to determine the segments of the interface that are most likely to rupture in the next large or great earthquake.

The part of the plate interface of the Kodiak segment between the trench and a depth of about 30–40 km (18.6–24.9 mi) is locked and accumulates strain. The dip of the subducting plate increases from about 10° in the shallow part to 30–45° at a 30–40-km (18.6–24.9 mi) depth, which also corresponds to the boundary between the locked and transition zones (Carver and Plafker, 2008). Locating the updip limit of the locked zone near Kodiak Island is hindered by the lack of geodetic data close to the Aleutian trench, and this zone is essentially unconstrained by the land-based geodetic data. Since we do not yet have seafloor GPS/acoustic measurements that are

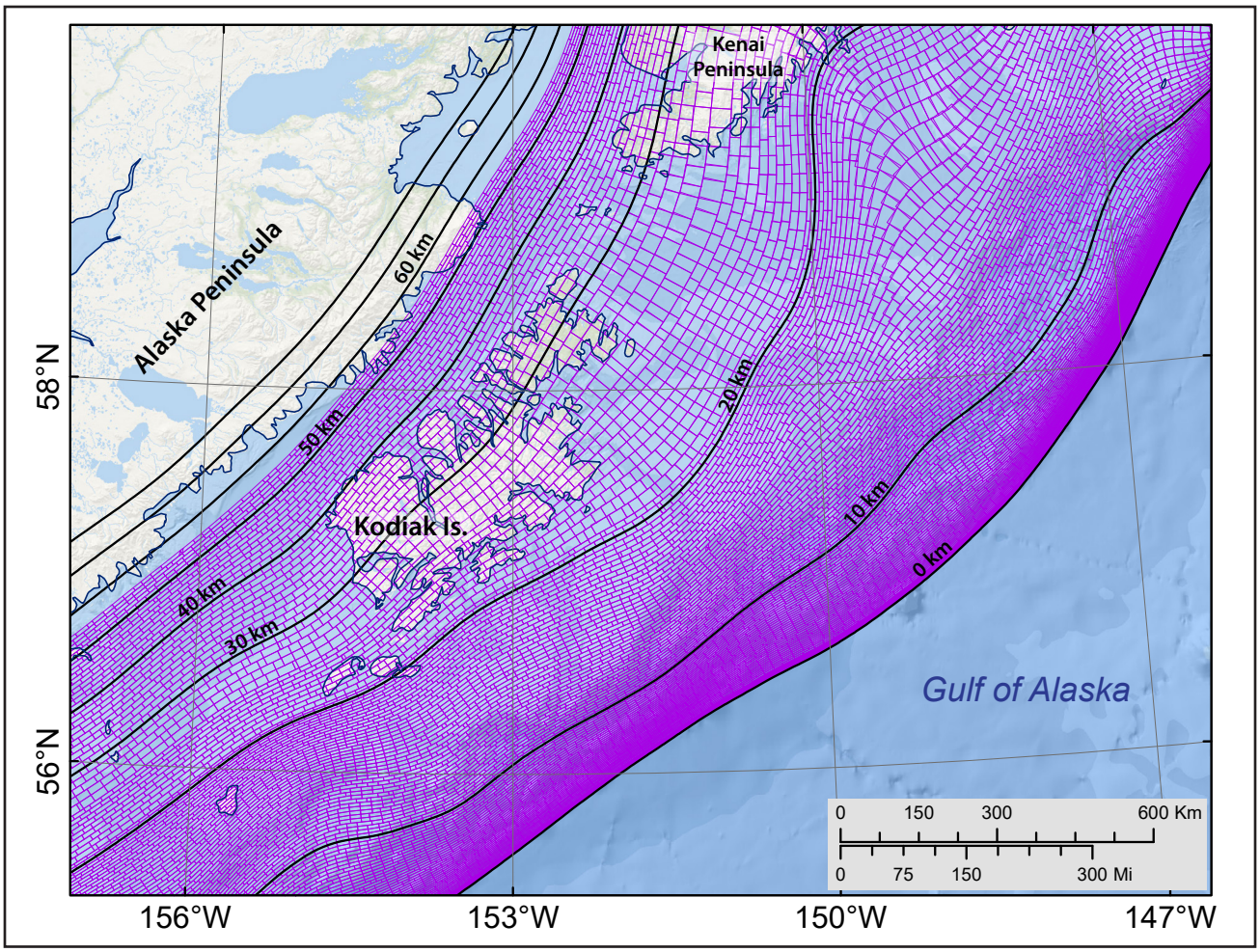

Figure 4. Discretization of the plate interface used to compute the coseismic vertical displacements with formulae developed by Okada (1985). Black lines mark depth contours (in kilometers) of the plate interface and the purple rectangles represent individual pieces of the place considered by the model.

necessary to determine the behavior of the uppermost portion of the plate interface, it was necessary to perform additional steps to construct maximum credible earthquake and tsunami scenarios for Kodiak. Recent studies comparing the Alaska and Tohoku tectonic margins (Kirby and others, 2013) suggest that there are several key geologic similarities between the two areas and that a hypothetical rupture might propagate to shallow depths on the Alaska-Aleutian megathrust, such as the M_W 9.0 Tohoku earthquake. Therefore, in our scenarios, we include earthquakes that rupture the shallow locked zone. Additionally, we conduct a sensitivity study to determine what effect the down-dip location of a rupture has on tectonic subsidence, uplift, and resulting tsunami waves. We then apply the results of the sensitivity study to construct the maximum credible scenarios.

Sensitivity study

We use the USGS SLAB2 model of the Alaska-Aleutian plate interface developed by Hayes (2018). After the initial analysis, we regularized a shallow part of the plate interface southeast of Kodiak Island in the Gulf of Alaska (151°W, 57°N) (Hayes, USGS, written communication, 2020). Similar to the plate interface model used by Zweck and others (2002), the SLAB2 plate interface model exhibits a relatively shallow dip beneath Kodiak Island and the Kenai Peninsula until it reaches a depth of 50 km (31 mi), at which point it steepens.

This area also corresponds to the unlocked or weakly coupled part of the plate interface (fig. 4).

The plate interface is discretized into a mesh of rectangles ranging from 1 to 6 km (0.6 to 3.7 mi) in the along-strike direction of the plate interface, with denser discretization in its shallow part (fig. 4). The upper and lower edges of each rectangle coincide with depth contours of the plate interface that are spaced at 0.5 km (0.3 mi), with spacing of 0.25 km (0.16 mi) at the shallowest part of the plate interface. The rectangles, called subfaults, are later used to compute coseismic ground deformation (Okada, 1985). Using this discretization of the plate interface, we model potential earthquake scenarios by prescribing a general pattern of slip distribution in the proposed rupture, then computing the slip at the center of each subfault using seismic moment as a constraint.

The Kodiak Island area of the Alaska-Aleutian megathrust is one of the two large segments of the 1964 rupture zone with a very wide locked region (200–250 km [124.3–155.3 mi] wide in the

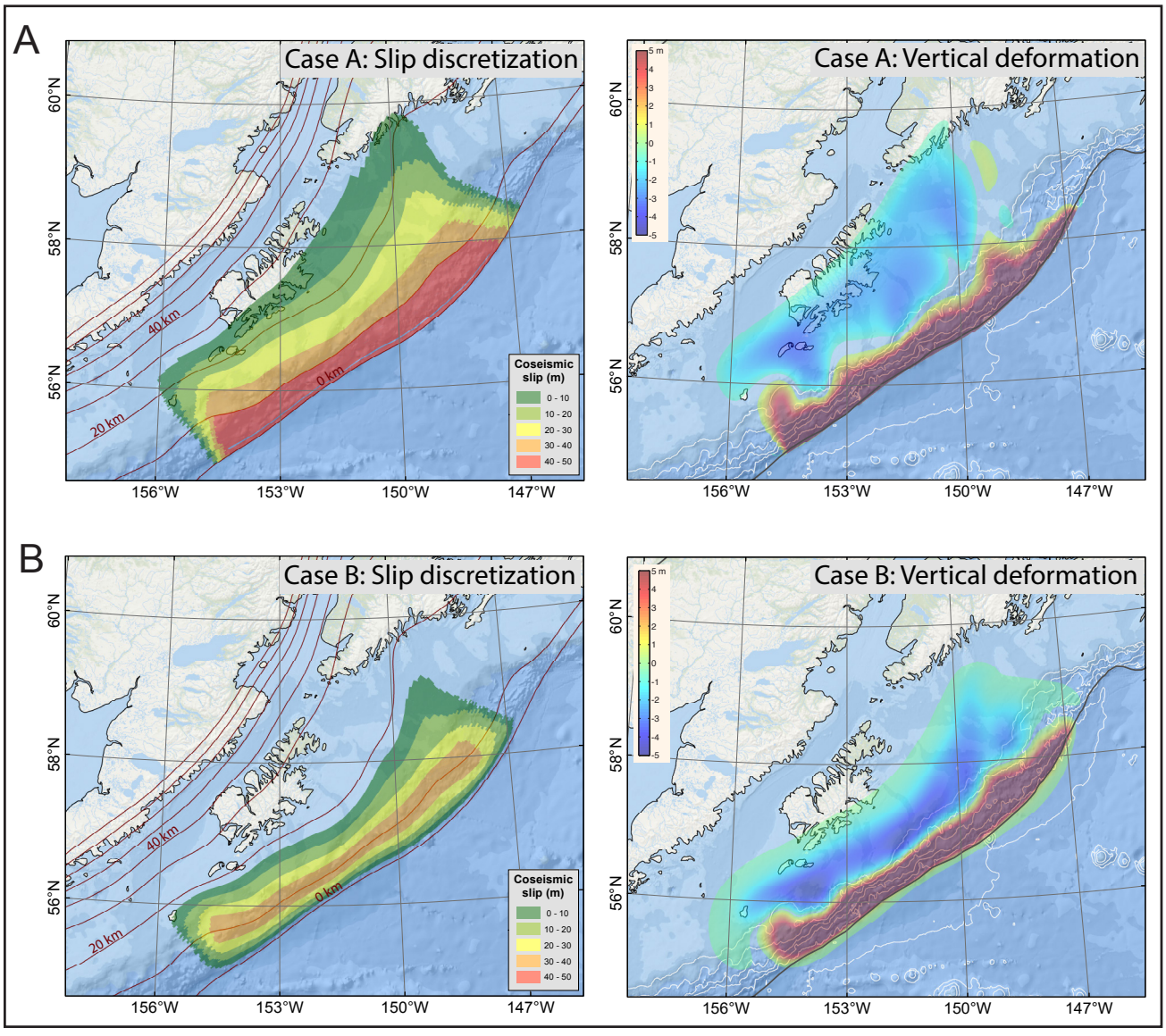

Figure 5. Imposed slip distribution along the plate interface (left) and computed vertical ground-surface deformation (right) for cases A and B, modeling M_w 9.0 ruptures in the area of Kodiak Island. The slip location varies in the downdip direction of the plate interface while preserving the same slip patch configuration. Red lines are depth contours of the subduction interface, in kilometers. White lines are bathymetry contours within the depth interval between 1 and 5 km. The black line in the deformation figures (right column) indicates the approximate location of the trench.

downdip direction), but the detailed shape of the locked region is uncertain (Freymueller and others, 2008). Earthquake ruptures with slip at different depths result in different distributions and amounts of subsidence and uplift in coastal communities, and therefore in different tsunami and permanent flooding characteristics. We develop four different slip cases (cases A–D) for M_W 9.0 earthquakes that could occur in the partially locked segment of the megathrust in the area of Kodiak Island (Freymueller and others, 2008), and calculate vertical deformations associated with each case (fig. 5). The slip distribution for all four cases is uniform in the along-strike direction with tapering at the ends of the rupture. The assumed slip distribution is consistent with earthquake source scenarios used by other tsunami modeling studies (for example, Butler, 2014; USGS SAFRR scenario, www2.usgs.gov/natural_hazards/safrr/projects/tsunamiscenario.asp). Between any two consecutive cases, the hypothetical rupture is offset by about 10 km (6.2 mi) in the downdip direction: case A corresponds to a shallow surface-breaching rupture with maximum amount of slip located close to the trench; case B

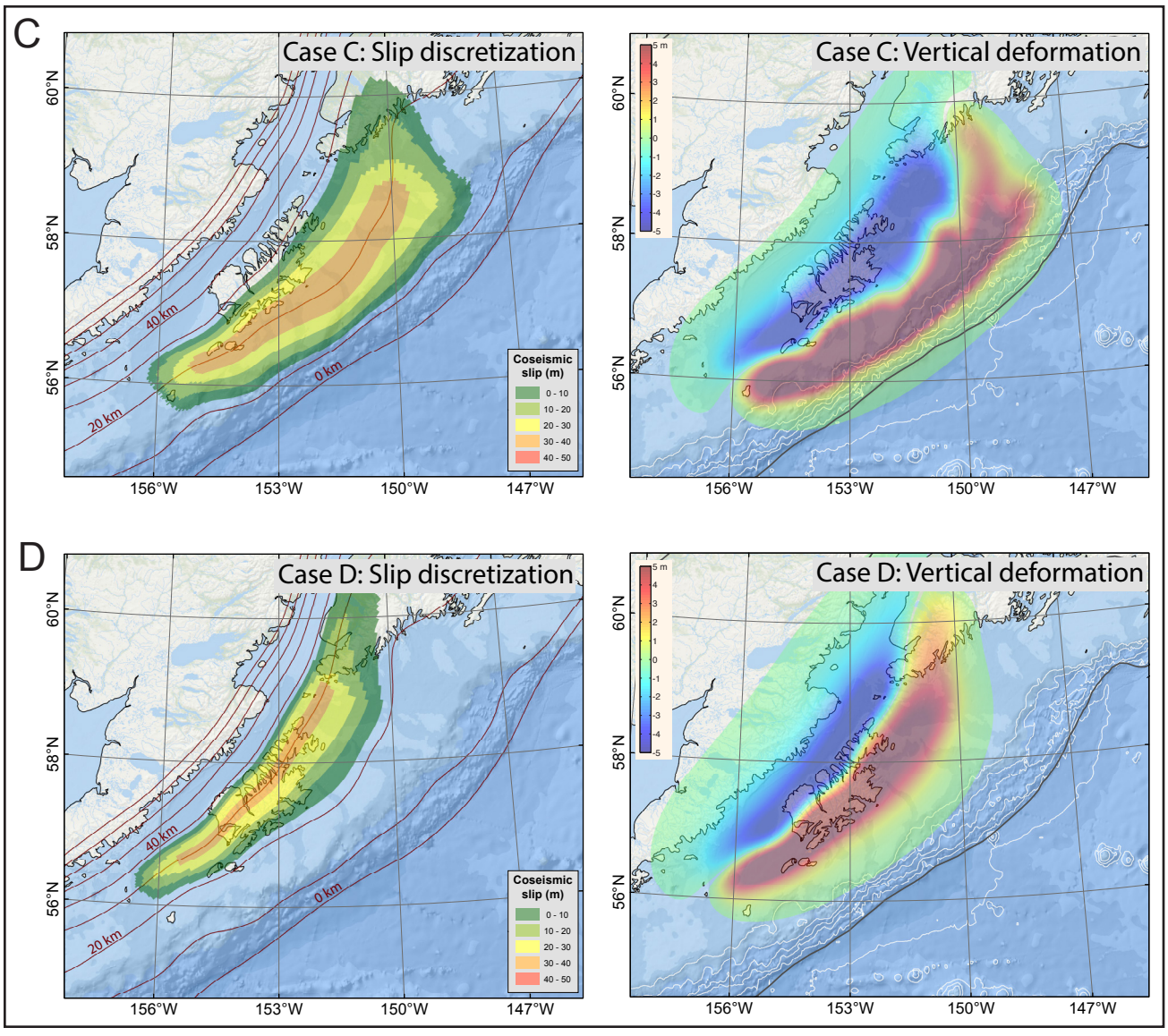

Figure 5, continued. Imposed slip distribution along the plate interface (left) and computed vertical ground-surface deformation (right) for cases C and D, modeling M_W 9.0 ruptures in the area of Kodiak Island. The slip location varies in the downdip direction of the plate interface while preserving the same slip patch configuration. Red lines are depth contours of the subduction interface, in kilometers. White lines are bathymetry contours within the depth interval between 1 and 5 km. The black line in the deformation figures (right column) indicates the approximate location of the trench.

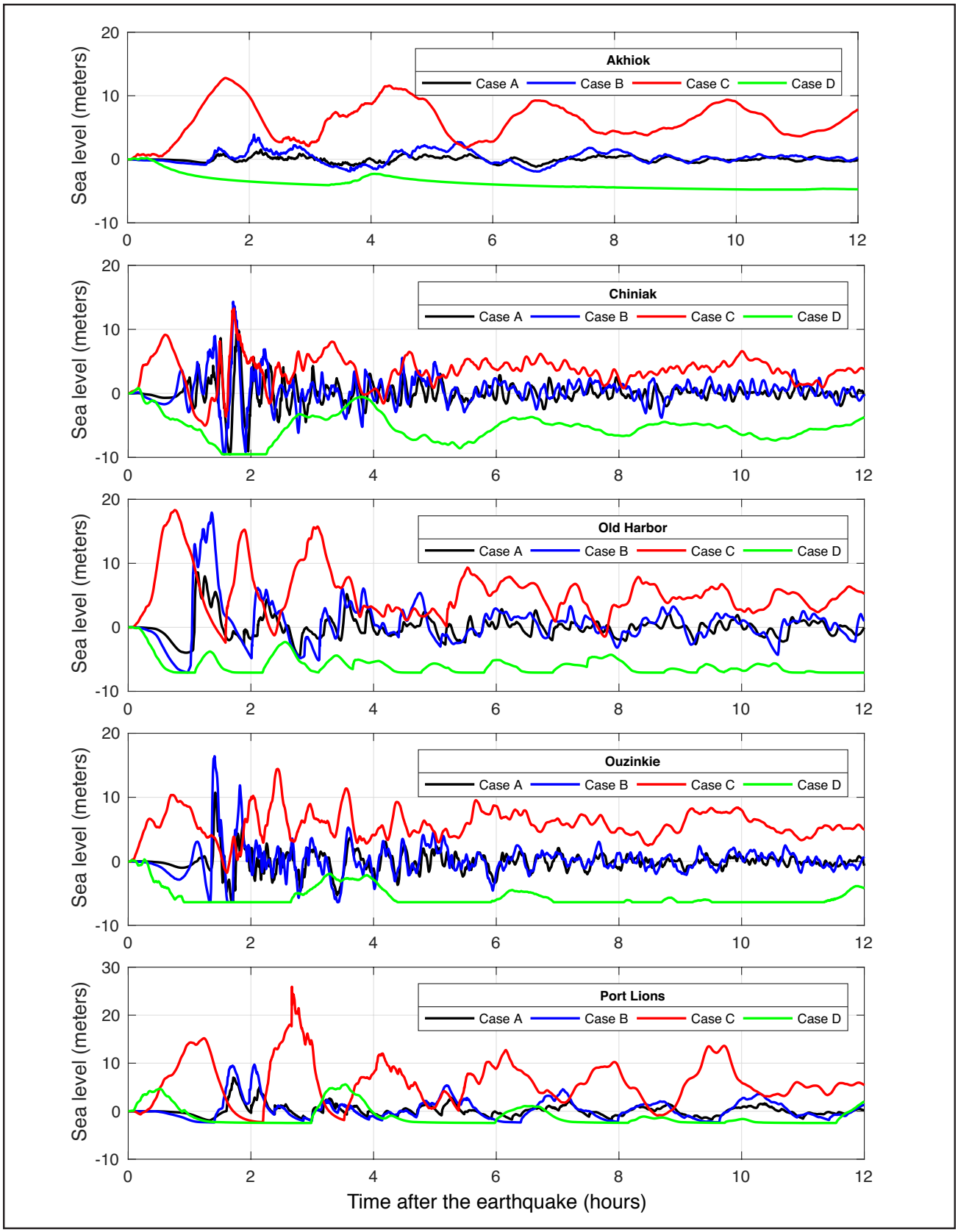

Figure 6. Modeled water-level dynamics (from the point of view of an observer standing at the shore) at the five Kodiak Island communities for the ground-surface deformations shown in figure 5.

corresponds to a rupture at 10 km (6.2 mi) depth; case C corresponds to a rupture at 20 km (12.4 mi) depth; and case D corresponds to a rupture at 30 km (18.6 mi) depth.

For each case, we calculate water dynamics at the Kodiak Island communities and notice that simulated water levels vary considerably according to different slip distributions (fig. 6), and that results are community-specific. The time series indicate that the rupture at 20 km (12.4 mi) depth (case C), which corresponds to the greatest coseismic subsidence in the communities, results in the highest wave amplitude at all locations except for Chiniak and Ouzinkie where case B, the rupture at 10 km (6.2 mi) depth, results in higher wave amplitudes, but with later arrivals. The deep rupture represented by case D produces sizable coseismic uplift along the eastern shore of Kodiak Island. As a result, the bay seabed and surrounding land surfaces become relatively higher with respect to post-earthquake sea level and the arriving waves effectively have much smaller amplitudes.

Based on these results, we develop hypothetical ruptures with maximum slip in the 10–20 km (6.2–12.4 mi) depth range (cases B–C). As in Nicolsky and others (2016), we develop maximum credible scenarios for the Kodiak Island communities by allowing up to 35 m (115 ft) of slip in the deep and intermediate sections of the Alaska–Aleutian megathrust and up to 50 m (164 ft) in the shallow sections of the megathrust. The maximum slip is imposed along regions of the megathrust that have the capability to generate the highest amplitude waves near Kodiak Island communities.

Table 3. The hypothetical megathrust scenarios used to model tsunami runup at the Kodiak Island communities. Asterisk indicates scenarios that have been considered in previous inundation mapping reports.

	Description	Rupture depth range km (mi)	Maximum slip depth range km (mi)	Maximum slip m (ft)	Maximum subsidence m (ft)	Maximum uplift m (ft)
1	M_w 9.2 earthquake in the area of Kodiak Island; 10 km depth	2–28 (1.2–17.4)	5–15 (3.1–9.3)	35.0 (115.0)	3.6 (11.8)	12.2 (40.0)
2	M_w 9.25 earthquake in the area of Kodiak Island; 20 km depth	2–28 (1.2–17.4)	15–25 (9.3–15.5)	35.0 (115.0)	7.3 (24.0)	7.4 (24.3)
3	M_w 9.3 earthquake in the area of Kodiak Island; 10–20 km depth	2–28 (1.2–17.4)	5–25 (3.1–15.5)	35.0 (115.0)	7.1 (23.3)	11.6 (38.0)
4	M_w 9.25 earthquake in the area of Kodiak Island; 10 km depth, slip extending to 0 km depth	0–28 (0–17.4)	5–15 (3.1–9.3)	35.0 (115.0)	4.0 (13.1)	12.0 (39.4)
5	M_w 9.3 earthquake in the area of Kodiak Island; 20 km depth, slip extending to 0 km depth	0–28 (0–17.4)	15–25 (9.3–15.5)	35.0 (115.0)	7.1 (23.3)	8.1 (26.6)
6	M_w 9.3 earthquake in the area of Kodiak Island; 10 km depth, slip extending to 0 km depth	0–30 (0–18.6)	0–15 (0–9.3)	50 (164.0)	4.9 (16.0)	26.4 (86.6)
7*	M_w 9.3 earthquake with 35 m of maximum slip for nearly the entire rupture patch	2–38 (1.2–23.6)	5–22 (3.1–13.7)	35.0 (115.0)	7.7 (25.3)	11.8 (38.7)
8*	M_w 9.25 earthquake with 50 m of maximum slip in the shallow part of the rupture	0–31 (0–19.2)	0–18 (0–11.2)	35.0 (115.0)	9.6 (31.5)	28 (91.9)
9*	M_w 9.1 earthquake in the Cascadia subduction zone	45.0 (150.0)	36.0 (120.0)	45.0 (148.0)	8.0 (25.0)	11.0 (35.0)

Hypothetical tsunami sources

In this section, we describe the development of scenarios for tsunamigenic earthquakes in the Kodiak area of the Alaska-Aleutian megathrust (table 3). Our goal is to determine geologically plausible scenarios that will result in maximum reasonable tsunami inundation in Kodiak communities—"credible worst-case scenarios." Scenarios 1–6 are based on results of the sensitivity study, geodetic data, and new thoughts regarding local megathrust behavior. Previously, the coseismic slip was limited to 18.5 m (60.7 ft) near the trench (fig. 6 in Suleimani and others, 2005). Now, following modeling results for the USGS SAFRR project and considering implications of the 2011 Tohoku earthquake (Wang and others, 2018), we suggest that the maximum slip near the trench could be up to 50 m (164 ft). To be consistent with previous reports (e.g., Nicolsky and others, 2016, 2017; Suleimani and others, 2016), we consider two events (scenarios 7 and 8) with slip parameterization according to research by Butler and others (2014). Scenario 9 models a rupture of the Cascadia subduction zone as an example of a distant tsunami source.

In all scenarios, we do not account for the finite speed of rupture propagation along the fault, and we consider the ocean-bottom displacements to be instantaneous. All proposed scenarios are summarized in table 3. The proposed slip distributions and vertical coseismic deformations are shown in figure 7A–D.

In scenarios 1–6, we assume maximum slip at depths with the greatest control over regional land-level changes and tsunami generation for Kodiak communities, i.e., depths of 10 and 20 km (6.2 and 12.4 mi), or around cases B and C of the sensitivity study. We consider various downdip locations for the maximum slip to parameterize various credible tsunamigenic earthquakes. In the downdip direction, the slip is determined by the slip skewness parameter q in the Freund and Barnett (1976) formulae, and the along-strike slip distribution is uniform. For each scenario, the maximum slip is assumed to be located at a different depth range. We note that the presented scenarios are intended to capture the maximum credible scenarios and to provide a starting point for development of more complex models.

Blind rupture scenarios

These scenarios simulate hypothetical ruptures of the Kodiak segment of the Alaska-Aleutian megathrust where the updip and downdip limits of the rupture are 2 km (1.2 mi) and 28 km (17.4 mi), respectively. The proposed slip distributions and vertical coseismic deformations for scenarios 1–3 are shown in figure 7.

Scenario 1: M_W 9.2 near Kodiak Island; 10 km (6.2 mi) depth	The depth of maximum slip corresponds to the depth for sensitivity case B. The slip skewness parameter, q, is set to 0.25 (bell-shaped curve skewed toward the trench) to model the maximum slip of 35 m (115 ft) at a depth of 10 km (6.2 mi).
Scenario 2: M_W 9.25 near Kodiak Island; 20 km (12.4 mi) depth	The depth of maximum slip corresponds to the depth for sensitivity case C. The slip skewness parameter, q, is set to 0.7 (bell-shaped curve skewed toward the deeper part of the rupture) to model the maximum slip of 35 m (115 ft) at a depth of 20 km (12.4 mi).
Scenario 3: M_W 9.3 near Kodiak Island; 10-20 km (6.2-12.4 mi) depth	The depth of maximum slip corresponds to that for the combination of sensitivity cases B and C, with the width of the maximum slip area extending from the 5 to 25 km (3.1 to 15.5 mi) depth contours of the plate interface.

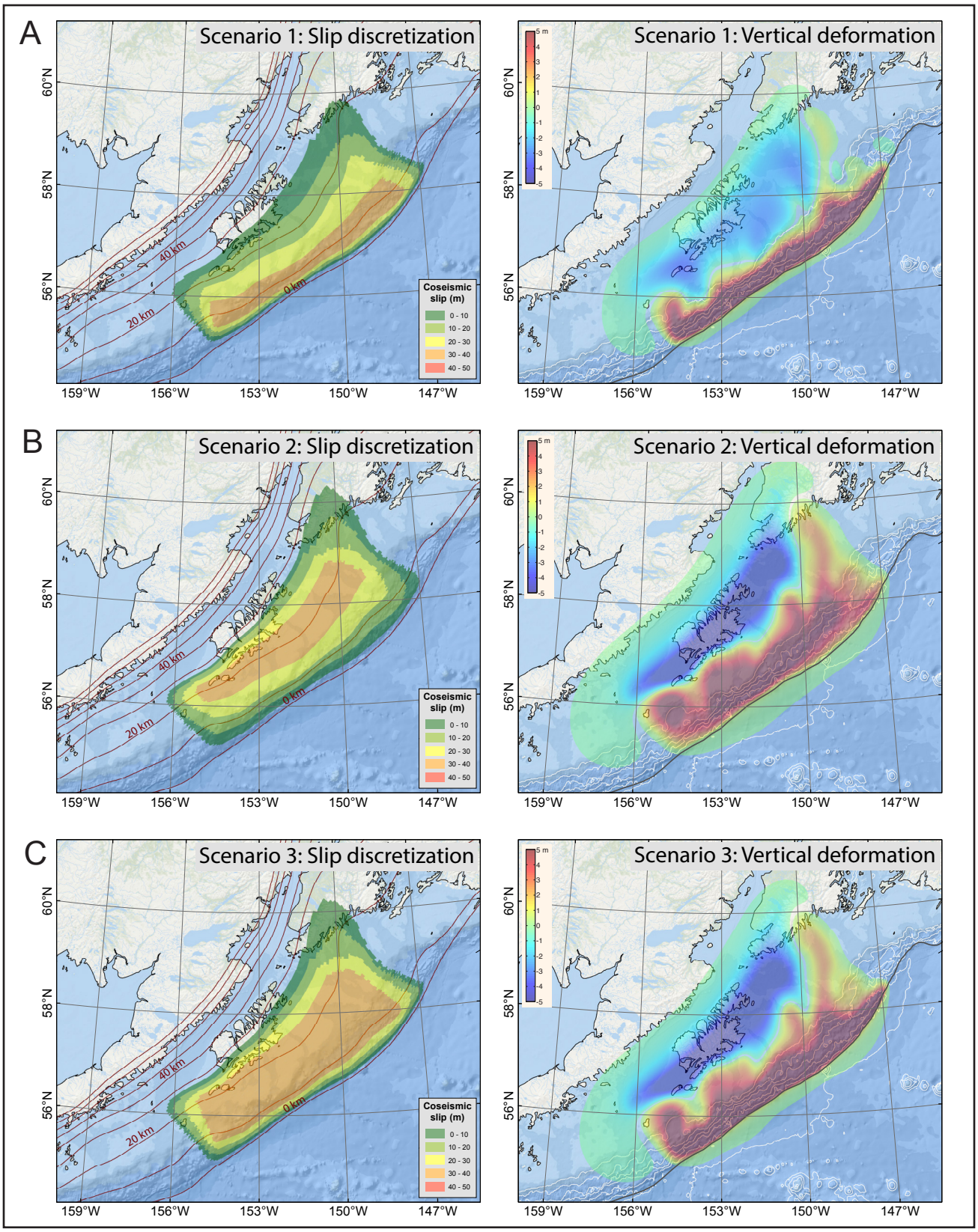

Figure 7. Estimated slip distribution along the plate interface for scenarios 1–8 and computed vertical ground-surface deformation for scenarios 1–9 (slip distribution is not provided for scenario 9). Red lines are depth contours of the subduction interface, in kilometers. White lines are bathymetry contours within the depth interval between 1 and 5 km. The black line in the deformation figures (right column) indicates the approximate location of the trench.

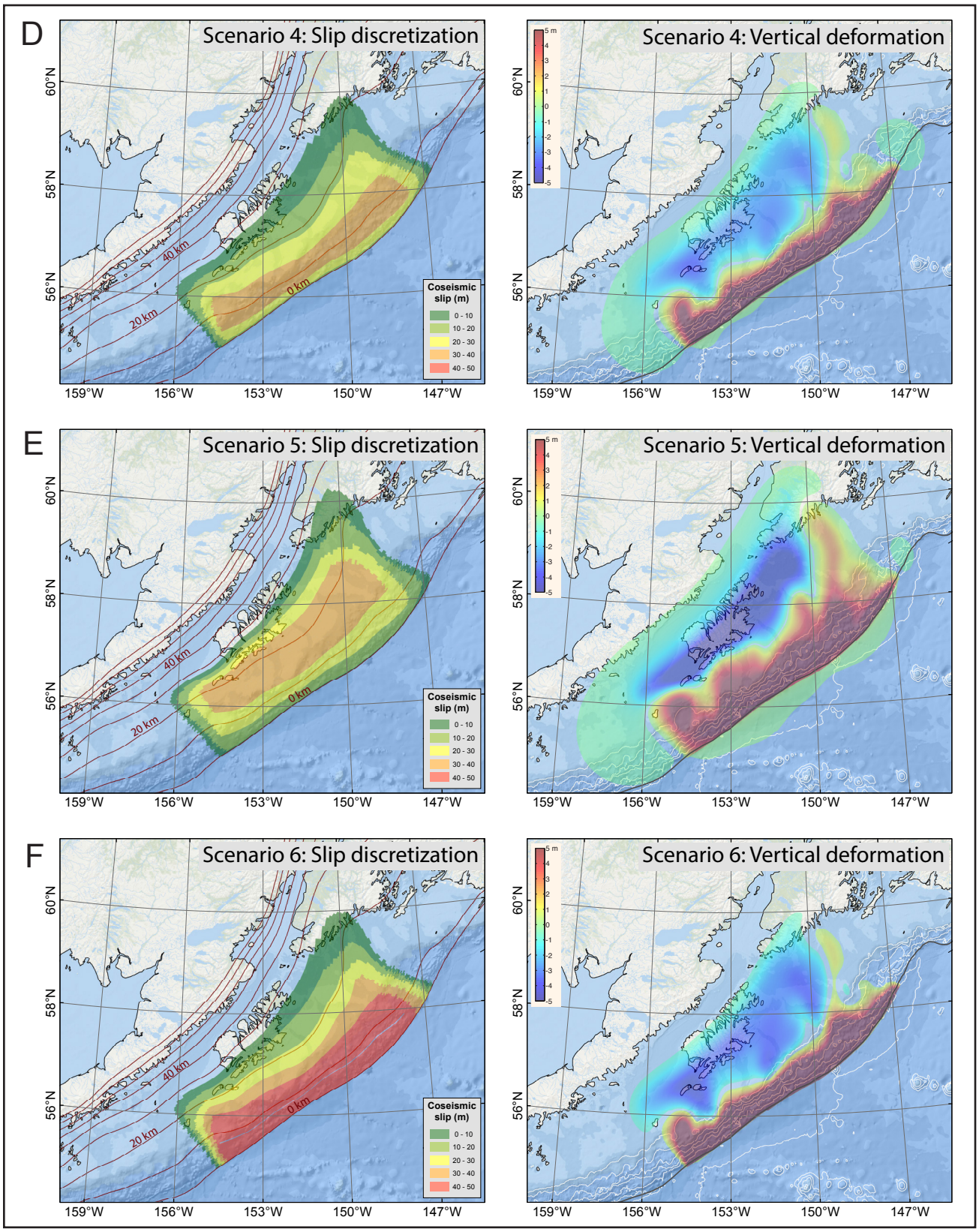

Figure 7, continued. Estimated slip distribution along the plate interface for scenarios 1–8 and computed vertical ground-surface deformation for scenarios 1–9 (slip distribution is not provided for scenario 9). Red lines are depth contours of the subduction interface, in kilometers. White lines are bathymetry contours within the depth interval between 1 and 5 km. The black line in the deformation figures (right column) indicates the approximate location of the trench.

Surface-breaching rupture scenarios

Scenarios 4–6 simulate hypothetical ruptures of the Kodiak segment of the Alaska-Aleutian megathrust where the updip and downdip limits of the rupture are 0 km and 30 km, respectively. The proposed slip distributions and vertical coseismic deformations for scenarios 4–6 are shown in figure 7.

Ryan and others (2012), and later Kirby and others (2013), compared the Alaska and Tohoku margins and suggested that a hypothetical rupture in the Alaska-Aleutian subduction zone might propagate to shallow depths, as it did in the M_W 9.0 Tohoku earthquake. Shallow fault rupture at the Tohoku margin resulted in a complex mix of seafloor rupture and blind (concealed) fault-bend

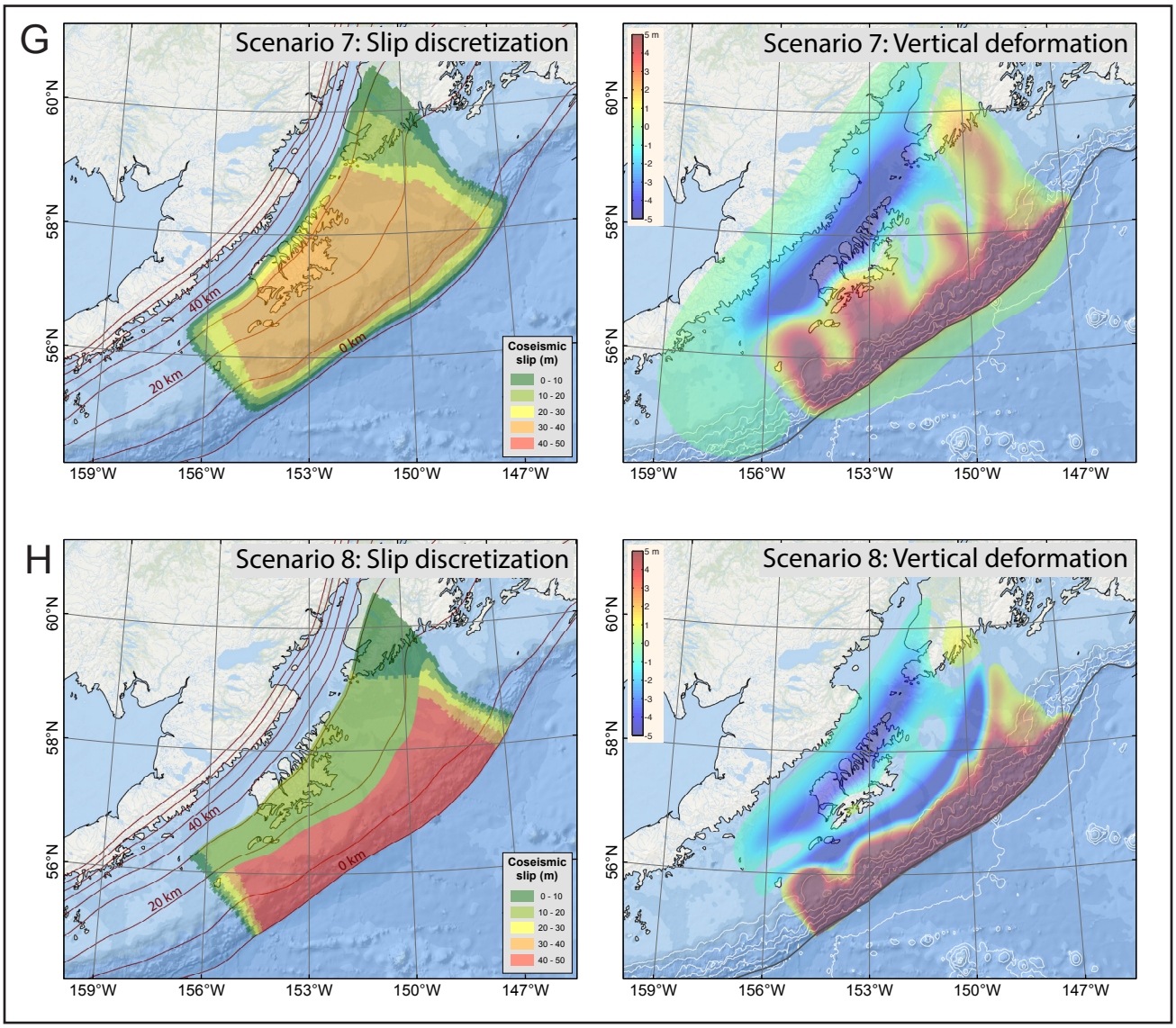

Figure 7, continued. Estimated slip distribution along the plate interface for scenarios 1–8 and computed vertical ground-surface deformation for scenarios 1–9 (slip distribution is not provided for scenario 9). Red lines are depth contours of the subduction interface, in kilometers. White lines are bathymetry contours within the depth interval between 1 and 5 km. The black line in the deformation figures (right column) indicates the approximate location of the trench.

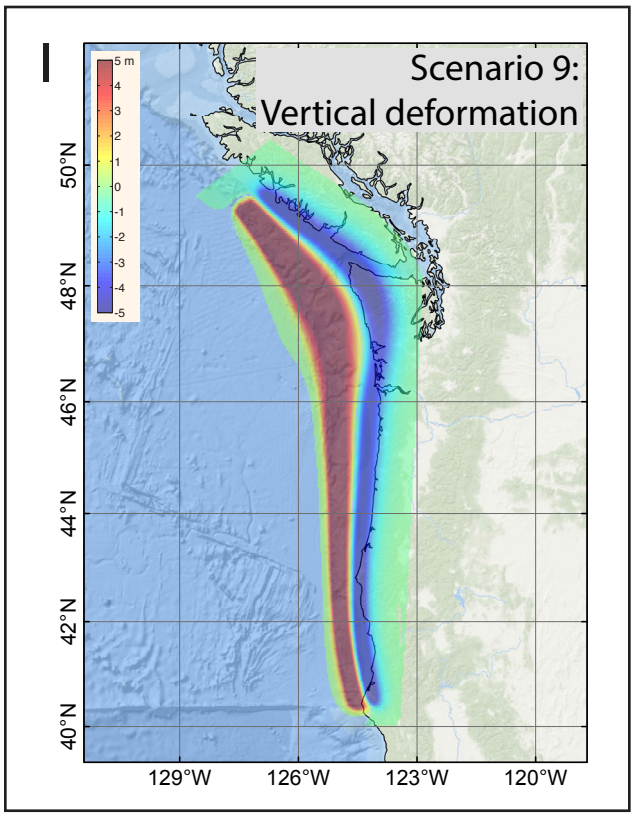

folding along the fault length—both of which contributed to a significant seafloor disturbance. Multibeam bathymetry in the Kodiak area suggests that the Alaska plate margin has similar mixed-behavior shallow ruptures. To account for the possibility that the earthquake rupture may reach the seafloor, we construct scenarios 4–6 with modeled fault slip that extend to the zero-depth contour. These scenarios modify scenarios 1–3 in which the slip extends only to about the 2-km-depth contour in the shallow part of the megathrust. The updip and downdip limits of the rupture are 0 km (0 mi) and 30 km (18.6 mi), respectively.

Figure 7, continued. Estimated slip distribution along the plate interface for scenarios 1–8 and computed vertical ground-surface deformation for scenarios 1–9 (slip distribution is not provided for scenario 9). Red lines are depth contours of the subduction interface, in kilometers. White lines are bathymetry contours within the depth interval between 1 and 5 km.

Scenario 4: M_W 9.25 near Kodiak Island; 10 km (6.2 mi) depth, slip extending upward to the ocean bottom	The depth of maximum slip corresponds to the depth for sensitivity case B. The slip skewness parameter, q, is set to 0.25 (bell-shaped curve skewed toward the trench) to model the maximum slip of 35 m (115 ft) at a depth of 10 km (6.2 mi), and a significant amount of slip near the trench.
Scenario 5: M_W 9.3 near Kodiak Island, 20 km (12.4 mi) depth, slip extending to the ocean bottom	The depth of maximum slip corresponds to the depth for sensitivity case C. The slip skewness parameter, q, is set to 0.7 (bell-shaped curve skewed toward the deeper part of the rupture) to model the maximum slip of 35 m (115 ft) at a depth of 20 km (12.4 mi), and a significant amount of slip near the trench. The width of the maximum slip extends from the 15 to 25 km (9.3 to 15.5 mi) depth contours of the plate interface.
Scenario 6: M_W 9.3 near Kodiak Island; 10 km (6.2 mi) depth, slip extending to the ocean bottom	The region of maximum slip of 50 m (164 ft) extends from the zero-depth contour to the depth of the plate interface at 15 km (9.3 mi), and then slip gradually reduces to about 10 m (33 ft) at 30 km (18.6 mi) depth.

Recently Butler and others (2014) described a layer of sand discovered in the Makauwahi sinkhole on the island of Kaua'i, Hawai'i. The origin of this layer was presumed to be inundation of the sinkhole by a giant paleotsunami following a M_W 9+ earthquake in the eastern Aleutian Islands. Butler (2012) provide an in-depth examination of previous great Aleutian earthquakes and tsunamis impacting Hawai'i. In subsequent research Butler (2014) considered several hypothetical events with a 35 m (114.8 ft) displacement on the megathrust and up to a 50 m (164 ft) displacement near the trench. Scenarios 7 and 8 consider similar hypothetical events that might occur near Kodiak Island. The proposed slip distribution and vertical coseismic deformations for scenarios 7 and 8 are shown in figure 7.

Scenario 7: M_W 9.3 earthquake near Kodiak Island with 35 m (114.8 ft) of maximum slip for nearly the entire rupture patch

In this scenario, similar to Butler (2014), we assume 35 m (114.8 ft) of slip for nearly the entire rupture patch between the 5 km (3.1 mi) and 35 km (21.7 mi) depth contours, with slip decreasing both toward the trench and to the deeper parts of the rupture. A similar scenario was proposed in the tsunami modeling study for Kodiak (scenario 8 of Suleimani and others, 2017).

Scenario 8: M_W 9.25 earthquake near Kodiak Island with 50 m (164.0 ft) of maximum slip

In this scenario, similar to Butler (2014), we assume 20 m (65.6 ft) slip on the plate interface between the 17.9 km (11.1 mi) and 30.8 km (19.1 mi) depth contours, and up to 50 m (164 ft) slip near the trench between 0 km (0 mi) and 17.9 km (11.1 mi) depth. A similar scenario was proposed in the tsunami modeling study for Kodiak (scenario 9 of Suleimani and others, 2017).

Scenario 9 considers a hypothetical tsunami generated along the coast of the Pacific Northwest U.S.—relatively distant from Kodiak Island. Although a rupture of the Cascadia subduction zone is not a worst-case scenario for the Kodiak area, this scenario is included for the sake of community preparedness.

Scenario 9: Rupture of the Cascadia subduction zone, including the entire megathrust between British Columbia and northern California

This scenario is the same as Scenario 16 in the tsunami modeling studies for King Cove and Cold Bay (Suleimani and others, 2016). The slip distribution model for this scenario is shown in figure 10 of Wang and others (2003). The vertical coseismic deformations for scenario 9 are shown in figure 7D.

TSUNAMI SOURCES WITH SPLAY FAULTS

Splay faults are important secondary tsunami sources in megathrust earthquakes. These steeply-dipping faults, which rise from the subduction zone to the seafloor, can produce large coseismic deformations that significantly increase tsunami runup heights in the near field (e.g., Lotto and others, 2019; Wang and Tréhu, 2016; Heidarzadeh, 2011). Also, tsunami waves produced by slip on a splay fault will arrive before the waves generated by slip on the megathrust; therefore, the initial tsunami wave can arrive sooner if slip on a splay fault is significant, thus reducing the time available for evacuation.

A number of studies published in the years following the 1964 Great Alaska Earthquake analyzed data on coseismic displacements and land features associated with the system of splay faults, as well as tsunami arrival times and tsunami amplitudes along the coast of the Kenai Peninsula and Kodiak Island (Plafker, 1965, 1967, 1969; Plafker and others, 1969). Plafker (1965) showed that slip during great megathrust earthquakes can be partitioned between the subducting boundary and splay faults. He demonstrated that the slip distribution in the 1964 rupture included a substantial amount of slip on intraplate splay faults, resulting in up to 10 meters of surface offset on the Patton Bay fault (fig. 1). Plafker suggested that the Patton Bay fault marks the northern end of a system of discontinuous faults in the ocean floor that continues well past where it was mapped at that time. More recently, Liberty and others (2013) analyzed high-resolution seismic reflection data for the Prince William Sound (PWS) area of the 1964 rupture and found that the greatest coseismic uplift in that region occurred on a series of splay faults. The authors examined the fault offsets on splay faults west of Montague Island (fig. 1) based on high frequency seismic reflection data and found that several splay faults had accumulated significant slip over the Holocene. Liberty and others (2019) showed that repeated ruptures of a set of splay faults had occurred along with past megathrust earthquakes, with a slip pattern similar to that seen in 1964. They concluded that the extent of rupture on the splay faults was linked to the along-strike limits of the PWS asperity (fig. 1), and that the asperity had been persistent over many earthquake cycles.

Using seismic reflection imagery, legacy seismic data, and high-resolution bathymetry, von Huene and others (2021) identified Aleutian trench backstops, which are splay fault zones that separate the accretionary prism from the continental margin, and are the boundaries along which weak sediment accreted. The authors suggest that the backstop splay fault zones extend along the entire Aleutian arc and contribute to regional tsunami hazards. From the analysis of slip distribution and coseismic displacements in the 1964 Great Alaska Earthquake, the authors proposed that the backstop splay faults in the Kodiak Island asperity (fig. 1) possibly contributed to generation of the 1964 tsunami. Suleimani and Freymueller (2020) presented a new coseismic slip model of the 1964 earthquake and showed that, along the south coast of Kodiak, coseismic slip on the megathrust alone is capable of producing tsunami arrivals and amplitudes that agree well with the observations, and that there is no evidence of the splay faults rupturing offshore Kodiak during the 1964 earthquake. Since the slip partitioning between the splay fault and megathrust is not well understood due to lack of direct seafloor measurements during earthquakes (Heidarzadeh, 2011; Li and others, 2014), both hypotheses are still valid and one cannot rule out the possibility of slip along splay faulting offshore of Kodiak Island in the next megathrust earthquake.

To avoid understating hazards, a tsunami hazard assessment must consider the effect of possible splay fault branching during a large subduction zone earthquake (Heidarzadeh, 2011; Wang and Tréhu, 2016). Therefore, in this report we consider several tsunami scenarios with added splay faults and study their effects on tsunami waves in the Kodiak Island communities. Figure 8 shows the shelf area in the Gulf of Alaska between the southern coast of Kodiak Island and the Aleutian trench. We assume that slip can be partitioned between the megathrust and a splay fault offshore Kodiak Island in one of the following three areas—in the mapped Kodiak shelf (KS), Albatross Bank (AB) fault zones, and the backstop (BS) splay fault zone described by von Huene and others (2021). The three solid lines between the island and trench—which go through these fault zones—are surface traces of the proposed splay faults. There are no direct constraints on the potential along-strike rupture extent of the splay faults in this area, but partially concealed faults are present along the entire length of the island (fig. 8), so we assume the length of the splay faults to be approximately the same as the rupture length in megathrust scenarios

(fig. 7). The A-A' cross-sectional profile across the Alaska-Aleutian megathrust (fig. 9) illustrates the splay faults rising from the megathrust. We develop splay fault scenarios based on these three possible locations of splay fault branching (fig. 10). For each KS and AB location, we make two splay fault scenarios with dips of 45° and 60°. The splay fault dips decrease with depth until the splay fault intersection with the plate interface. For the BS location, we select 30° dip at the surface, based on the values between 21° and 39° derived from seismic imagery for the eastern part of the Alaska-Aleutian megathrust (von Huene and others, 2021). The resultant splay fault geometry was checked to ensure that it is tightly connected to the plate interface, and then was discretized (similarly to the plate interface) into several rectangular subfaults.

The goal of adding a splay fault to a megathrust earthquake is to create a scenario that accounts for potential increases in tsunami height due to more complex earthquake ruptures. Another effect of a splay fault is a shorter wave arrival time, an important factor considered by emergency managers during evacuation planning, as well as by pedestrian evacuation modeling tools. Therefore, we construct the splay fault scenarios based on the following considerations:

Distance from the coast. To determine how the distance from the coast affects wave height, we consider three different locations of the splay fault surface traces with respect to the coast of Kodiak Island: in the KS, AB, and BS zones (fig. 8).

Selection of the megathrust scenarios. We have chosen to augment three aforementioned megathrust scenarios by adding a splay fault. The selected scenarios are those which result in the largest tsunami inundation areas (see Modeling Results section; several scenarios can produce a similar extent of inundation), and also satisfy one of following conditions: either the scenario has the maximum amount of slip in the area of the rupture where the splay fault connects to the megathrust, or the scenario results in the maximum amount of ground subsidence in the community. Scenarios 3, 6, and 8 (table 3) fit these criteria.

Slip partitioning. Because the pattern of slip partitioning between the megathrust and splay faults is poorly understood (Wendt and others, 2009), we consider two different ways to divide the slip in combined megathrust/splay fault ruptures.

If the slip on a megathrust at the base of the splay fault is large (40–50 m [131.2–164 ft]), we assume uniform slip along the splay fault all the way to the surface, and no slip on the megathrust updip of the splay fault.

If the slip on a megathrust at the base of the splay fault is moderate (20 m [65.6 ft]), we similarly assume uniform slip along the splay fault all the way to the surface, but reduce the slip on the megathrust updip of the splay fault by 50 percent.

To build a set of combined megathrust/splay fault ruptures, we add each of the splay fault ruptures outlined in the scenario tree (fig. 10) to megathrust scenarios 3, 6, and 8. Figure 11 illustrates this process using the example of scenario 6. The proposed slip distributions and vertical coseismic deformations are shown in the left and right columns, respectively. Figure 11A shows scenario 6 without the splay fault for reference. Figures 11B–D show the splay fault slip patterns and the combined coseismic deformations for KS, AB, and BS splay faults. The left columns are the slip patterns for splay faults shown on top of the megathrust rupture area to illustrate the proximity of splay faults to Kodiak Island. The coseismic deformations in the right column illustrate that for the cases of KS and AB splay faults, there is an area of second maximum uplift that is much closer to the coast than the maximum in the trench area.

The full list of scenarios and splay fault parameters is given in table 4. Note that the first column lists the overall number of scenarios for the purpose of referencing them in the time series plots (apps. A–E); the second column shows scenario numbers for megathrust-only scenarios given in table 3; and the third column refers to the splay fault scenario numbers.

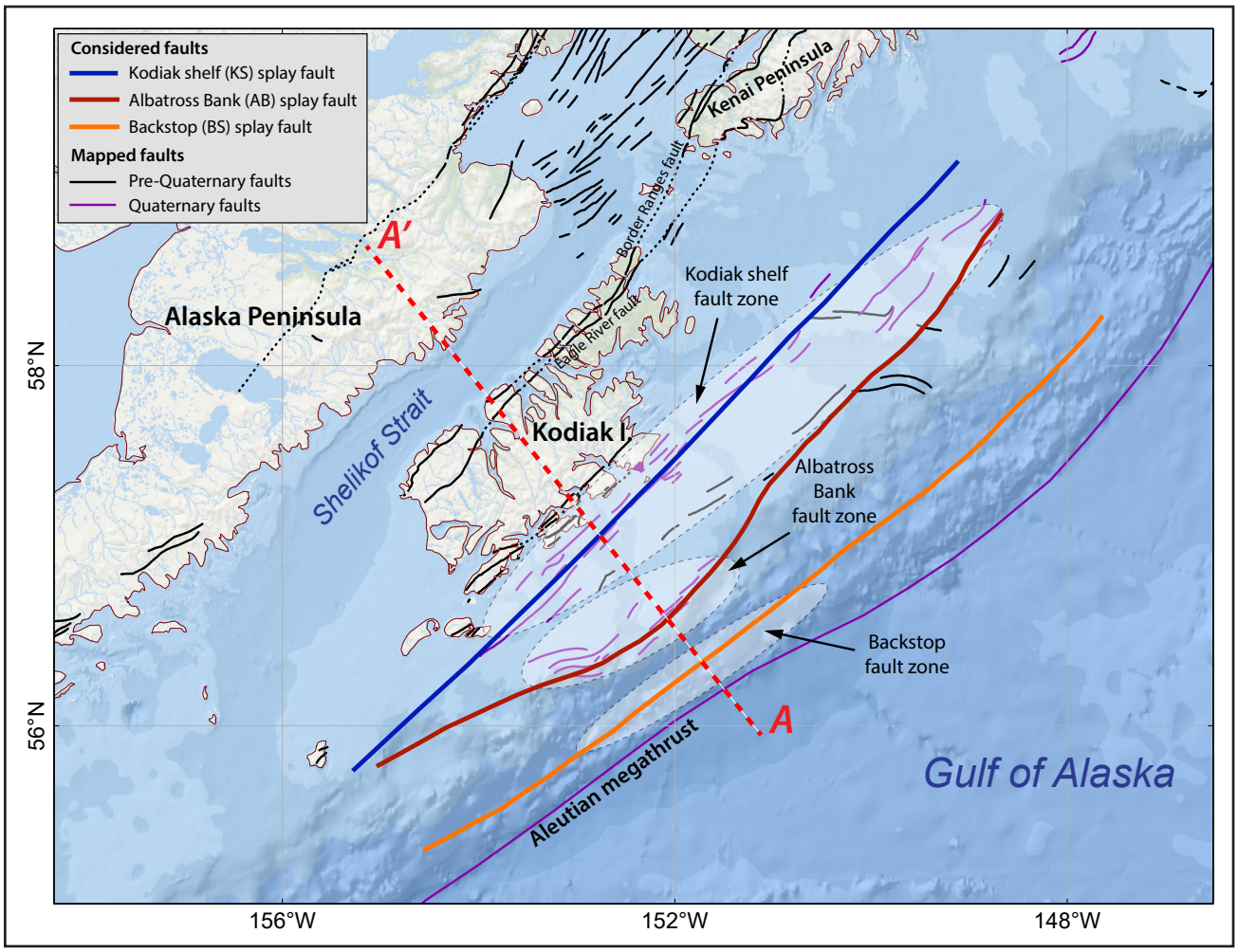

Figure 8. Shelf area in the Gulf of Alaska between the southern coast of Kodiak Island and the Aleutian trench, with locations of the Kodiak shelf (KS), Albatross Bank (AB), and the backstop (BS) splay faults. The A-A' profile across the Aleutian megathrust is shown in figure 9.

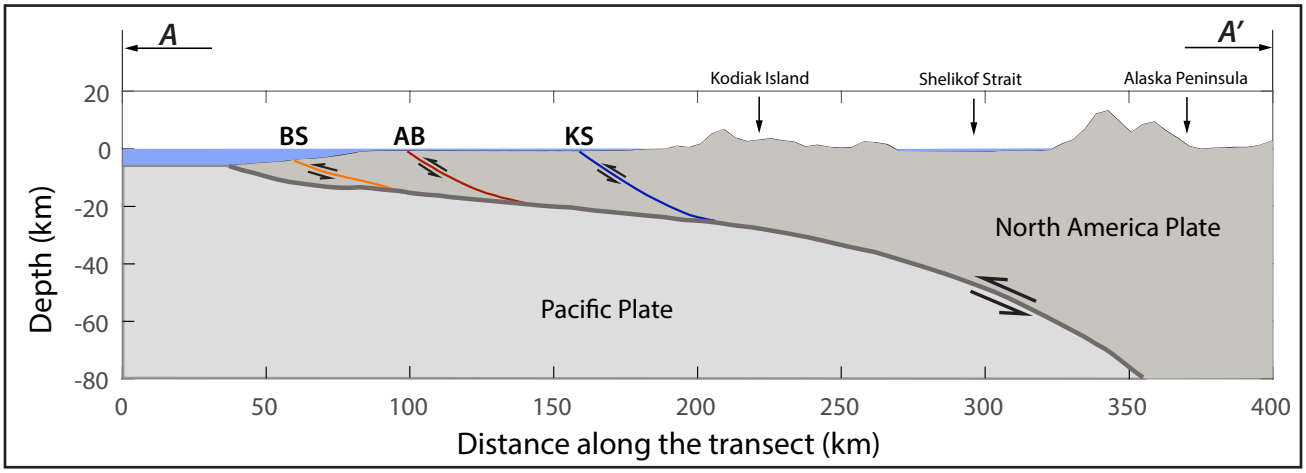

Figure 9. The A-A' cross-sectional profile across the Aleutian megathrust. The AB and KS splays are shown here with 45° dips. The elevation values are exaggerated by a factor of 10 to illustrate the topography of Kodiak Island and the Alaska Peninsula.

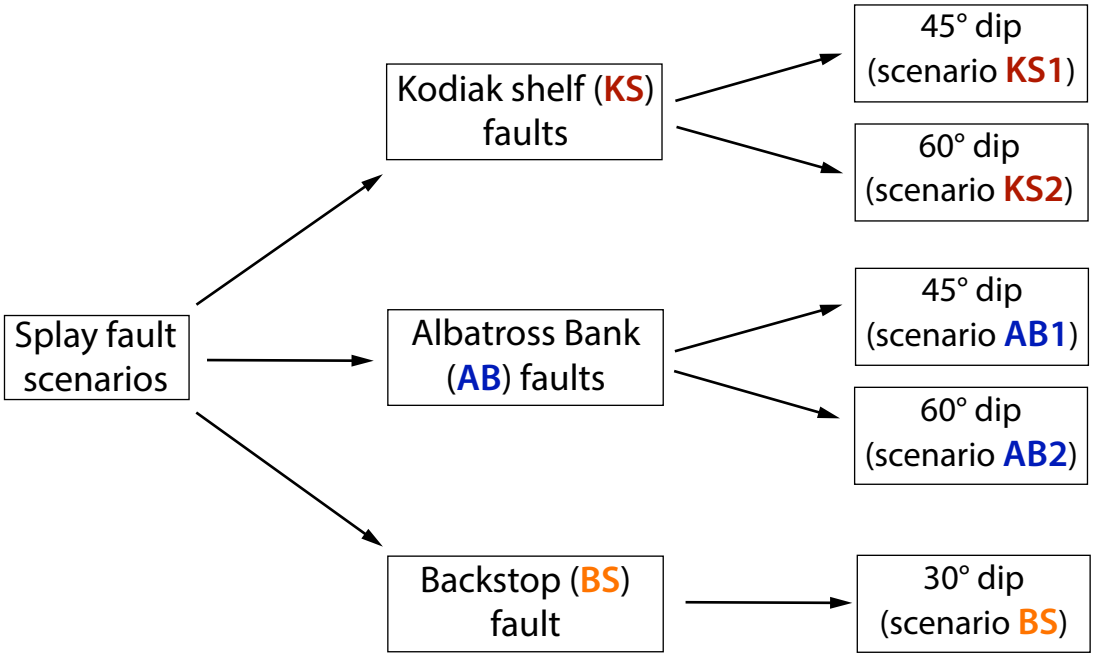

Figure 10. Scenario tree illustrating the development of the splay fault scenarios.

Time series

The arrival time of the first wave, the maximum wave amplitude, and the duration of wave action are all important factors that should be considered by emergency managers during evacuation planning. Therefore, we supplement the inundation maps with time series of modeled water level and velocity dynamics at certain locations in the Kodiak communities. Appendices A–E contain plots of sea level and velocity time series for selected scenarios at critical locations. For each location—shown by a number in figures A1 through E1, we plot the sea level and water velocity (figs. A2–E2, respectively) for selected scenarios (scenarios 3, 3-KS2, 3-AB1, 6-BS, 8, and 9). Scenarios 3, 6, and 8 are the megathrust scenarios that result in the largest areas of tsunami inundation in the communities. We show the three splay fault scenarios with different locations of a splay fault (scenarios 3-KS2, 3-AB1, and 6-BS) to illustrate how the distance between the splay fault and the coast affects the arrival time of the first wave. Scenario 9 is included as an example of a potential far-field event.

In all plots in appendices A–E, zero time corresponds to the time at which the earthquake occurs. The pre-earthquake elevation/depth with respect to the MHHW is stated for each location. The post-earthquake elevation/depth corresponding to the MHHW datum is also listed for each scenario in tables A1-E1. To show the height of arriving tsunamis for offshore locations, we use a vertical datum with a zero mark corresponding to the pre-earthquake sea level. Velocity was computed only where the water depth is greater than 0.3 m (1.0 ft). The velocity magnitude is calculated as water flux divided by water depth, thus the uncertainty can be large when the water depth is small.

The maximum water level for all 24 considered scenarios are listed in appendix tables A2 through E2, and maximum velocity values are given in tables A3 through E3.

MODELING RESULTS

Water dynamics were modeled for each of the scenarios described above and summarized in table 4 for each grid (table 2; fig. 3). The extent of inundation and flow depths were calculated only for the level 4 high-resolution grids. Map sheets 1–5 show the maximum composite extent of inunda-

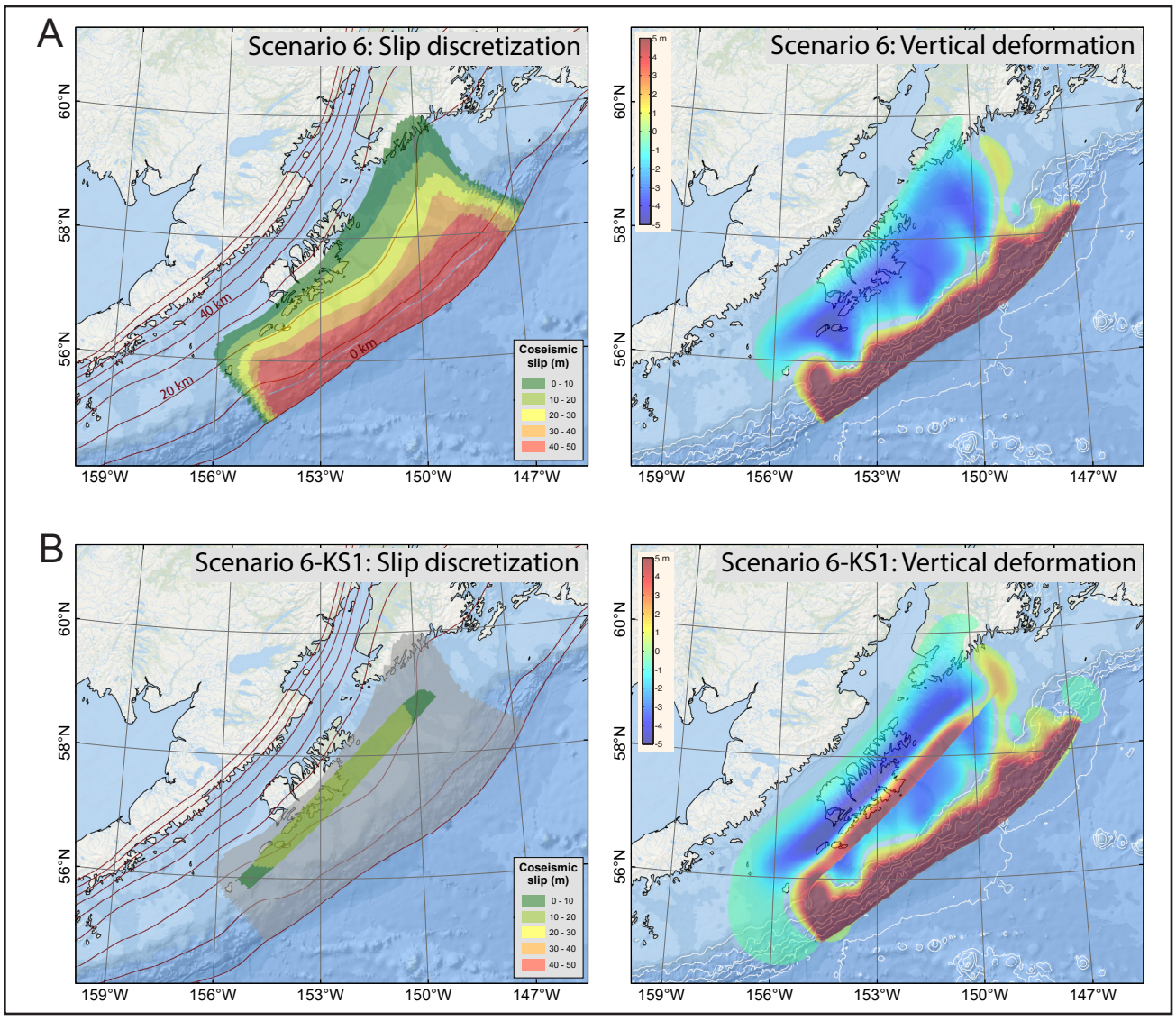

Figure 11. Assumed slip distribution along the plate interface (left) and computed vertical ground-surface deformation (right) for (**A**) the megathrust-only scenario 6 and (**B**) scenario 6-KS1 with an added splay fault in the KS zone.

tion for all scenarios, and the maximum composite flow depths over dry land. The calculated extent of inundation accounts for coseismic deformation in the communities.

First, we modeled tsunami inundation in all communities for every megathrust scenario listed in table 3. Scenario 3 resulted in the worst inundation at Akhiok; scenario 6 in Chiniak and Old Harbor; and scenario 8 in Ouzinkie and Port Lions. For each of these three scenarios, we made five sub-scenarios by adding splay faults of different geometries and locations of their surface traces with respect to the southeastern shore of Kodiak Island (table 4). We use the community of Old Harbor to illustrate our analysis of modeling results for the splay fault scenarios and their comparison to the megathrust-only scenario results. In figure 12A, we plot the inundation lines for the three worst-case megathrust scenarios (3, 6, and 8), as well as scenario 9 as an example of a far-field tsunami event that can potentially inundate communities on Kodiak Island. All four scenarios result in substantial inundation at Old Harbor; scenarios 6 and 8 flood the entire community. While the inundation area for scenario 9 is much smaller, it still covers a substantial part of

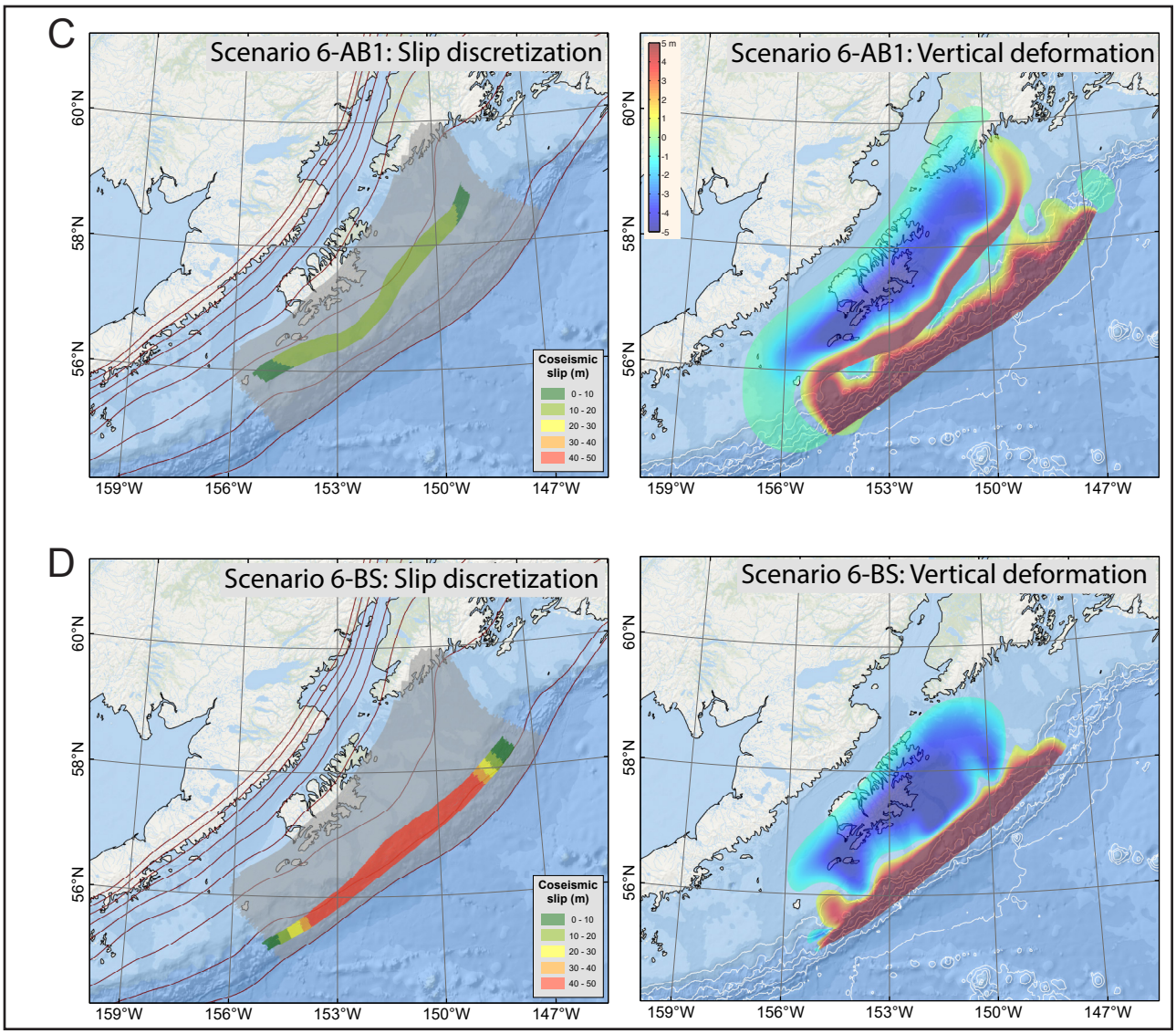

Figure 11, continued. Assumed slip distribution along the plate interface (left), and computed vertical ground-surface deformation (right) for (**C**) scenario 6-AB1 with an added splay fault in the AB zone and (**D**) scenario 6-BS with an added splay fault in the BS zone.

the coastline, including the road along the bay and part of the village adjacent to the harbor.

Next, we analyze the inundation areas due to scenarios with added splay faults. Figures 12B–D show the inundation zones for splay fault scenarios, which correspond to megathrust scenarios 3, 6, and 8, respectively. The maps show that some scenarios result in comparable inundation zones. However, for every megathrust scenario there is at least one corresponding splay fault scenario that results in a larger inundation zone, namely scenarios 3-AB1, 6-BS, and 8-BS. We perform this type of analysis for the rest of the communities and identify the worst-case splay fault scenario for each of them.

Finally, we investigate how the location of a splay fault with respect to the Kodiak Island coast affects the arrival time of the first wave. Figure 13 shows time series plots for each community for four scenarios: the worst-case megathrust scenario for the community and the three splay fault scenarios corresponding to three different locations of the splay fault in the KS, AB, and BS zones (fig. 8).

Below we describe the community-specific tsunami modeling results. To illustrate the three

Table 4. All hypothetical megathrust and splay fault scenarios used to model tsunami runup at the Kodiak Island communities.

#	Mega-thrust scenario number	Splay fault scenario number	Description	Dip	Maximum slip on splay fault, m (ft)	Slip reduction on the plate interface updip of the splay fault
1	1		M_w 9.2 earthquake in the area of Kodiak Island; 10 km depth			
2	2		M_w 9.25 earthquake in the area of Kodiak Island; 20 km depth			
3	3		M_w 9.3 earthquake in the area of Kodiak Island; 10–20 km depth			
4		3-KS1	Megathrust scenario #3 with the added splay fault in the Kodiak shelf zone	45°	20.0 (65.6)	50%
5		3-KS2	Megathrust scenario #3 with added splay fault in the Kodiak shelf zone	60°	20.0 (65.6)	50%
6		3-AB1	Megathrust scenario #3 with added splay fault in the Albatross Bank zone	45°	20.0 (65.6)	50%
7		3-AB2	Megathrust scenario #3 with added splay fault in the Albatross Bank zone	60°	20.0 (65.6)	50%
8		3-BS	Megathrust scenario #3 with added splay fault in the backstop zone	30°	40.6 (133.2)	100%
9	4		M_w 9.25 earthquake in the area of Kodiak Island; 10 km depth			
10	5		M_w 9.3 earthquake in the area of Kodiak Island; 20 km depth, slip extending to 0 km depth			
11	6		M_w 9.3 earthquake in the area of Kodiak Island; 10 km depth, slip extending to 0 km depth			
12		6-KS1	Megathrust scenario #6 with added splay fault in the Kodiak shelf zone	45°	20.0 (65.6)	50%
13		6-KS2	Megathrust scenario #6 with added splay fault in the Kodiak shelf zone	60°	20.0 (65.6)	50%
14		6-AB1	Megathrust scenario #6 with added splay fault in the Albatross Bank zone	45°	20.0 (65.6)	50%
15		6-AB2	Megathrust scenario #6 with added splay fault in the Albatross Bank zone	60°	20.0 (65.6)	50%
16		6-BS	Megathrust scenario #6 with added splay fault in the backstop zone	30°	62.8 (206.0)	100%
17	7		M_w 9.3 earthquake with 35 m of maximum slip for nearly the entire rupture patch			
18	8		M_w 9.25 earthquake with 50 m of maximum slip in the shallow part of the rupture			
19		8-KS1	Megathrust scenario #8 with added splay fault in the Kodiak shelf zone	45°	20.0 (65.6)	50%
20		8-KS2	Megathrust scenario #8 with added splay fault in the Kodiak shelf zone	60°	20.0 (65.6)	50%
21		8-AB1	Megathrust scenario #8 with added splay fault in the Albatross Bank zone	45°	20.0 (65.6)	50%
22		8-AB2	Megathrust scenario #8 with added splay fault in the Albatross Bank zone	60°	20.0 (65.6)	50%
23		8-BS	Megathrust scenario #8 with added splay fault in the backstop zone	30°	50.0 (164.0)	100%
24	9		M_w 9.1 earthquake in the Cascadia subduction zone			

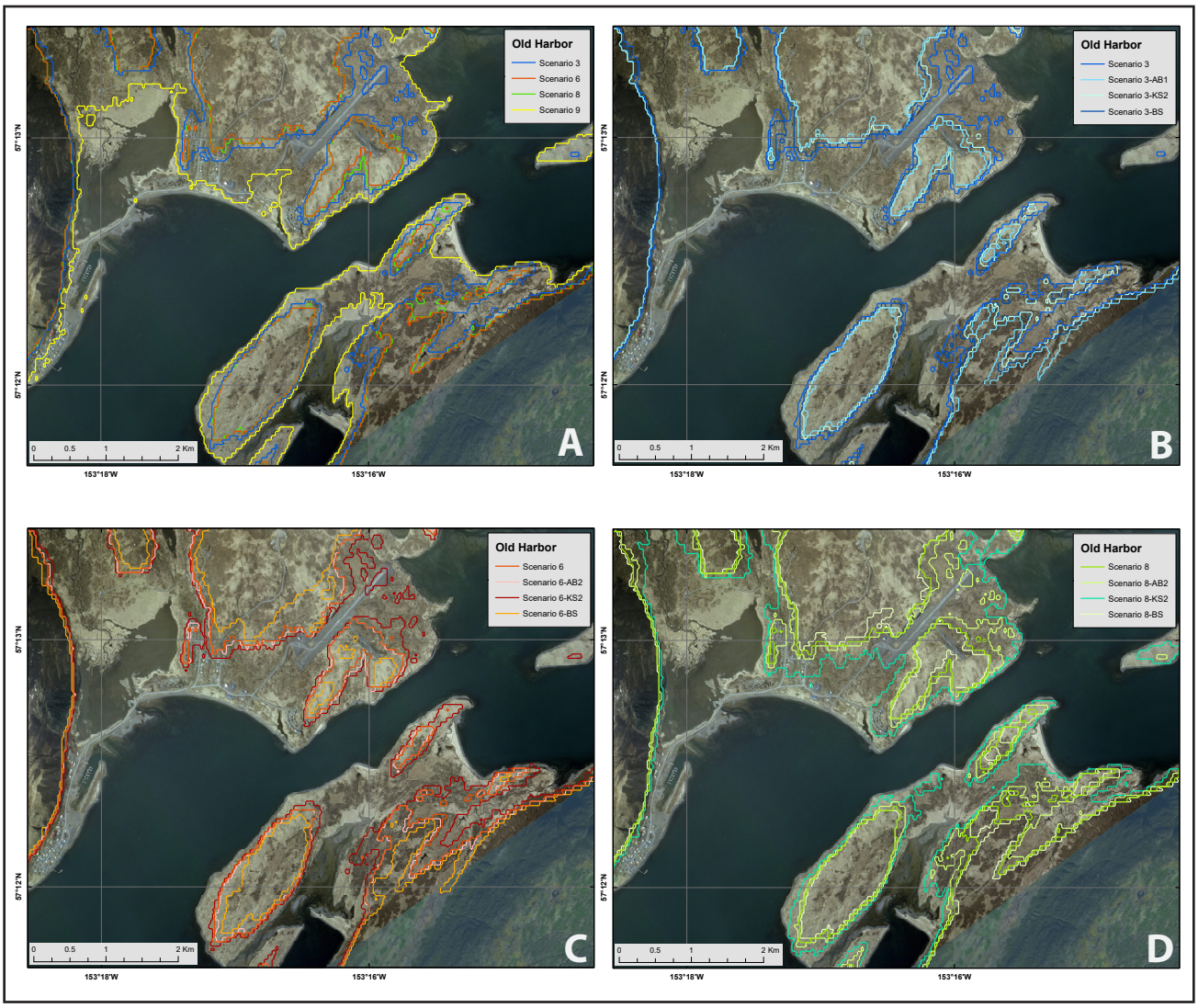

Figure 12. Extents of tsunami inundation at Old Harbor for (**A**) megathrust-only scenarios 3, 6, 8 and 9; (**B**) splay fault scenarios corresponding to scenario 3; (**C**) splay fault scenarios corresponding to scenario 6; (**D**) splay fault scenarios corresponding to scenario 8.

major types of tsunami scenarios that could be potentially damaging to Kodiak Island communities we plot the extent of inundation for each community in figure 14 for three scenarios: the worst-case megathrust; splay fault scenarios that are specific to that community: and scenario 9 as an example of a far-field tsunami event.

Akhiok

In Akhiok, both scenarios 3 and 3-AB2 flood the entire community, while scenario 9 results in minimal inundation (fig. 14A). According to the time series plot (fig. 13A), inclusion of a splay fault does not significantly affect the time of arrival of the first wave. Akhiok is located on the coast of Alitak Bay, which is sheltered by Aliulik Peninsula from waves coming from the Gulf of Alaska (fig. 2A). As waves enter Alitak Bay through a shallow entrance between Aliulik Peninsula and Sitkinak Island they slow down and their energy partially dissipates. As a result, the tsunami signal at Akhiok has only a long-wave component; high-frequency waves are filtered out by a combination of local bathymetric features and location of the village inside a sheltered bay.

Map sheet 1 shows the composite inundation line and flow depths over dry land for the village

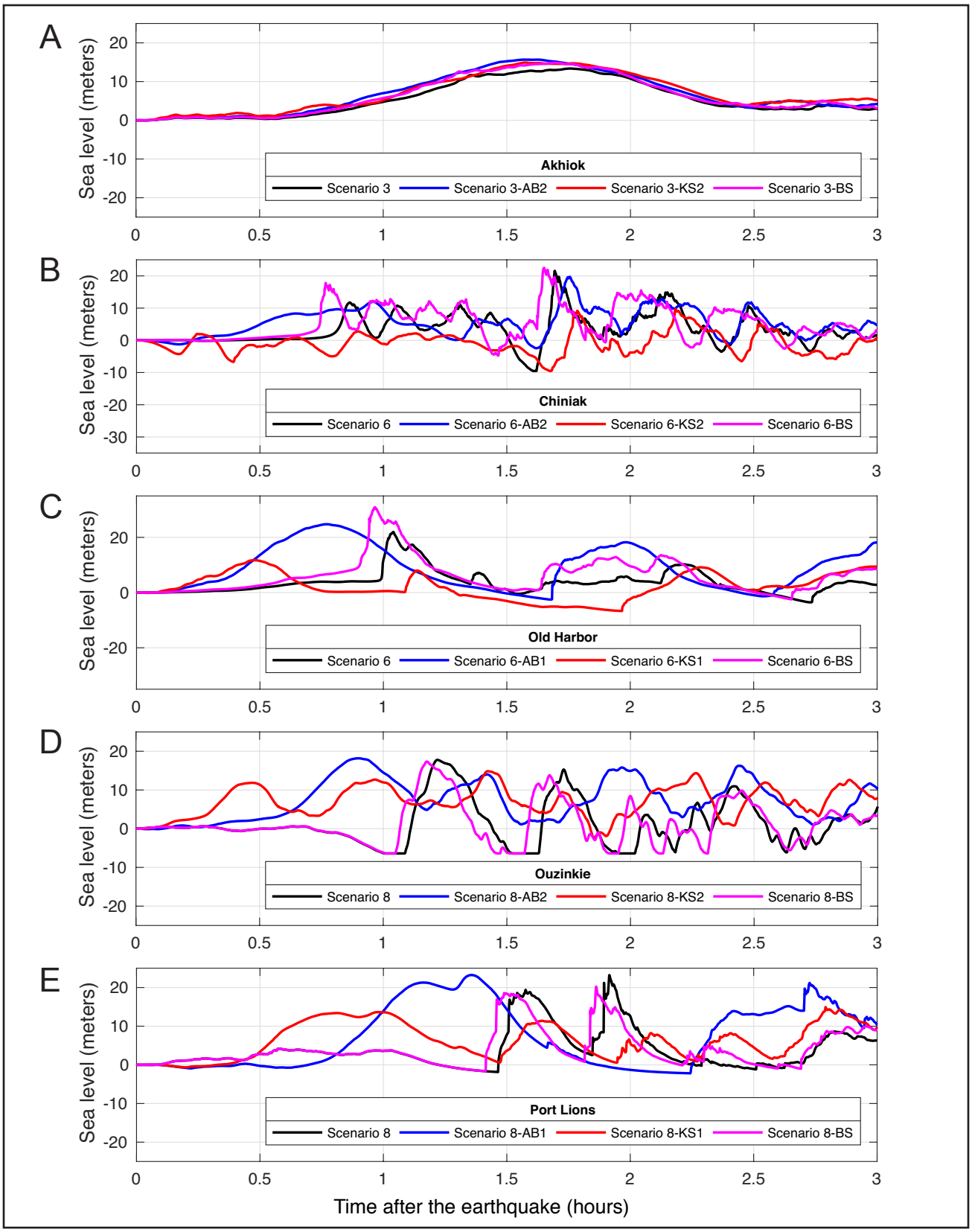

Figure 13. Modeled water-level dynamics (from the point of view of an observer standing at the shore) at the five Kodiak Island communities for the worst-case megathrust scenario in each community, and three splay fault scenarios corresponding to this megathrust scenario.

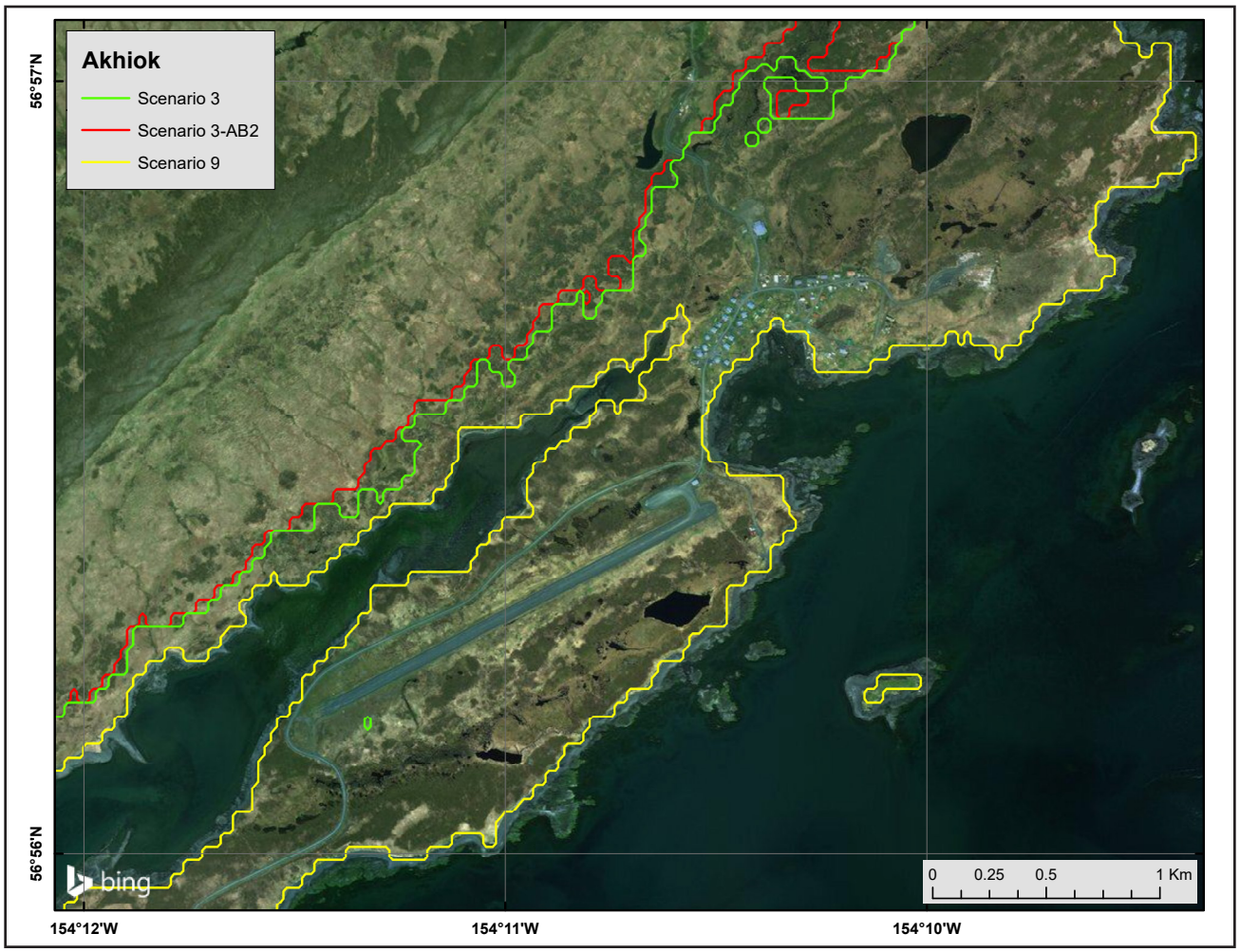

Figure 14A. Modeled potential tsunami inundation for selected scenarios in Akhiok.

of Akhiok. The entire community is inside the inundation zone, with flow depths reaching 15 m (49.2 ft). The numerical simulations reveal that the first wave—which is the highest one—could arrive at Akhiok about 30 minutes after the earthquake. As demonstrated by the time series data shown in figure A2, significant wave activity could continue in Akhiok for at least 12 hours after the earthquake, and the predicted average time interval between successive waves is two to three hours.

Chiniak

Both scenarios 6 and 6-BS flood the entire coastal area along Chiniak Bay including the Chiniak Highway, except for the small area at Chiniak Point where elevations are higher (figs. 14B and B1). Scenario 9 results in minimal inundation. According to the time series plot shown in figure 13B, all splay fault scenarios result in an earlier arrival of the first wave. Scenario 6-KS2 results in the first negative wave—which manifests itself as a water withdrawal from the coastline—as soon as 10 minutes after the earthquake, with the wave crest following five minutes later.

Map sheet 2 shows the composite inundation line and flow depths over dry land for the community of Chiniak. The major part of the community is inside the inundation zone, with flow depths reaching 20 m (65.6 ft) along the Chiniak Highway. The numerical simulations reveal that the first wave could start arriving at Chiniak about 15 minutes after the earthquake. The second wave (the largest one) would arrive about 1.5 hours after

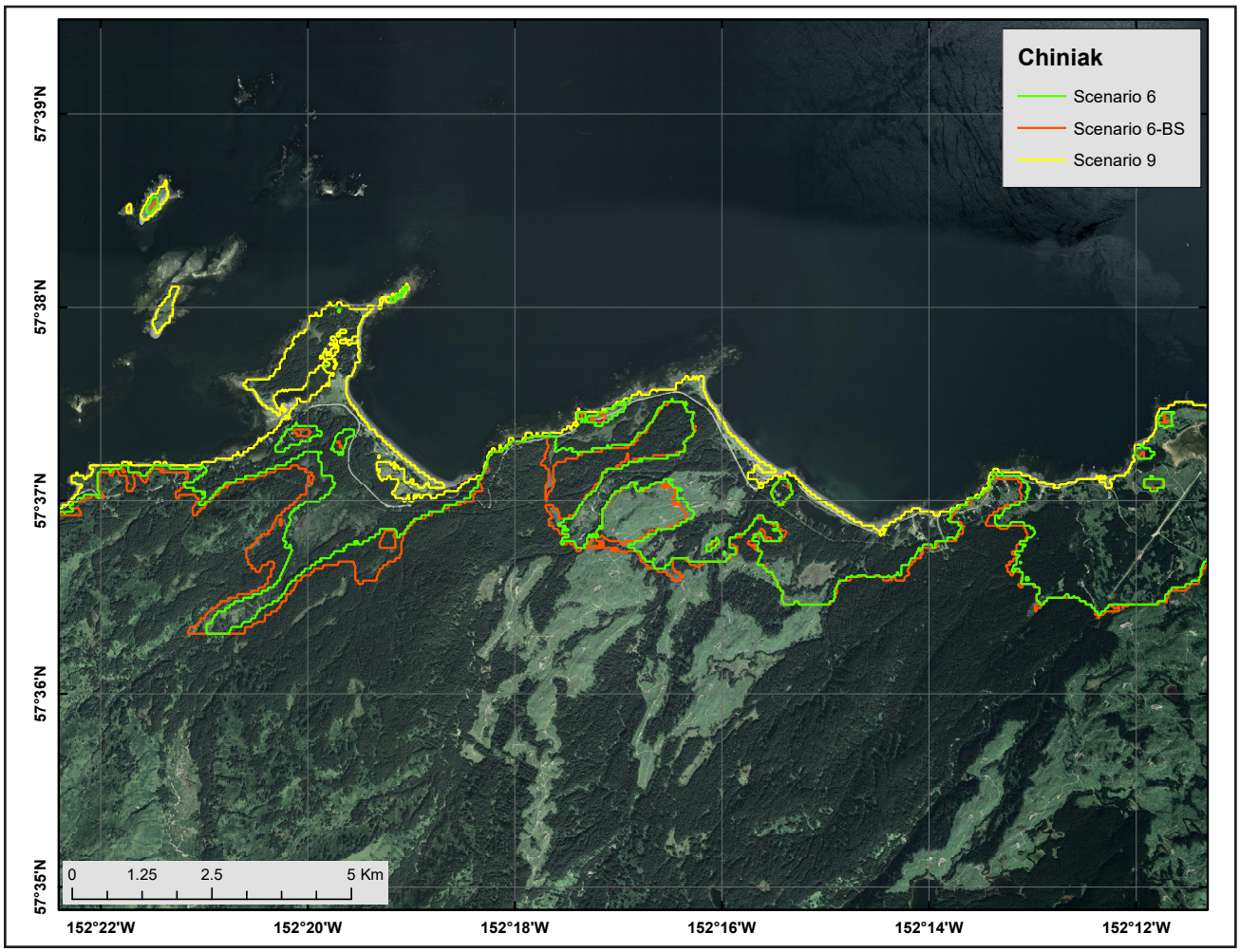

Figure 14B. Modeled potential tsunami inundation for selected scenarios in Chiniak.

the earthquake. As demonstrated by the time series shown in figure B2, significant wave activity could continue in Chiniak for at least 12 hours after the earthquake, and the predicted average time interval between successive waves is about 1.5 hours.

Old Harbor

The simulated extents of tsunami inundation in Old Harbor are shown in figure 14C. All three scenarios result in substantial inundation at Old Harbor. Scenarios 6 and 6-BS flood the entire community. While the inundation area for scenario 9 is much smaller, it still covers a substantial part of the coastline, including the road that goes along the bay, and part of the village adjacent to the harbor. According to the time series plot shown in figure 13C, all splay fault scenarios result in an earlier time of arrival of the first wave. Scenario 6-KS1 results in a large wave that arrives as soon as 15 minutes after the earthquake. The first wave in scenario 6-BS arrives five minutes earlier than the first wave in the megathrust-only scenario 6.

Map sheet 3 shows the composite inundation line and flow depths over dry land for the community of Old Harbor. The entire community is inside the inundation zone, with flow depths reaching 30 m (98.4 ft) in the area adjacent to the harbor and along the road that follows the bay. The numerical simulations reveal that the first wave, which is the largest one, could arrive at Old Harbor about 15 minutes after the earthquake. As demonstrated by the time series shown in figure C2, significant wave activity could continue in Old Harbor for at least

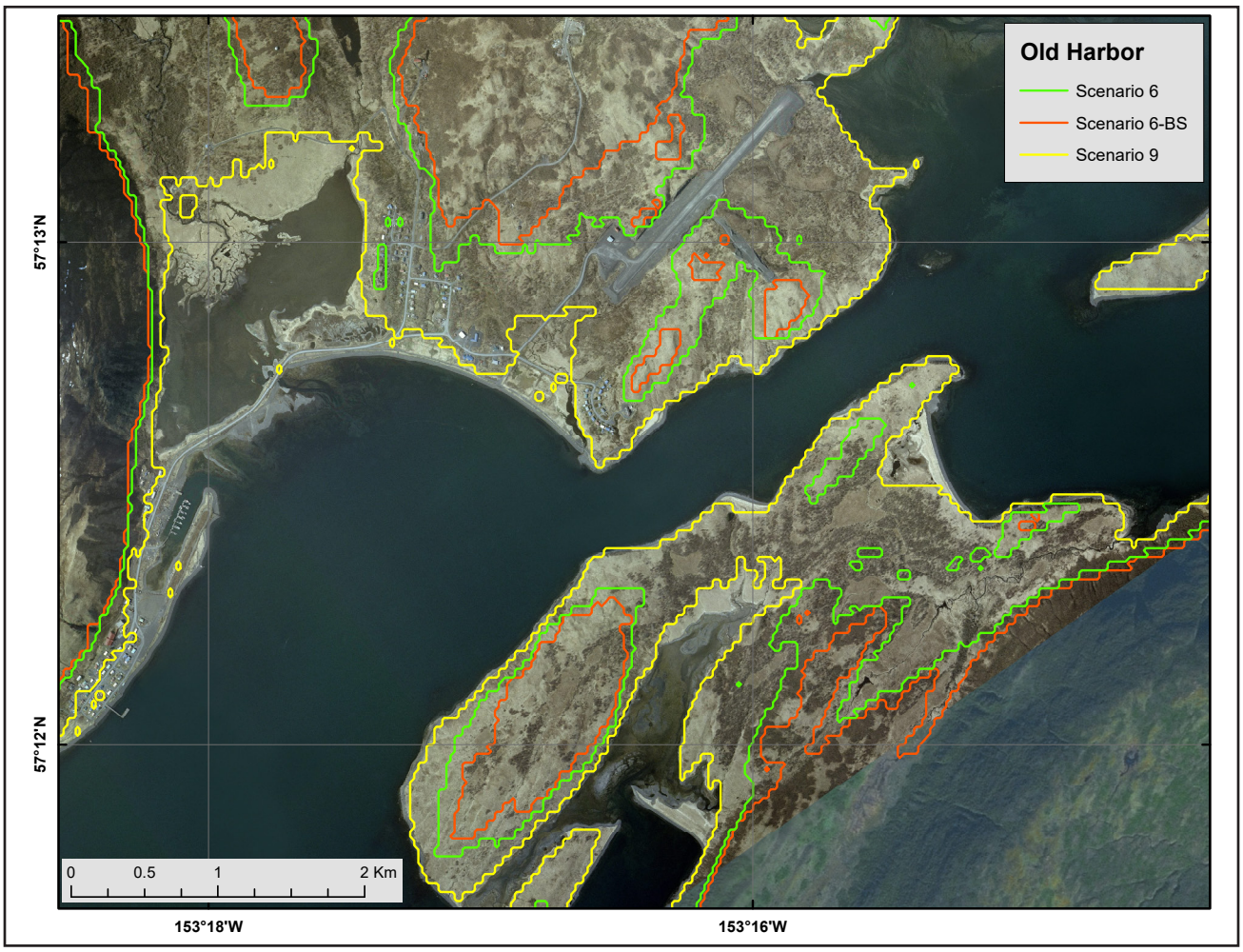

Figure 14C. Modeled potential tsunami inundation for selected scenarios in Old Harbor.

12 hours after the earthquake, and the predicted average time interval between successive waves is approximately 1 to 1.5 hours.

Ouzinkie

Both scenarios 6-BS and 8 result in substantial inundation in this community, while scenario 9 results in minimal inundation (fig. 14D). According to the time series plot shown in figure 13D, all splay fault scenarios result in earlier first wave arrival times. Scenario 8-KS2 results in a large wave that arrives as soon as 15 minutes after the earthquake. The crest in scenario 8-AB2 arrives about 50 minutes after the earthquake, and the wave in scenario 8-BS arrives just two minutes earlier than the first wave in megathrust-only scenario 8.

Map sheet 4 shows the tsunami hazard for Ouzinkie. The composite inundation line and flow depths over dry land are shown for the area covered by the high-resolution level 4 grid (table 2). However, in order to include the air strip—critical infrastructure that could potentially be affected— we have adjusted the map extent and added the inferred tsunami hazard boundary from the Kodiak regional tsunami hazard study (Suleimani and others, 2019). A major part of the community is inside the inundation zone, with flow depths reaching 20 m (65.6 ft) in the area adjacent to the harbor and along the road that follows the bay. The numerical simulations reveal that the first wave, which is the largest for the majority of scenarios, could start arriving at Ouzinkie about 15 minutes after the earthquake. The second wave is the largest one only for scenario 3-AB1 and arrives about 2.5 hours after the earthquake. As demonstrated by the time series shown in figure D2, significant wave activity could continue in Ouzinkie

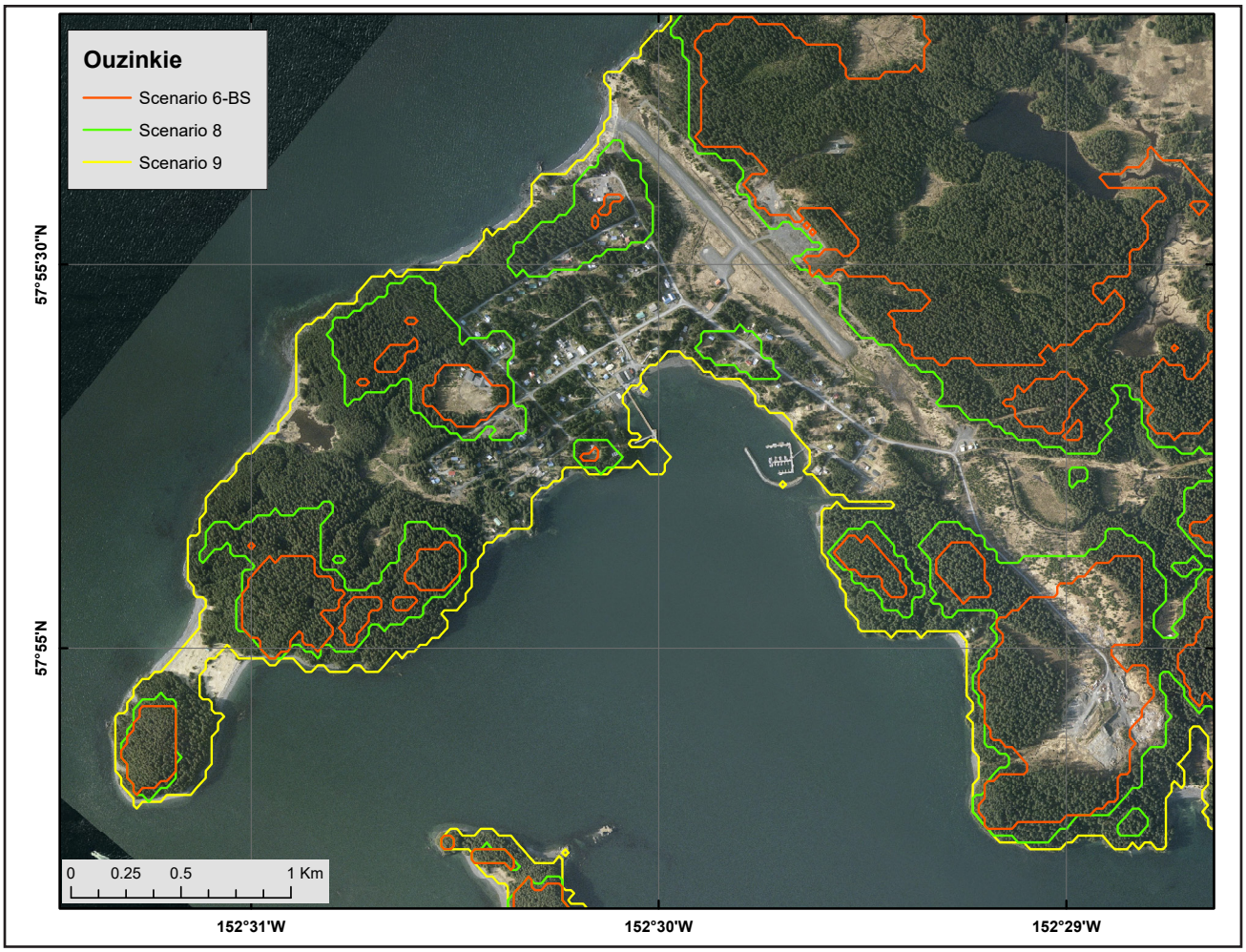

Figure 14D. Modeled potential tsunami inundation for selected scenarios in Ouzinkier.

for at least 12 hours after the earthquake, and the predicted average time interval between successive waves is approximately 30 minutes to 1 hour.

Port Lions

Both scenarios 6-BS and 8 flood almost the entire community, while scenario 9 results in minimal inundation (fig. 14E). According to the time series plot shown in figure 13E, all splay fault scenarios result in earlier first wave arrival times. The wave produced by scenario 8-KS1 arrives as soon as 30 minutes after the earthquake. Scenario 8-AB1 results in a wave with the largest amplitude among all four scenarios and arrives about 45 minutes after the earthquake. The first wave in scenario 8-BS arrives just two minutes earlier than the first wave in megathrust-only scenario 8.

Map sheet 5 shows the composite inundation line and flow depths over dry land for the community of Port Lions. A major part of the community is inside the inundation zone, with flow depths reaching 20 m (65.6 ft) in the low-elevation coastal area, and along the road that goes around the bay. The numerical simulations reveal that the first wave, which is the largest for most scenarios, could start arriving at Port Lions about 30 minutes after the earthquake. The second wave is largest for scenario 8 and arrives about 1.5 hours after the earthquake. As demonstrated by the time series shown in figure E2, significant wave activity could continue in Port Lions for at least 12 hours after the earthquake, and the predicted average time interval between successive waves is approximately 1 to 1.5 hours.

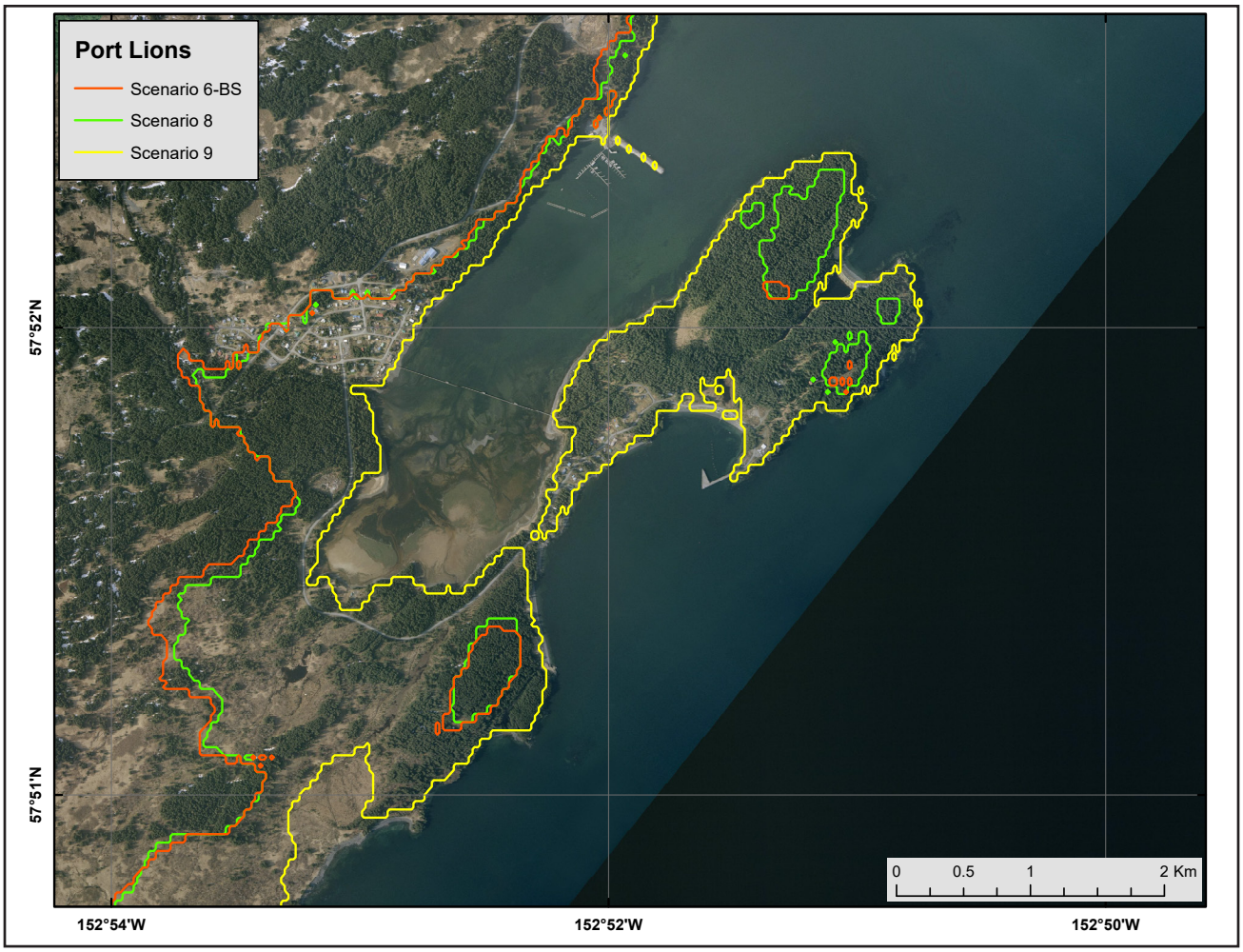

Figure 14E. Modeled potential tsunami inundation for selected scenarios in Port Lions.

SOURCES OF ERRORS AND UNCERTAINTIES

The hydrodynamic model used to calculate propagation and run-up of tectonic tsunamis is a nonlinear, flux-formulated, shallow-water model (Nicolsky, Suleimani, and Hansen, 2011) that passed the verification and validation tests required for numerical codes used to produce tsunami inundation maps (Synolakis and others, 2007; NTHMP, 2012). Most of the errors/uncertainties in the numerical predictions originate from the tsunami sources used in the numerical models. Furthermore, our assessment of potential earthquake scenarios is not exhaustive and represents a best estimate of the locations and sizes of potential tsunami-generating events. It is possible that other unrecognized earthquake scenarios or slope failures could present hazards to Kodiak Island communities. However, the scenarios presented are intended to cover the range of potential situations about which the communities should be aware.

The spatial resolution of the grid used to calculate tsunami inundation at Kodiak Island communities is about 16 m (52.5 ft) and satisfies NOAA minimum recommended requirements for computation of tsunami inundation (NTHMP, 2010). Although this resolution is high enough to describe major relief features, small topographic features, buildings, and other facilities cannot be resolved accurately by the existing model. We also note that uncertainty in grid-cell elevation/depth propagates into the modeling results and eventually contributes

to horizontal uncertainty in the location of the inundation line. One contribution to this uncertainty is the paucity of data in the intertidal zone. However, no established practices exist to directly propagate the DEM uncertainty into the uncertainty of the inundation line (Hare and others, 2011). In addition to the uncertainty related to the grid cell elevation/depth, uncertainties in the tsunami source (earthquake and splay fault geometry) are the largest source of error in tsunami modeling efforts. The direction of the incoming waves, their amplitudes, and times of arrival are primarily determined by displacements of the ocean in the source area. Therefore, the inundation modeling results for local sources are especially sensitive to the fine structure of the tsunami source. The modeling process is highly sensitive to errors when the complexity of the source function is combined with its proximity to the coastal zone. The current practice is for communities to create an additional buffer around the modeled inundation line when developing community-specific tsunami evacuation plans.

SUMMARY

We present the results of numerical modeling of earthquake-generated tsunamis for the communities of Akhiok, Chiniak, Old Harbor, Ouzinkie, and Port Lions on Kodiak Island, Alaska. The earthquake scenarios considered in this report include a range of different earthquake ruptures in the Kodiak Island segment of the Alaska-Aleutian megathrust. Hypothetical scenario 3-AB2 (M_W 9.3 earthquake in the area of Kodiak Island with maximum slip distributed between the 10 and 20 km [6.2–12.4 mi] depth, with a splay fault dipping 60° in the Albatross Bank zone) results in the "worst case" tsunami-inundation hazards for Akhiok. Scenario 6-BS (M_W 9.3 earthquake in the area of Kodiak Island with maximum slip distributed between a depth of 0–10 km [0–6.2 mi], with a splay fault dipping 30° in the backstop splay zone) is the "worst case" scenario for the rest of the communities. The results show that the maximum predicted tsunami flow depth in the communities ranges from 10 to 25 m (32.8 to 82 ft), and the currents in community harbors can be as strong as 8.4 m/sec (16.3 knots). Dangerous wave activity is expected to last for at least 12 hours after the earthquake.

Each scenario considered is geologically reasonable and presents potential hazards to the communities. Map sheets 1–5, which show the potential extent of inundation and the tsunami flow depths, have been completed using the best information available and are believed to be accurate; however, their preparation required many assumptions. We considered several tsunami scenarios and have provided an estimate of maximum credible tsunami inundation. Actual conditions during a tsunami event may vary from those considered, so the accuracy of predictions based on the modeling presented in this report cannot be guaranteed. The limits of inundation shown should only be used as a guideline for emergency planning and response action. Actual inundated areas will depend on specifics of earthquake deformation, on-land construction, and tide level, and may differ from areas shown on the map. The information on this map is intended to assist state and local agencies in planning for emergency evacuation and tsunami response actions in the event of a major tsunamigenic earthquake. These results are not intended for land-use regulation or building-code development.

ACKNOWLEDGMENTS

This report was funded by the U.S. Department of Commerce/National Oceanic and Atmospheric Administration (NOAA) through National Tsunami Hazard Mitigation Program Award NA20NWS4670057 to the Alaska Division of Homeland Security and Emergency Management. This does not constitute an endorsement by NOAA. Numerical calculations for this work were supported by High Performance Computing (HPC) resources at the Research Computing Systems unit at the Geophysical Institute, University of Alaska Fairbanks. We thank our reviewers, Roland von Huene and Richard Thomson, for their insightful comments, suggestions and discussions, which helped improve the report.

REFERENCES

Briggs, R.W., Engelhart, S.E., Nelson, A.R., Dura, T., Kemp, A.C., Haeussler, P.J., Corbett, D.R., Angster, S.J., and Bradley, L.-A., 2014, Uplift and subsidence reveal a nonpersistent megathrust rupture boundary (Sitkinak Island, Alaska): Geophysical Research Letters, v. 41, no. 7, p. 2,289–2,296. doi.org/10.1002/2014GL059380

Butler, Rhett, 2012, Re-examination of the potential for great earthquakes along the Aleutian island arc with implication for tsunamis in Hawai'i: Seismological Research Letters, v. 83, no. 1, p. 30–39. doi.org/10.1785/gssrl.83.1.29

———2014, Great Aleutian tsunamis: Honolulu, HI, University of Hawai'i at Manoa, Hawai'i Institute of Geophysics & Planetology, Peer-Reviewed Report HIGP-2014-1, 170 p. www.higp.hawaii.edu/reports/2014

Butler, Rhett, Burney, David, and Walsh, David, 2014, Paleo-tsunami evidence on Kaua'i and numerical modeling of a great Aleutian tsunami: Geophysical Research Letters, v. 41, no. 19, p. 6,795–6,802. doi.org/10.1002/2014GL061232

Carignan, K.S., McLean, S.J., Eakins, B.W., Love, M.R., and Sutherland, M., 2013, Digital elevation models of Kodiak, Alaska—Procedures, data sources, and analysis: Boulder, CO, NOAA National Centers for Environmental Information (NCEI). www.ngdc.noaa.gov/dem/report/download/5055

Carver, G.A., and Plafker, George, 2008, Paleoseismicity and neotectonics of the Aleutian subduction zone—An overview, in Freymueller, J.T., Haeussler, P.J., Wesson, R.L, and Ekström, G., eds., Active tectonics and seismic potential of Alaska: American Geophysical Union Geophysical Monograph 179, p. 43–63.

Christensen, D.H., and Beck, S.L., 1994, The rupture process and tectonic implications of the Great 1964 Prince William Sound Earthquake: Pure and Applied Geophysics, v. 142, no. 1, p. 29–53. doi.org/10.1007/BF00875967

DeMets, Charles, Gordon, R.C., Argus, D.F., and Stein, Seth, 1990, Current plate motions: Geophysical Journal International, v. 101, no. 2, p. 425–478. doi.org/10.1111/j.1365-246X.1990.tb06579.x

Department of Commerce, Community, and Economic Development (DCCED)/Division of Community and Regional Affairs (DCRA), 2015, Community Database Online, accessed November 22, 2016. www.commerce.alaska.gov/dcra/DCRAExternal

Dunbar, P.K., and Weaver, C.S., 2008, U.S. states and territories national tsunami hazard assessment—Historical record and sources for waves: Technical Report, National Oceanic and Atmospheric Administration and U.S. Geological Survey, 59 p. nthmp.tsunami.gov/documents/Tsunami_Assessment_Final.pdf

Eberhart-Phillips, Donna, Christensen, D.H., Brocher, T.M., Hansen, Roger, Ruppert, N.A., Haeussler, P.J., and Abers, G.A., 2006, Imaging the transition from Aleutian subduction to Yakutat collision in central Alaska, with local earthquakes and active source data: Journal of Geophysical Research, v. 111, no. B11, p. 303. doi.org/10.1029/2005JB004240

Ferris, Aaron, Abers, G.A., Christensen, D.H., and Veenstra, Elizabeth, 2003, High resolution image of the subducted Pacific(?) plate beneath central Alaska, 50–150 km depth: Earth and Planetary Science Letters, v. 214, no. 3–4, p. 575–588. doi.org/10.1016/S0012-821X(03)00403-5

Fine, I.V., Thomson, R.E., Lupton, L.M., and Mundschutz, Stephen, 2018a, Numerical modeling of an Alaska 1964-type tsunami at the Canadian Coast Guard Base in Seal Cove, British Columbia: Canadian Technical Report of Hydrography and Ocean Sciences 321, Ocean Sciences Division, Fisheries and Oceans Canada, Institute of Ocean Sciences, Sidney, BC.

———2018b, Numerical modeling of an Alaska 1964-type tsunami at the Canadian Coast Guard Base in Victoria, British Columbia: Canadian Technical Report of Hydrography and Ocean Sciences 323, Ocean Sciences Division, Fisheries and Oceans Canada, Institute of Ocean Sciences, Sidney, BC.

Freund, L.B., and Barnett, D.M., 1976, A two-dimensional analysis of surface deformation due to dip-slip faulting: Bulletin of the Seismological Society of America, v. 66, no. 3, p. 667–675.

Freymueller, J.T., Woodard, Hillary, Cohen, S.C., Cross, Ryan, Elliott, Julie, Larsen, C.F., Hreinsdóttir, Sigrún, 2008, Active deformation processes in Alaska, based on 15 years of GPS measurements, *in* Freymueler, J.T., Haeussler, P.J., Wesson, R.L., and Ekström, Göran, eds., Active Tectonics and Seismic Potential of Alaska: Geophysical Monograph Series: Washington, D. C., American Geophysical Union, p. 1–42. https://doi.org/10.1029/179GM02

Geist, E.L., and Parsons, Tom, 2006, Probabilistic analysis of tsunami hazards: Natural Hazards, v. 37, no. 3, p. 277–314. doi.org/10.1007/s11069-005-4646-z

Gulick, S.P.S., Reece, R.S., Christenson, G.L., Van Avendonk, H.J.A., Worthington, L.L., and Pavlis, T.L., 2013, Seismic images of the Transition fault and the unstable Yakutat–Pacific–North American triple junction: Geology, v. 41, no. 5, p. 571–574. doi.org/10.1130/G33900.1

Hare, Rob, Eakins, B.W., and Amanate, Christopher, 2011, Modelling bathymetric uncertainty: International Hydrographic Review, p. 31–42. journals.lib.unb.ca/index.php/ihr/article/view/20888

Hayes, Gavin, 2018, Slab2-A Comprehensive Subduction Zone Geometry Model: U.S. Geological Survey data release. doi.org/10.5066/F7PV6JNV

Heidarzadeh, Mohammad, 2011, Major tsunami risk from splay faulting, *in* Mörner, N.A., ed., The tsunami threat: research and technology, p. 67–80. doi.org/10.5772/13375

Holdahl, S.R., and Sauber, Jeanne, 1994, Co-seismic slip in the 1964 Prince William Sound earthquake—A new geodetic inversion: Pure and Applied Geophysics, v. 142, no. 1, p. 55–82.

Ichinose, Gene, Somerville, Paul, Thio, H.K., Graves, Robert, and O'Connell, Dan, 2007, Rupture process of the 1964 Prince William Sound, Alaska, earthquake from the combined inversion of seismic, tsunami, and geodetic data: Journal of Geophysical Research, v. 112, no. B07, p. 306, 21 p. doi.org/10.1029/2006JB004728

Johnson, J.M., Satake, Kenji, Holdahl, S.R., and Sauber, Jeanne, 1996, The 1964 Prince William Sound earthquake—Joint inversion of tsunami waveforms and geodetic data: Journal of Geophysical Research, v. 101, no. B1, p. 523–532. doi.org/10.1029/95JB02806

Kachadoorian, Reuben, and Plafker, George, 1967, Effects of the earthquake of March 27, 1964, on communities of Kodiak Area: U.S. Geological Survey Professional Paper 542-F, 41 p. pubs.usgs.gov/pp/0542f/

Kanamori, Hiroo, 1970, The Alaska earthquake of 1964—Radiation of long-period surface waves and source mechanism: Journal of Geophysical Research, v. 75, no. 26, p. 5,029–5,040. doi.org/10.1029/JB075i026p05029

Kirby, Stephen, Scholl, David, von Huene, Roland, and Wells, Ray, 2013, Alaska earthquake source for the SAFRR tsunami scenario, chapter B, *in* Ross, S.L., and Jones, L.M., eds., The SAFRR (Science Application for Risk Reduction) Tsunami Scenario: U.S. Geological Survey Open-File Report 2013–1170, 40 p. pubs.usgs.gov/of/2013/1170/b/

Kulikov, E.A., Rabinovich, A.B., Fine, I.V., Bornhold, B.D., and Thomson, R.E., 1998, Tsunami generation by landslides at the Pacific coast of North America and the role of tides: Oceanology, v. 38, no. 3, p. 323–328.

Lander, J.F., 1996, Tsunamis affecting Alaska, 1737–1996: Boulder, CO, National Oceanic and Atmospheric Administration, National Geophysical Data Center (NGDC), Key to Geophysical Research Documentation, v. 31, 155 p. ftp.ngdc.noaa.gov/hazards/publications/Kgrd-31.pdf

Larsen, C.F., Motyka, R.J., Freymueller, J.T, Echelmeyer, K.A., and Ivins, E.R., 2004, Rapid uplift of southern Alaska caused by recent ice loss: Geophysical Journal International, v. 158, issue 3, p. 1,118–1,133. doi.org/10.1111/j.1365-246X.2004.02356.x

Lee, H.J., Ryan, Holly, Kayen, R.E., Haeussler, P.J., Dartnell, Peter, and Hampton, M.A., 2006, Varieties of submarine failure morphologies of seismically-induced landslides in Alaskan fjords: Norwegian Journal of Geology (Norsk Geologisk Tidsskrift), v. 86, no. 3, p. 221–230.

Li, Shaoyang, Moreno, Marcos, Rosenau, Matthias, Melnick, Daniel, and Oncken, Onno, 2014, Splay fault triggering by great subduction earthquakes inferred from finite element models: Geophysical Research Letters, v. 41, no. 2, p. 385–391. doi.org/10.1002/2013GL058598

Liberty, L.M., Brothers, D.S., and Haeussler, P. J., 2019, Tsunamigenic splay faults imply a long-term asperity in southern Prince William Sound, Alaska: Geophysical Research Letters, v. 46, p. 3,764–3,772. doi.org/10.1029/2018GL081528

Liberty, L.M., Finn, S.P., Haeussler, P.J., Pratt, T.L., and Peterson, Andrew, 2013, Megathrust splay faults at the focus of the Prince William Sound asperity, Alaska, Journal of Geophysical Research, 118, p. 1–14. doi.org/10.1002/jgrb.50372

Lim, E., Eakins, B.W., and Wigley, R., 2009, Southern Alaska coastal relief model—Procedures, data sources, and analysis: National Geophysical Data Center, NOAA, 25 p. www.ngdc.noaa.gov/mgg/coastal/s_alaska.html

Lotto, G.C., Jeppson, T.N., and Dunham, E.M., 2019, Fully Coupled Simulations of Megathrust Earthquakes and Tsunamis in the Japan Trench, Nankai Trough, and Cascadia Subduction Zone: Pure and Applied Geophysics, v. 176, p. 4,009–4,041. doi.org/10.1007/s00024-018-1990-y

National Centers for Environmental Information (NCEI/WDS), in progress, Global historical tsunami database at NCEI, 2100 BC to present (interactive map): National Centers for Environmental Information, NOAA. doi.org/10.7289/V5PN93H7

National Tsunami Hazard Mapping Program (NTHMP), 2010, Guidelines and best practices for tsunami inundation modeling for evacuation planning: National Oceanic and Atmospheric Administration (NOAA), NTHMP Mapping & Modeling Subcommittee.

———2012, Proceedings and results of the 2011 NTHMP Model Benchmarking Workshop: Boulder, CO, U.S. Department of Commerce/NOAA/NTHMP, NOAA Special Report, 436 p. nthmp.tsunami.gov

Nicolsky, D.J., Suleimani, E.N., Combellick, R.A., and Hansen, R.A., 2011, Tsunami inundation maps of Whittier and western Passage Canal, Alaska: Alaska Division of Geological & Geophysical Surveys Report of Investigation 2011-7, 65 p. doi.org/10.14509/23244

Nicolsky, D.J., Suleimani, E.N., Freymueller, J.T., and Koehler, R.D., 2015, Tsunami inundation maps of Fox Islands communities, including Dutch Harbor and Akutan, Alaska: Alaska Division of Geological & Geophysical Surveys Report of Investigation 2015-5, 67 p., 2 sheets, scale 1:12,500. doi.org/10.14509/29414

Nicolsky, D.J., Suleimani, E.N., Haeussler, P.J., Ryan, H.F., Koehler, R.D., Combellick, R.A., and Hansen, R.A., 2013, Tsunami inundation maps of Port Valdez, Alaska: Alaska Division of Geological & Geophysical Surveys Report of Investigation 2013-1, 77 p., 1 sheet, scale 1:12,500. doi.org/10.14509/25055

Nicolsky, D.J., Suleimani, E.N., and Hansen, R.A., 2011, Validation and verification of a numerical model for tsunami propagation and runup: Pure and Applied Geophysics, v. 168, no. 6, p. 1,199–1,222. doi.org/10.1007/s00024-010-0231-9

Nicolsky, D.J., Suleimani, E.N., and Koehler, R.D., 2014, Tsunami inundation maps of Cordova and Tatitlek, Alaska: Alaska Division of Geological & Geophysical Surveys Report of Investigation 2014-1, 49 p. doi.org/10.14509/27241

———2016, Tsunami inundation maps for the communities of Chignik and Chignik Lagoon, Alaska: Alaska Division of Geological & Geophysical Surveys Report of Investigation 2016-8, 48 p., 2 sheets, scale 1:12,500. doi.org/10.14509/29675

Nicolsky, D.J., Suleimani, E.N., Koehler, R.D., and Salisbury, J.B., 2017, Tsunami inundation maps for Juneau, Alaska: Alaska Division of Geological & Geophysical Surveys Report of Investigation 2017-9, 66 p., 5 sheets. doi.org/10.14509/29741

Nishenko, S.P., 1991, Circum-Pacific seismic potential, 1989–1999: Pure and Applied Geophysics, v. 135, no. 2, p. 169–259. doi.org/10.1007/BF00880240

Nishenko, S.P., and Jacob, K.H., 1990, Seismic potential of the Queen Charlotte–Alaska–Aleutian seismic zone: Journal of Geophysical Research, v. 95, no. B3, p. 2,511–2,532. doi.org/10.1029/JB095iB03p02511

Okada, Yoshimitsu, 1985, Surface deformation due to shear and tensile faults in a half-space: Bulletin of the Seismological Society of America, v. 75, no. 4, p. 1,135–1,154.

Oppenheimer, Michael, Glavovic, B.C., Hinkel, Jochen, van de Wal, Roderik, Magnan, A.K., Abd-Elgawad, Amro, Cai, Rongshuo, Cifuentes-Jara, Miguel, DeConto, R.M., Ghosh, Tuhin, Hay, John, Isla, Federico, Marzeion, Ben, Meyssignac, Benoit, Sebesvari, Zita, 2019, Sea level rise implications for low-lying islands, coasts and communities, *in* Pörtner, H.-O., Roberts, D.C., Masson-Delmotte, V., Zhai, P., Tignor, M., Poloczanska, E., Mintenbeck, K., Alegría, A., Nicolai, M., Okem, A., Petzoid, J., Rama, B., Weyer, N.M., eds., IPCC Special Report on the ocean and cryosphere in a changing climate. www.ipcc.ch/site/assets/uploads/sites/3/2019/11/08_SROCC_Ch04_FINAL.pdf

Plafker, George, 1965, Tectonic deformation associated with the 1964 Alaska earthquake: Science, v. 148, no. 3,678 p. 1,675–1,687.

———1967, Surface faults on Montague Island associated with the 1964 Alaska earthquake: U.S. Geological Survey Professional Paper 543-G, p. G1–G42. pubs.usgs.gov/pp/0543g/

———1969, Tectonics: U.S. Geological Survey Professional Paper 543-I, p. G1–G74.

Plafker, George, and Kachadoorian, Reuben, 1966, Geologic effects of the March 1964 earthquake and associated seismic sea waves on Kodiak and nearby islands, Alaska: U.S. Geological Survey Professional Paper 543–D, 46 p. pubs.usgs.gov/pp/0543d/

Plafker, George, Kachadoorian, Reuben, Eckel, E.B., and Mayo, L.R., 1969, Effects of the earthquake of March 27, 1964, on various communities: U.S. Geological Survey Professional Paper 542-G, 50 p. pubs.usgs.gov/pp/0542g/

Rabinovich, A.B., Thomson, R.E., Krassovski, M.V., Stephenson, F.E., and Sinnott, D.C., 2019, Five Great Tsunamis of the 20th Century as Recorded on the Coast of British Columbia: Pure and Applied Geophysics, v. 176, p. 2,887–2,924. doi.org/10.1007/s00024-019-02133-3

Ryan, Holly, von Huene, Roland, Scholl, Dave, and Kirby, Steve, 2012, Tsunami hazards to U.S. coasts from giant earthquakes in Alaska: Eos AGU, v. 93, no. 19, 185 p.

Shennan, Ian, Barlow, Natasha, Carver, Gary, Davies, Frank, Garrett, Ed, and Hocking, Emma, 2014, Great tsunamigenic earthquakes during the past 1,000 yr on the Alaska megathrust: Geology, v. 42, no. 8, p. 687–690. doi.org/10.1130/G35797.1

Shennan, Ian, Bruhn, Ronald, Barlow, Natasha, Good, Kelly, and Hocking, Emma, 2014, Late Holocene great earthquakes in the eastern part of the Aleutian megathrust: Quaternary Science Reviews, v. 84, p. 86–97. doi.org/10.1016/j.quascirev.2013.11.010

Shirzaei, Manoochehr, Freymueller, Jeffrey, Törnqvist, T.E., Galloway, D.L., Dura, Tina, and Minderhoud, P.S.J., 2021, Measuring, modelling and projecting coastal land subsidence: Nature Reviews Earth & Environment, no. 2, p. 40–58. doi.org/10.1038/s43017-020-00115-x

Soloviev, S.L., 1968, The Sanak Kodiak Island tsunami of 1788 [in Russian]: Moscow, Nauka, The Tsunami Problem, p. 232–237. [English translation in Science of Tsunami Hazards, v. 8, no. 1, p. 34–38, 1990.] library.lanl.gov/tsunami/00394733.pdf

Suito, Hisashi, and Freymueller, J.T., 2009, A viscoelastic and afterslip postseismic deformation model for the 1964 Alaska earthquake: Journal of Geophysical Research, v. 114, no. B11, p. 404–426. doi.org/10.1029/ 2008JB005954

Suleimani, E.N., Combellick, R.A., Marriott, D., Hansen, R.A., Venturato, A.J., and Newman, J.C., 2005, Tsunami hazard maps of the Homer and Seldovia areas, Alaska: Alaska Division of Geological & Geophysical Surveys Report of Investigation 2005-2, 28 p., 2 sheets, scale 1:12,500. doi.org/10.14509/14474

Suleimani, E.N, and Freymueller, J.T., 2020, Near-field modeling of the 1964 Alaska tsunami: The role of splay faults and horizontal displacements: Journal of Geophysical Research: Solid Earth, v. 125. doi.org/10.1029/2020JB019620

Suleimani, E.N., Nicolsky, D.J., and Koehler, R.D., 2013, Tsunami inundation maps of Sitka, Alaska: Alaska Division of Geological & Geophysical Surveys Report of Investigation 2013-3, 76 p., 1 sheet, scale 1:250,000. doi.org/10.14509/26671

———2015, Tsunami inundation maps of Elfin Cove, Gustavus, and Hoonah, Alaska: Alaska Division of Geological & Geophysical Surveys Report of Investigation 2015-1, 79 p. doi.org/10.14509/29404

———2017, Updated tsunami inundation maps of the Kodiak area, Alaska: Alaska Division of Geological & Geophysical Surveys Report of Investigation 2017-8, 38 p., 10 sheets. doi.org/10.14509/29740

Suleimani, E.N., Nicolsky, D.J., Koehler, R.D., Freymueller, J.T., and Macpherson, A.E., 2016, Tsunami inundation maps for King Cove and Cold Bay communities, Alaska: Alaska Division of Geological & Geophysical Surveys Report of Investigation 2016-1, 73 p., 2 sheets, scale 1:12,500. doi.org/10.14509/29565

Suleimani, E.N., Nicolsky, D.J., West, D.A., Combellick, R.A., and Hansen, R.A., 2010, Tsunami inundation maps of Seward and northern Resurrection Bay, Alaska: Alaska Division of Geological & Geophysical Surveys Report of Investigation 2010-1, 47 p., 3 sheets, scale 1:12,500. doi.org/10.14509/21001

Synolakis, C.E., Bernard, E.N., Titov, V.V., Kânoğlu, U., and González, F.I., 2007, Standards, criteria, and procedures for NOAA evaluation of tsunami numerical models: National Oceanic and Atmospheric Administration (NOAA)/Pacific Marine Environmental Laboratory (PMEL) Technical Memorandum OAR PMEL-135, 55 p. www.pmel.noaa.gov/pubs/PDF/syno3053/syno3053.pdf

von Huene, Roland, Miller, J.J., and Krabbenhoeft, Anne, 2021, The Alaska convergent margin backstop splay fault zone, a potential large tsunami generator between the frontal prism and continental framework: Geochemistry, Geophysics, Geosystems, v. 22, no. 1. doi.org/10.1029/2019GC008901

Wang, Kelin, Sun, Tianhaozhe, Brown, Lonn, Hino, Ryota,Tomita, Fumiaki, Kido, Moyoyuki, Iinuma, Takeshi, Kodaira, Shuichi, and Fujiwara,Toshiya, 2018, Learning from crustal deformation associated with the M9 2011 Tohoku-oki earthquake: Geosphere, v. 14, no. 2, p. 552–571. doi.org/10.1130/GES01531.1

Wang, Kelin, and Tréhu, A.M., 2016, Invited review paper: Some outstanding issues in the study of great megathrust earthquakes—The Cascadia example: Journal of Geodynamics, v. 98, p. 1–18.

Wang, Kelin, Wells, R.E., Mazzotti, Stephane, Hyndman, R.D., and Sagiya, Takeshi, 2003, A revised dislocation model of interseismic deformation of the Cascadia subduction zone: Journal of Geophysical Research, v. 108, no. B1, p. 2,026–2,038. doi.org/10.1029/2001JB001227

Wendt, James, Oglesby, D.D., and Geist, E.L., 2009, Tsunamis and splay fault dynamics: Geophysical Research Letters, v. 36, no. 15. doi.org/10.1029/2009GL038295

Worthington, L.L., Gulick, S.P.S., and Pavlis, T.L., 2010, Coupled stratigraphic and structural evolution of a glaciated orogenic wedge, offshore St. Elias orogen, Alaska: Tectonics, v. 29, no. 6, TC6013. doi.org/10.1029/2010TC002723

Worthington, L.L., Van Avendonk, H.J.A., Gulick, S.P.S., Christeson, G.L., and Pavlis, T.L., 2012, Crustal structure of the Yakutat terrane and the evolution of subduction and collision in southern Alaska: Journal of Geophysical Research, v. 117, no. B1, B01102. doi.org/10.1029/2011JB008493

Zweck, Chris, Freymueller, J.T., Cohen, S.C., 2002, Three-dimensional elastic dislocation modeling of the postseismic response to the 1964 Alaska earthquake: Journal of Geophysical Research, v. 107, no. B4. doi.org/10.1029/2001JB000409

Table A1. Longitude and latitude locations of time series points in Akhiok. The pre-earthquake onshore (S) and offshore (O) locations are specified in the third column. The minimum elevation (sixth column) above the post-earthquake MHHW datum is provided for onshore locations, while the minimum post-earthquake depth is provided for offshore locations. The horizontal datum used is World Geodetic System of 1984.

#	Label	S/O	Longitude (°W)	Latitude (°N)	Minimum elevation/ depth, m (ft)
1	Alitak Bay	O	-154.109722	56.896667	74.7 (245.1)
2	Moser Bay	O	-154.126667	56.973333	22.7 (74.5)
3	Akhiok Bay	O	-154.156944	56.938056	3.5 (11.5)
4	Pryor Point	O	-154.206389	56.931667	5.9 (19.4)
5	Lagoon	O	-154.173611	56.943056	1.8 (5.9)
6	Airport Way	S	-154.17500	56.944167	-1.5 (-4.9)
7	Post Office	S	-154.168056	56.944722	-0.3 (-1.0)
8	Third Street	S	-154.170278	56.945556	-3.1 (-10.2)
9	Airport East	S	-154.175833	56.940556	1.9 (6.2)
10	Airport West	S	-154.189722	56.936389	3.6 (11.8)

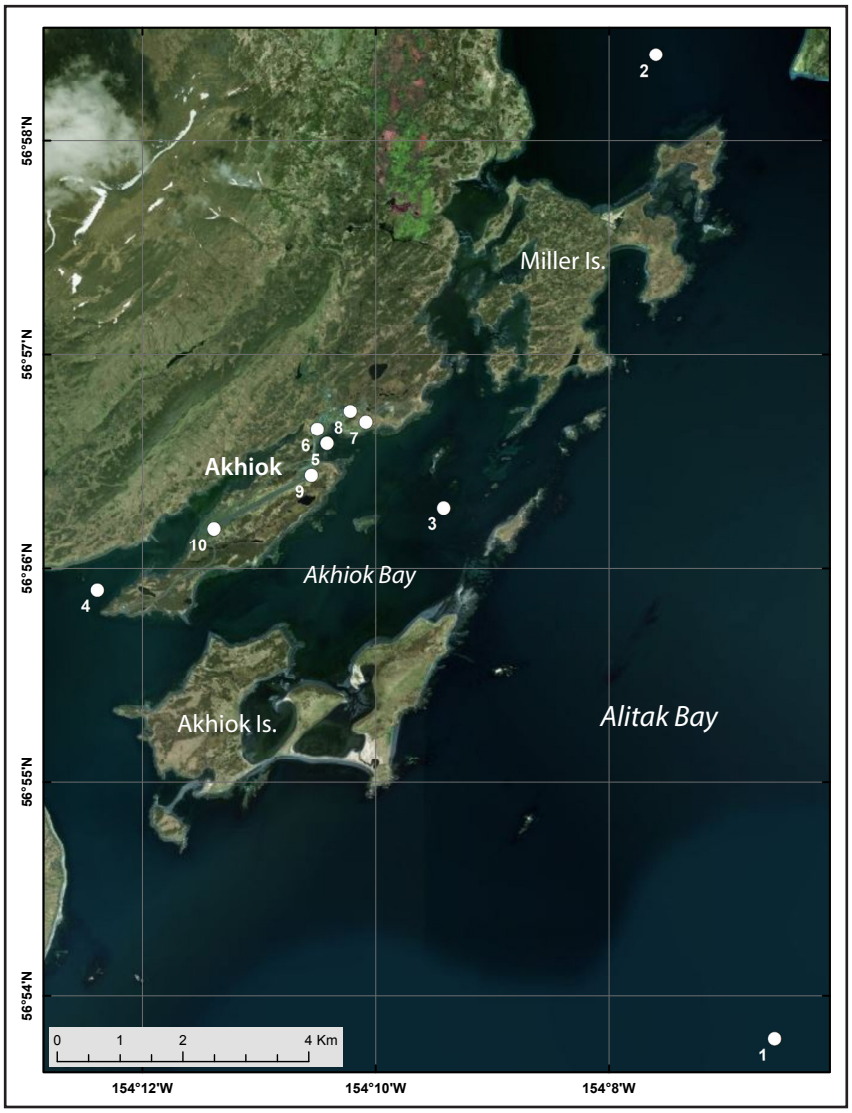

Figure A1. Locations of time series points in and around Akhiok. The longitude and latitude locations of the time series points are listed in table A1.

Table A2. Maximum water levels for all tsunami scenarios at time series points near Akhiok, which are listed in table A1. The maximum water depth above ground is provided for onshore (S) locations, whereas the maximum water level above the pre-earthquake MHHW is provided for offshore (O) locations.

#	Label	Maximum water depth above ground/sea level (meters)																							
		Scenario																							
		1	2	3	4	5	6	7	8	9	10	11	12	13	14	15	16	17	18	19	20	21	22	23	24
1	Alitak Bay	7.6	12.1	12.5	10.2	13.7	14.6	14.8	13.9	8.2	12.3	10.6	9.3	10.9	11.6	12.1	11.7	5.2	4.8	2.9	3.4	3.1	3.1	5.0	0.7
2	Moser Bay	7.8	13.6	13.6	12.8	15.9	16.3	16.4	15.1	8.7	13.4	11.3	10.1	11.2	12.1	11.8	11.7	5.5	4.7	4.2	4.2	3.8	3.6	4.8	0.9
3	Akhiok Bay	8.2	13.0	13.4	11.9	14.9	15.7	15.7	14.9	9.1	13.0	11.6	10.2	11.0	11.2	12.2	12.4	5.9	6.0	4.2	4.3	4.0	4.0	6.4	0.8
4	Pryor Point	9.1	13.1	13.6	11.9	15.2	15.9	15.6	15.1	10.0	13.3	12.1	10.4	11.7	12	12.9	12.5	7.2	7.8	4.3	4.6	5.2	5.8	7.9	1.2
5	Lagoon	8.3	13.3	13.7	12.4	15.2	15.9	16.0	15.1	9.2	13.2	12.0	10.5	11.6	11.5	12.3	12.5	6.6	6.4	4.9	4.8	4.6	4.5	6.8	1.1
6	Airport Way	1.6	6.6	7.1	5.8	8.6	9.3	9.3	8.5	2.5	6.5	5.4	3.9	5.0	4.9	5.7	5.9	0.2	0.2	0	0	0	0	0.2	0
7	Post Office	0.5	5.4	5.8	4.6	7.3	8.0	8.1	7.2	1.4	5.3	4.0	2.5	3.6	3.6	4.4	4.6	0	0	0	0	0	0	0	0
8	Third Street	3.2	8.3	8.7	7.5	10.2	10.9	11	10.1	4.1	8.2	6.9	5.4	6.5	6.5	7.3	7.5	1.6	1.2	0.2	0	0	0	1.7	0
9	Airport East	0	3.0	3.6	2.2	5.0	5.7	5.6	5.0	0	3.0	2.0	0.4	1.6	1.3	2.2	2.5	0	0	0	0	0	0	0	0
10	Airport West	0	1.1	1.8	0.3	3.2	4	3.8	3.2	0	1.3	0.2	0	0	0.4	1.0	0.9	0	0	0	0	0	0	0	0

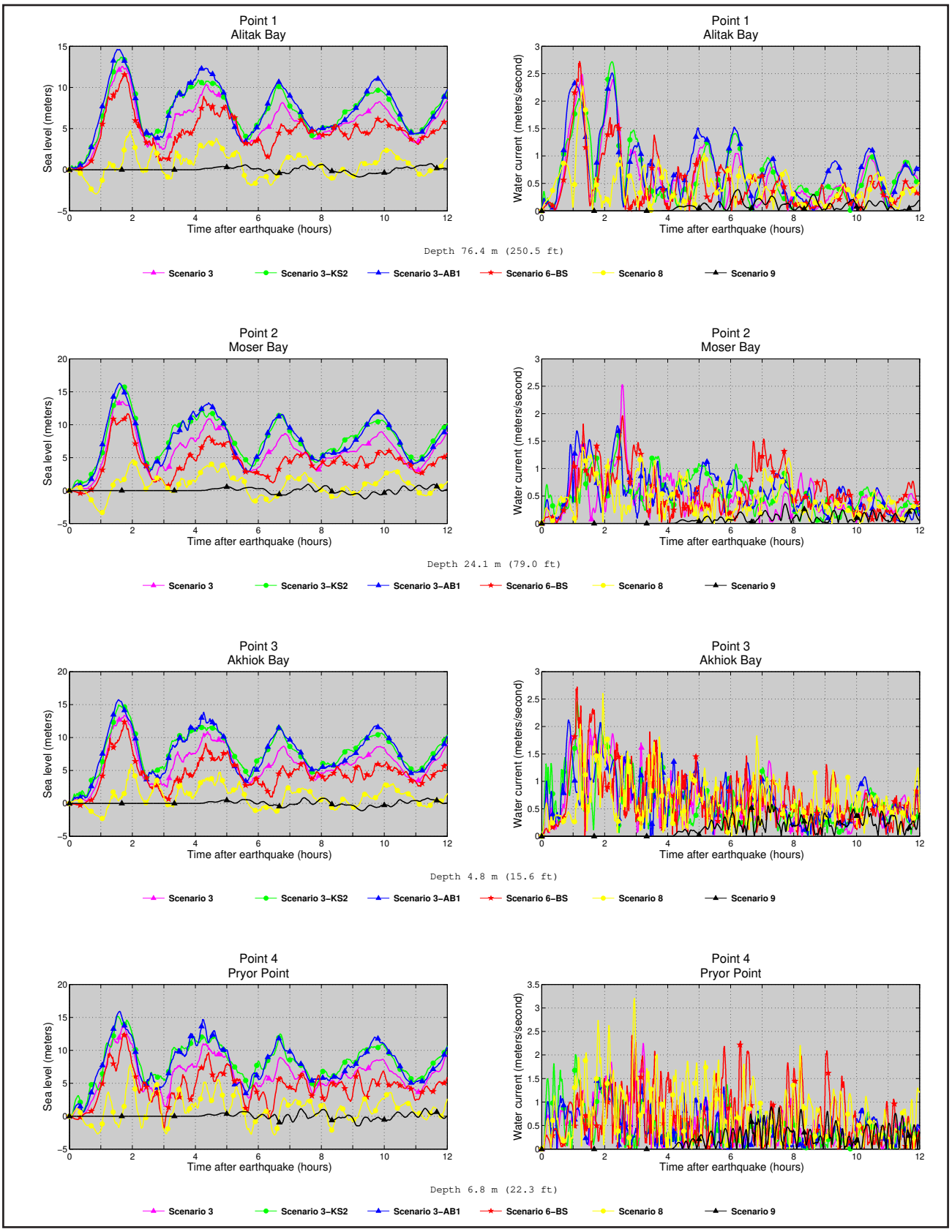

Figure A2. Time series of water level (left column) and velocity (right column) for selected scenarios at locations shown in figure A1. Elevations of onshore locations and ocean depth at offshore locations are given based on the pre-earthquake MHHW datum.

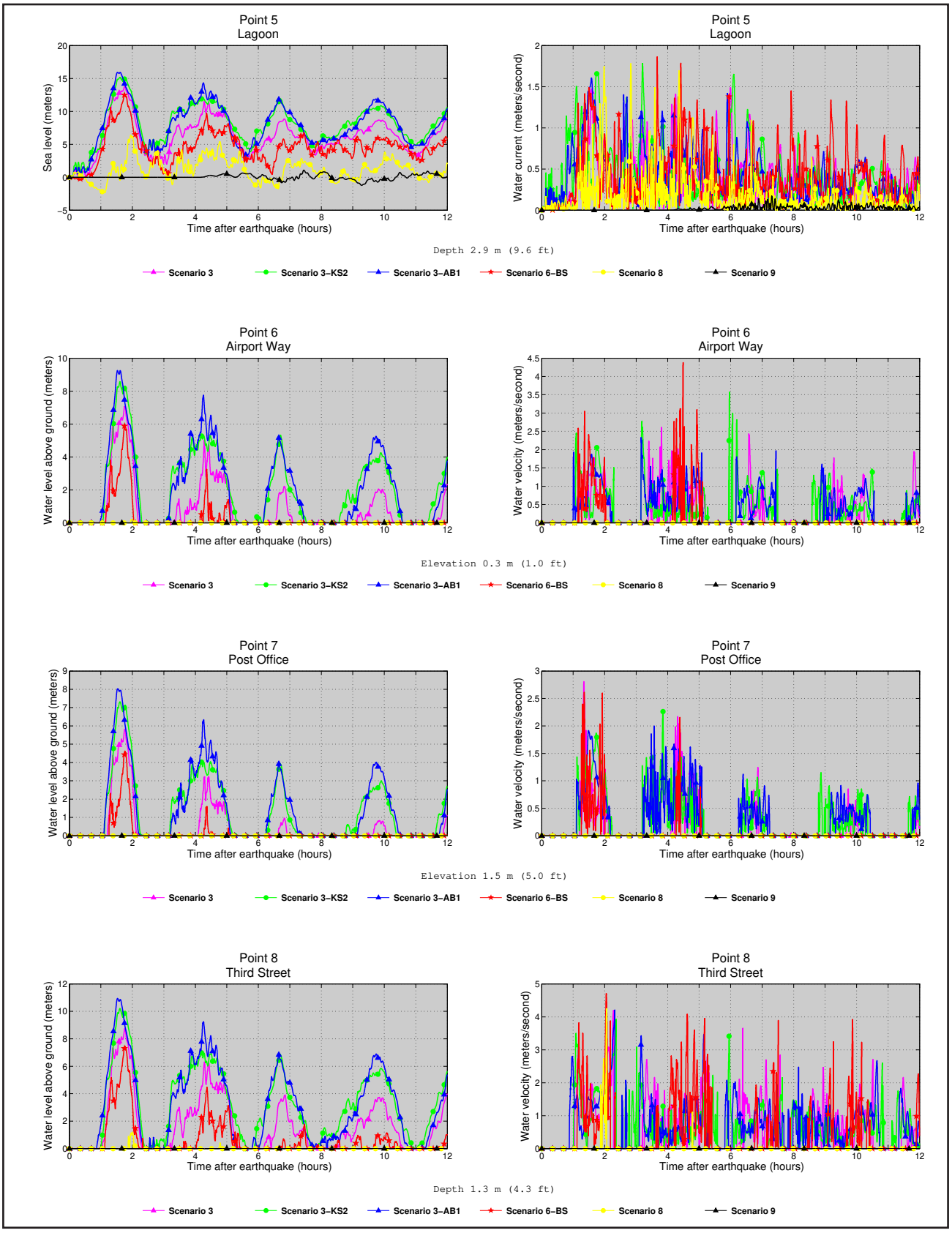

Figure A2, continued. Time series of water level (left column) and velocity (right column) for selected scenarios at locations shown in figure A1. Elevations of onshore locations and ocean depth at offshore locations are given based on the pre-earthquake MHHW datum.

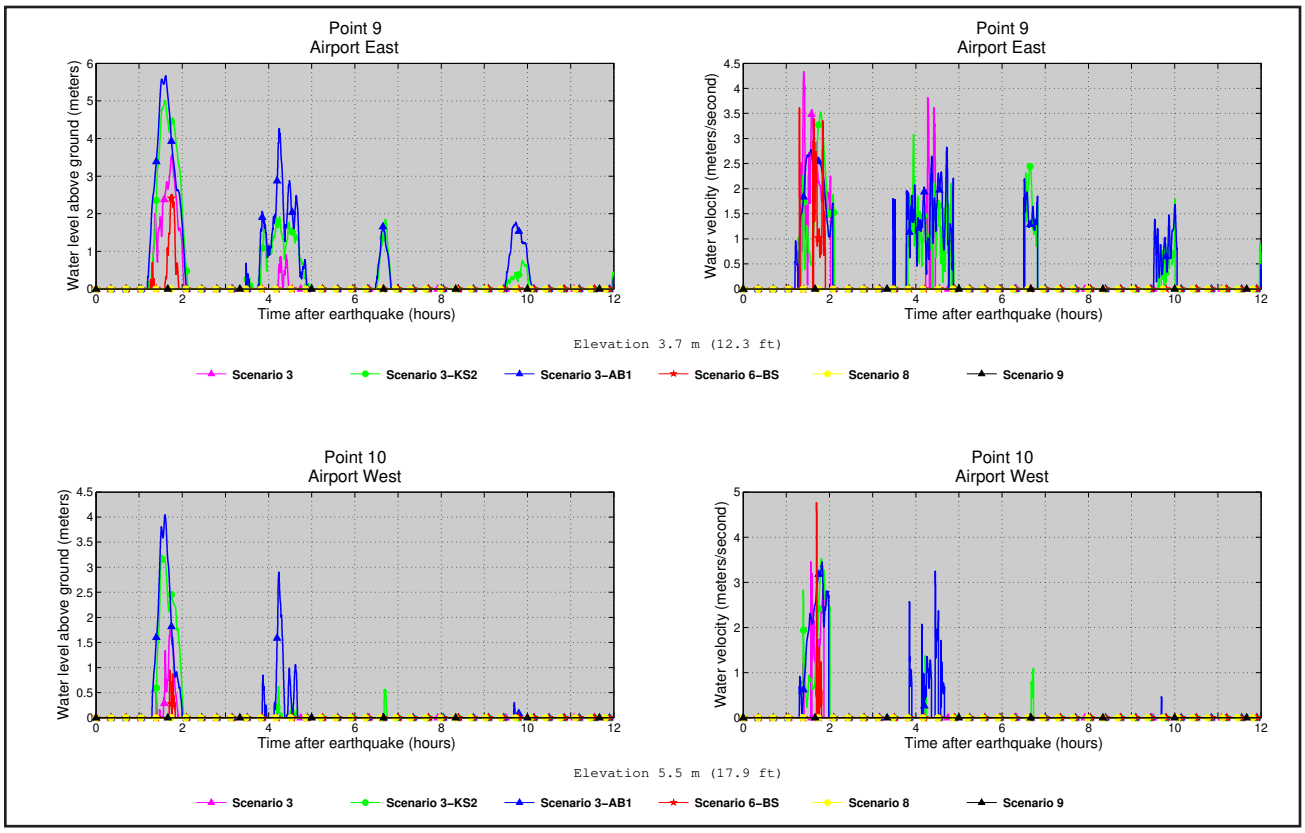

Figure A2, continued. Time series of water level (left column) and velocity (right column) for selected scenarios at locations shown in figure A1. Elevations of onshore locations and ocean depth at offshore locations are given based on the pre-earthquake MHHW datum.

Table A3. Maximum water velocities for all tsunami scenarios at time series points near Akhiok, which are listed in Table A1.

#	Label	Maximum water velocity (meters/second)																							
		Scenario																							
		1	2	3	4	5	6	7	8	9	10	11	12	13	14	15	16	17	18	19	20	21	22	23	24
1	Alitak Bay	1.8	2.5	2.5	2.4	2.7	2.5	2.5	2.7	1.9	2.4	2.6	1.7	2	2.1	2.4	2.7	1.5	2.3	1	1.1	1.2	1.3	2.3	0.4
2	Moser Bay	1.7	1.7	2.5	1.6	1.6	1.8	1.9	2.8	1.5	2.0	1.8	1.1	1.5	1.8	1.9	2.0	1.4	1.4	0.8	1.1	1.3	1.5	1.6	0.4
3	Akhiok Bay	2.3	2.0	2.0	1.8	2.4	2.1	2.2	3.0	2.5	1.9	3.3	2.3	2.7	2.4	2.5	2.7	1.9	2.6	1.3	1.5	1.7	2.0	2.4	0.6
4	Pryor Point	2.1	1.6	2.2	2.6	2.0	1.6	1.5	2.8	2.3	1.9	2.5	1.8	2.4	2.0	2.4	2.4	2.1	3.2	2.5	3.1	2.8	2.8	3.4	0.9
5	Lagoon	1.7	1.5	1.5	1.5	1.8	1.6	1.8	1.8	1.6	1.4	2.1	1.8	2.2	2.3	2.3	1.9	1.6	1.8	1.3	1.3	1.8	2.1	1.7	0.2
6	Airport Way	3.3	2.8	2.6	2.4	3.6	2.3	2.3	4.4	4.7	2.4	4.2	3.0	3.5	4.0	3.3	4.4	0	0	0	0	0	0	0	0
7	Post Office	0.6	1.9	2.8	2.0	2.3	2.0	2.7	3.0	1.4	2.4	2.1	2.1	2.5	2.9	3.0	2.6	0	0	0	0	0	0	0	0
8	Third Street	4.2	4.2	4.2	4.2	3.9	4.2	4.2	4.0	4.2	4.1	4.5	4.7	4.7	4.1	4.2	4.7	4.2	4.2	0	0	0	0	4.2	0
9	Airport East	0	3.9	4.3	2.5	3.5	2.8	3.5	4.8	0	3.9	3.3	2.1	2.7	3.8	3.8	3.6	0	0	0	0	0	0	0	0
10	Airport West	0	2.4	3.4	2.6	3.5	3.4	3.6	4.1	0	3	0	0	0	1.6	2.7	4.8	0	0	0	0	0	0	0	0

Table B1. Longitude and latitude locations of time series points in Chiniak. The pre-earthquake onshore (S) and offshore (O) locations are specified in the third column. The minimum elevation (sixth column) above the post-earthquake MHHW datum is provided for onshore locations, while the minimum post-earthquake depth is provided for offshore locations. The horizontal datum used is World Geodetic System of 1984.

#	Label	S/O	Longitude (°W)	Latitude (°N)	Minimum elevation/ depth, m (ft)
1	Post Office	S	-152.364444	57.616944	19.6 (64.3)
2	Kalsin Bay	O	-152.355833	57.623333	8.3 (27.2)
3	Isthmus Bay	O	-152.313611	57.623333	1.5 (4.9)
4	Pony Point	O	-152.249167	57.620556	2.3 (8.2)
5	Ninth Wave	S	-152.335278	57.623333	13.2 (43.3)
6	Distant Loon	S	-152.307778	57.617778	16.6 (54.5)
7	Midway Point	S	-152.271389	57.625278	2.8 (9.2)
8	Sawmill Lake	S	-152.249722	57.615833	-2.7 (-8.9)
9	Clay Creek Pottery	S	-152.22500	57.616389	31.2 (102.4)
10	Chiniak Lake	S	-152.195278	57.622778	5.1 (16.7)

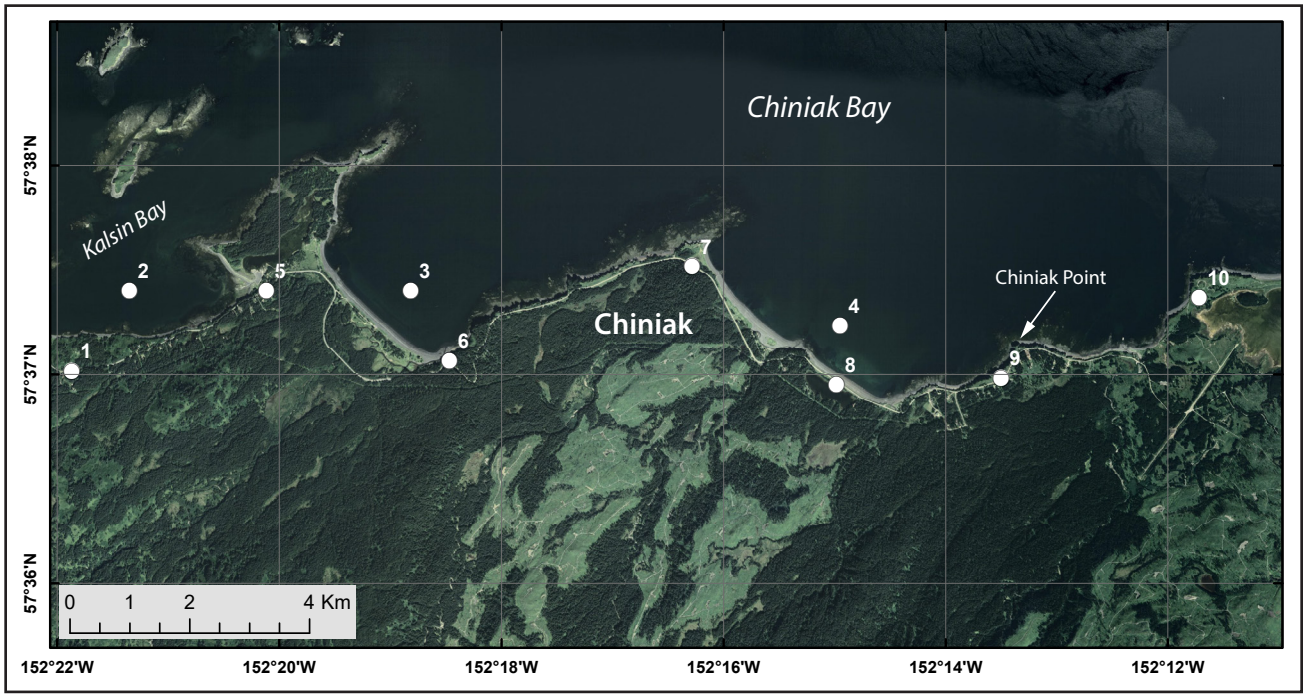

Figure B1. Locations of time series points in and around Chiniak. The longitude and latitude locations of the time series points are listed in table B1.

Table B2. Maximum water levels for all tsunami scenarios at time series points near Chiniak, which are listed in table B1. The maximum water depth above ground is provided for onshore (S) locations, whereas the maximum water level above the pre-earthquake MHHW is provided for offshore (O) locations.

#	Label	Maximum water depth above ground/sea level (meters)																						
		Scenario																						
		1	**2**	**3**	**4**	**5**	**6**	**7**	**8**	**9**	**10**	**11**	**12**	**13**	**14**	**15**	**16**	**17**	**18**	**19**	**20**	**21**	**22**	**23**	**24**
1	Post Office	0	0	0	0	0	0	0	0	0	0	0	0	0	0	0	0	0	0	0	0	0	0	0	0
2	Kalsin Bay	9.2	14.4	17.0	4.6	8.8	16.4	21.8	20.7	10.6	17.8	13.9	7.2	11.2	13.4	17.6	22.1	7.0	12.4	0	4.0	8.7	8.6	10.5	1.4
3	Isthmus Bay	15.9	16.6	20.8	7.9	9.9	19.2	20.3	22.8	16.5	19.2	18.6	9.9	13.9	18.7	20.6	24.2	13.6	15.6	0.6	5.0	13.3	13.1	14.7	2.1
4	Pony Point	18.9	15.4	20.9	7.7	9.7	18.2	19.7	21.7	19.7	18.1	21.6	9.2	10.6	19.6	21.7	22.5	13.0	17.6	2.7	5.1	12.3	12.5	16.7	1.5
5	Ninth Wave	0	0	0	0	0	0	0	0.5	0	0	0	0	0	0	0	0.6	0	0	0	0	0	0	0	0
6	Distant Loon	0	0	0.2	0	0	0	0.1	1.5	0	0	0	0	0	0.4	0	3.7	0	0	0	0	0	0	0	0
7	Midway Point	10.5	7.3	12.0	2.8	2.3	9.3	9.6	13.0	12.0	9.6	14.0	4.0	4.4	11.1	10.8	15.3	4.2	13.9	0	0	5.1	4.7	7.9	0
8	Sawmill Lake	18.7	14.8	20	4.9	7.0	16.5	18.5	20.6	19.7	17.5	21.8	7.4	8.9	19.5	20.5	24.1	11.9	16.5	0.9	2.0	10.6	10.6	16.0	0
9	Clay Creek Pottery	0	0	0	0	0	0	0	0	0	0	0	0	0	0	0	0	0	0	0	0	0	0	0	0
10	Chiniak Lake	1.9	0.7	5.8	0	0	4.3	4.8	4.2	3.1	3.0	6.2	0	0	3.9	5.7	6.1	0	0.5	0	0	0	0	0.8	0

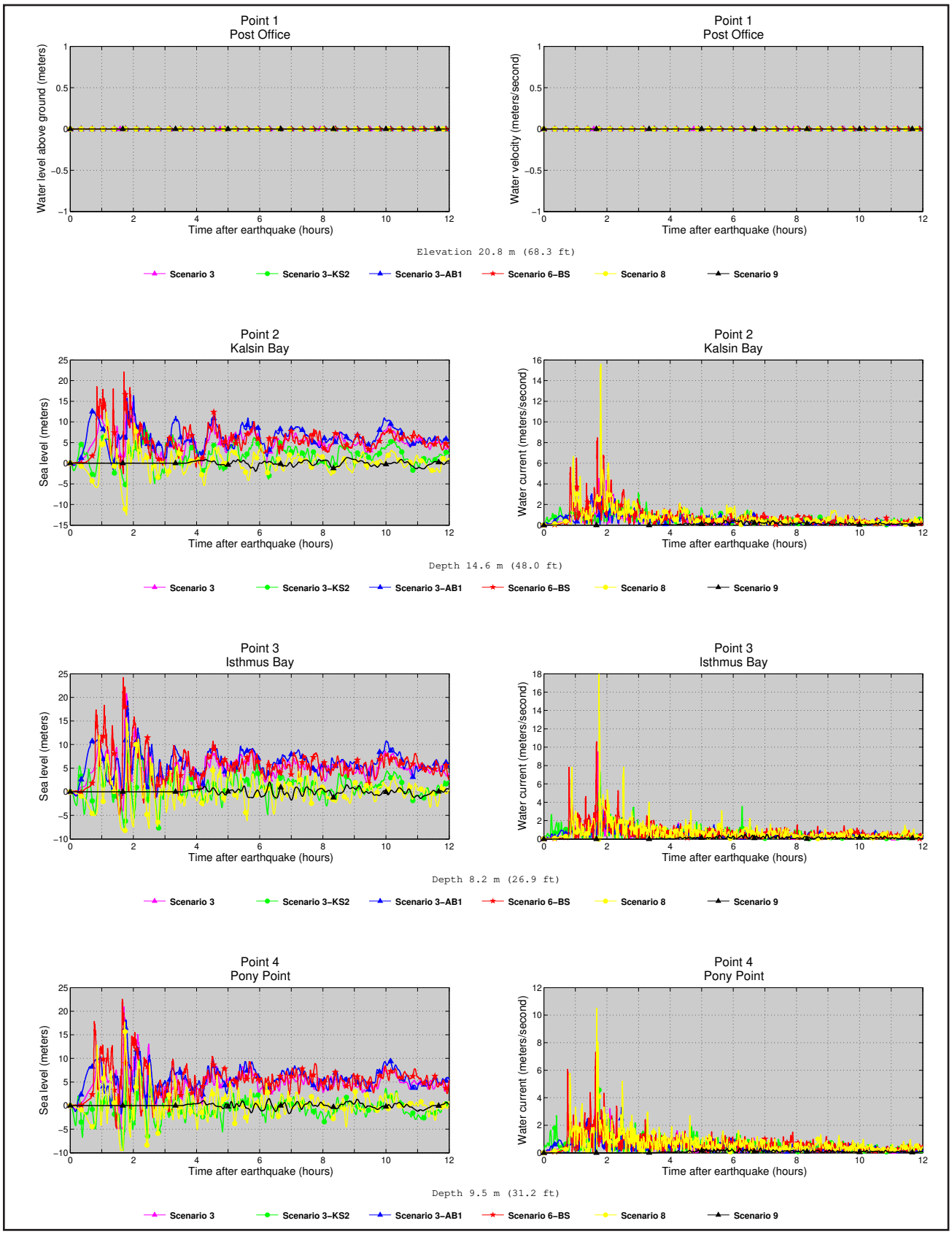

Figure B2. Time series of water level (left column) and velocity (right column) for selected scenarios at locations shown in figure B1. Elevations of onshore locations and ocean depth at offshore locations are given based on the pre-earthquake MHHW datum.

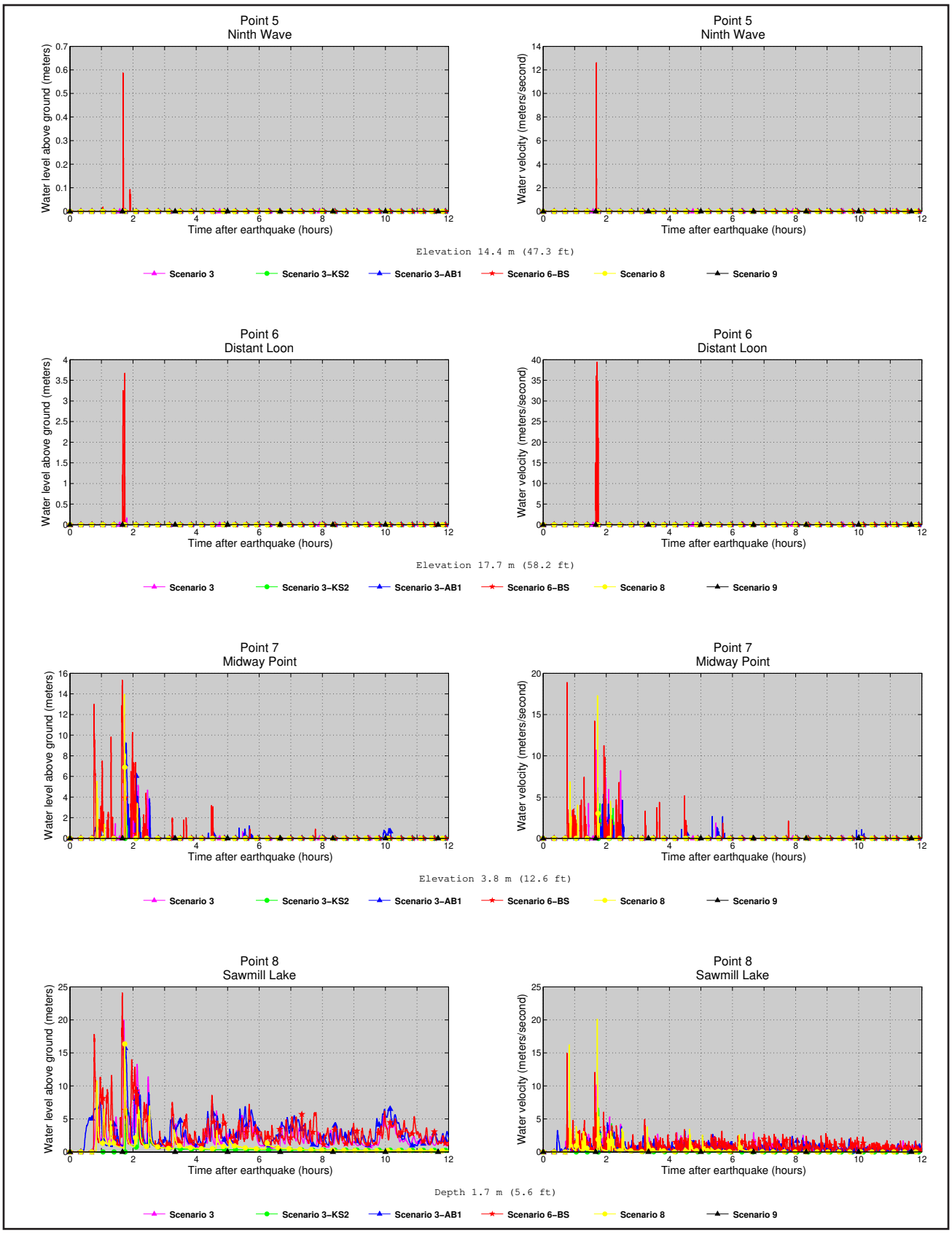

Figure B2, continued. Time series of water level (left column) and velocity (right column) for selected scenarios at locations shown in figure B1. Elevations of onshore locations and ocean depth at offshore locations are given based on the pre-earthquake MHHW datum.

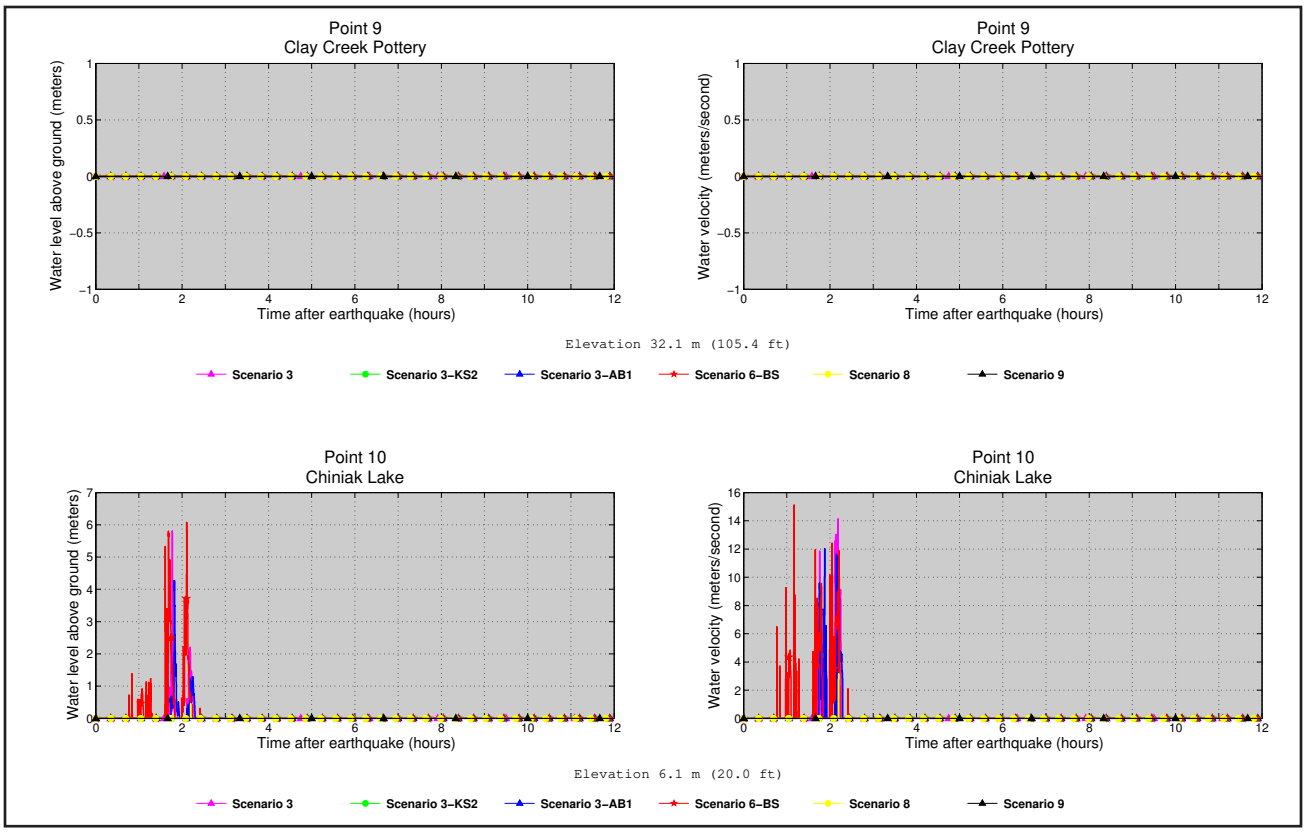

Figure B2, continued. Time series of water level (left column) and velocity (right column) for selected scenarios at locations shown in figure B1. Elevations of onshore locations and ocean depth at offshore locations are given based on the pre-earthquake MHHW datum.

Table B3. Maximum water velocities for all tsunami scenarios at time series points near Chiniak, which are listed in table B1.

#	Label	Maximum water velocity (meters/second)																							
		Scenario																							
		1	2	3	4	5	6	7	8	9	10	11	12	13	14	15	16	17	18	19	20	21	22	23	24
1	Post Office	0	0	0	0	0	0	0	0	0	0	0	0	0	0	0	0	0	0	0	0	0	0	0	0
2	Kalsin Bay	5.8	4.3	8.2	10.7	3.5	4.2	5.5	9.1	6.0	5.0	7.7	12.5	5.8	6.2	6.9	8.5	18.1	15.6	9.0	10.3	7.2	9.4	13.7	0.5
3	Isthmus Bay	11.9	5.1	9.5	16.6	7.3	6.1	7.0	9.4	10.9	7.1	13.1	14.8	8.5	7.5	10.3	10.6	17.8	17.9	14.1	15.1	11.2	19.4	16.8	0.5
4	Pony Point	14.3	3.6	5.4	15.2	8.2	3.3	3.6	6.2	7.2	4.6	12.7	16.2	6.6	5.6	5.4	7.3	7.6	10.5	10.7	15.2	13.5	16.6	13.8	0.3
5	Ninth Wave	0	0	0	0	0	0	0	81.8	0	0	0	0	0	0	0	12.6	0	0	0	0	0	0	0	0
6	Distant Loon	0	0	0	0	0	0	0	28.3	0	0	0	0	0	5.5	0	39.4	0	0	0	0	0	0	0	0
7	Midway Point	8.3	7.3	10.7	4.3	4.2	6.1	5.3	14.2	7.9	11.1	10.5	8.2	10.2	7.9	25.2	18.9	5.9	17.3	0	0	13.1	7.7	12.6	0
8	Sawmill Lake	8.6	6.0	10.1	8.4	6.6	5.5	4.7	8.7	9.7	9.1	13.1	5.8	4.6	6.5	6.8	14.9	14.8	20.1	3.4	4.6	10.7	6.3	21	0
9	Clay Creek Pottery	0	0	0	0	0	0	0	0	0	0	0	0	0	0	0	0	0	0	0	0	0	0	0	0
10	Chiniak Lake	6.0	6.7	14.1	0	0	12	17.1	12.5	6.2	10.8	12.9	0	0	16.6	13.9	15.1	0	3.2	0	0	0	0	7.2	0

Table C1. Longitude and latitude locations of time series points in Old Harbor. The pre-earthquake onshore (S) and offshore (O) locations are specified in the third column. The minimum elevation (sixth column) above the post-earthquake MHHW datum is provided for onshore locations, while the minimum post-earthquake depth is provided for offshore locations. The horizontal datum used is World Geodetic System of 1984.

#	Label	S/O	Longitude (°W)	Latitude (°N)	Minimum elevation/ depth, m (ft)
1	Sitkalidak Strait	O	-153.314722	57.180278	31.6 (103.7)
2	Sitkalidak Passage	O	-153.266667	57.210000	2.9 (9.5)
3	Port Hobron	O	-153.200000	57.200000	14.0 (45.9)
4	The Church	O	-153.306111	57.201667	-6.2 (20.3)
5	Post Office	S	-153.305000	57.204722	-0.8 (2.6)
6	The Harbor	O	-153.301667	57.207222	1.9 (6.2)
7	Mountain View Dr.	O	-153.297500	57.210833	-3.9 (12.8)
8	Beach Road	S	-153.276111	57.210833	7.2 (23.6)
9	Airport West	S	-153.274444	57.215278	7.1 (23.3)
10	Airport East	S	-153.259167	57.224167	13.9 (45.6)

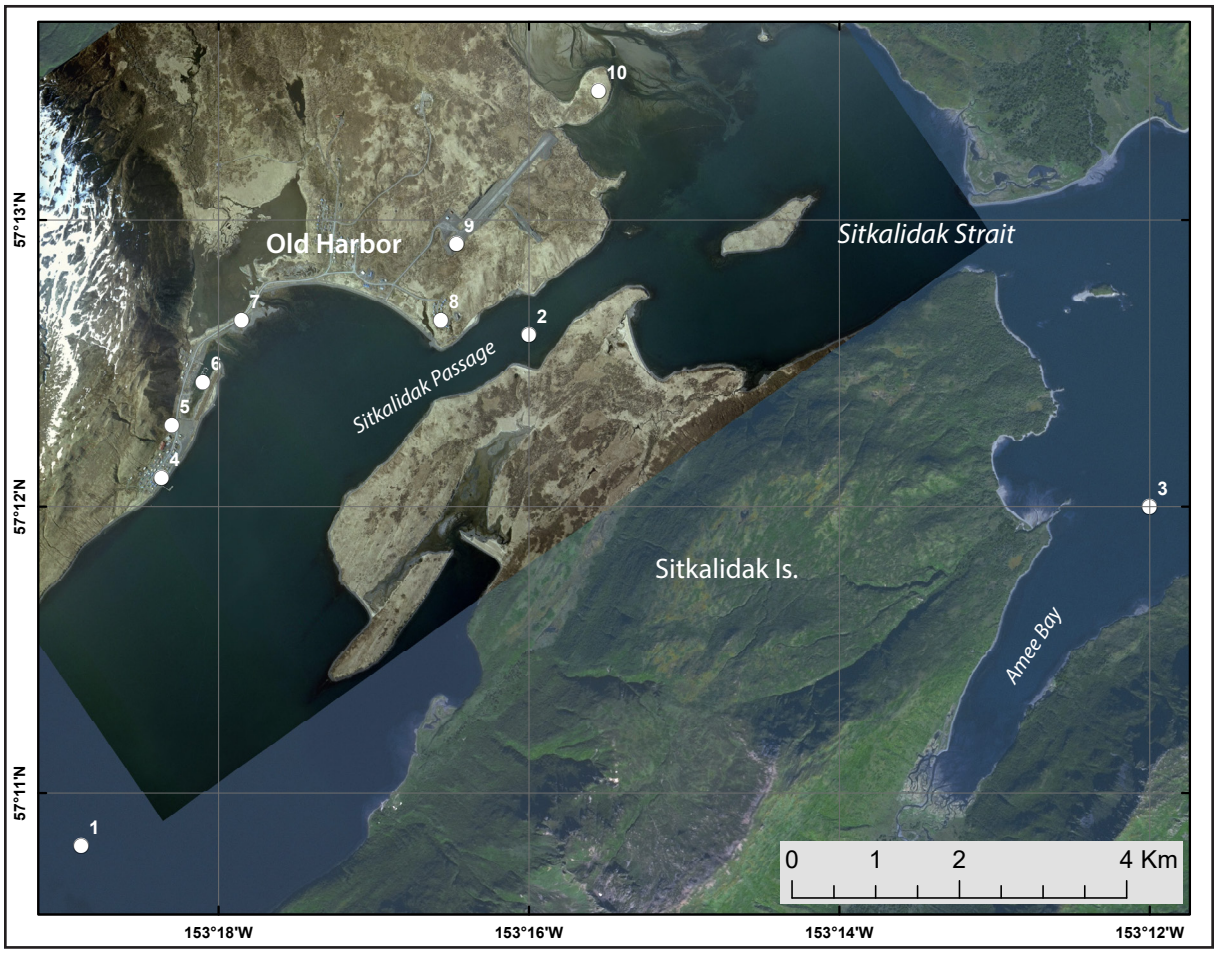

Figure C1. Locations of time series points in and around Old Harbor. The longitude and latitude locations of the time series points are listed in table C1.

Table C2. Maximum water levels for all tsunami scenarios at time series points near Old Harbor, which are listed in table C1. The maximum water depth above ground is provided for onshore (S) locations, whereas the maximum water level above the pre-earthquake MHHW is provided for offshore (O) locations.

#	Label	Maximum water depth above ground/sea level (meters)																						
		Scenario																						
		1	**2**	**3**	**4**	**5**	**6**	**7**	**8**	**9**	**10**	**11**	**12**	**13**	**14**	**15**	**16**	**17**	**18**	**19**	**20**	**21**	**22**	**23**	**24**
1	Sitkalidak Strait	10.7	14.8	14.2	11.5	19.9	23.9	21.4	17.5	11.2	14.5	14.6	9.2	14.2	19.7	19.7	23.1	4.2	15.1	3.6	8.1	12.4	13.8	17.7	2.4
2	Sitkalidak Passage	15.8	15.5	16.0	11.7	20.7	24.8	22.4	19.3	16.2	15.4	22.0	15.1	16.7	20.7	21.1	30.8	7.8	19.6	7.6	9.3	13.4	15.6	22.2	2.6
3	Port Hobron	13.6	13.9	13.8	12.7	16.5	22.8	20.8	19.5	14.6	13.1	18.1	10.0	12.8	17.5	17.4	24.6	7.6	17.8	5.1	7.3	11.6	12.4	19.5	1.9
4	The Church	9.7	13.7	13.3	11.0	20.5	22.6	19.8	17.0	10.4	13.7	16.7	11.9	14.0	18.6	18.9	26.4	3.5	16.7	2.6	6.5	12.9	14.3	20.0	0.3
5	Post Office	8.6	11.0	10.7	8.5	18.3	20.0	17.1	14.5	9.2	10.9	15.3	7.6	11.6	16.0	16.6	25.5	1.1	14.7	1.0	4.2	10.4	12.2	17.4	0
6	The Harbor	14.9	16.4	16.0	14.2	23.3	25.3	22.4	19.6	15.3	16.2	22.0	13.6	17.3	21.2	21.9	32.4	6.9	20.5	6.7	10.1	15.4	17.3	23.5	2.8
7	Mountain View Dr.	15.5	16.7	16.6	14.4	24.1	25.2	22.4	20.0	16.0	16.5	23.0	15.6	18.1	21.5	22.3	32.5	7.4	21.8	7.9	10.7	16.4	18.6	24.9	2.6
8	Beach Road	2.8	2.7	2.6	1.0	9.9	12.1	9.4	6.2	3.0	2.5	9.3	2.2	4.1	8.1	8.8	17.9	0	8.0	0	0	3.0	5.2	10.3	0
9	Airport West	3.5	3.4	4.1	2.5	11.3	12.7	9.7	7.5	4.0	3.5	10.3	4.7	5.3	8.8	9.6	20.6	0	10.5	0	0	4.3	6.7	13.4	0
10	Airport East	0	0	0	0	0	4.3	1.5	0	0	0	0	0	0	0.3	0.3	8.5	0	0	0	0	0	0	0.6	0

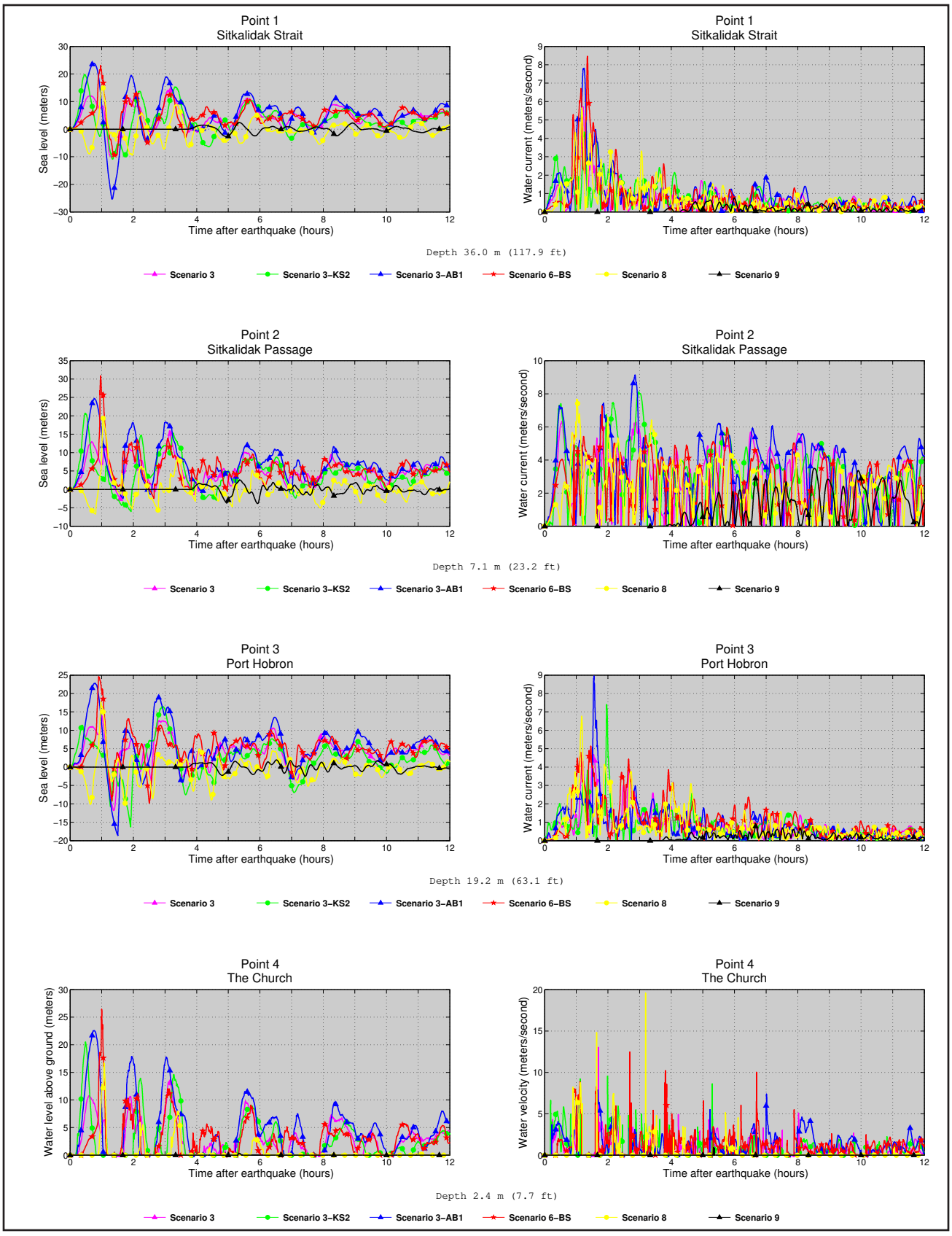

Figure C2. Time series of water level (left column) and velocity (right column) for selected scenarios at locations shown in figure C1. Elevations of onshore locations and ocean depth at offshore locations are given based on the pre-earthquake MHHW datum.

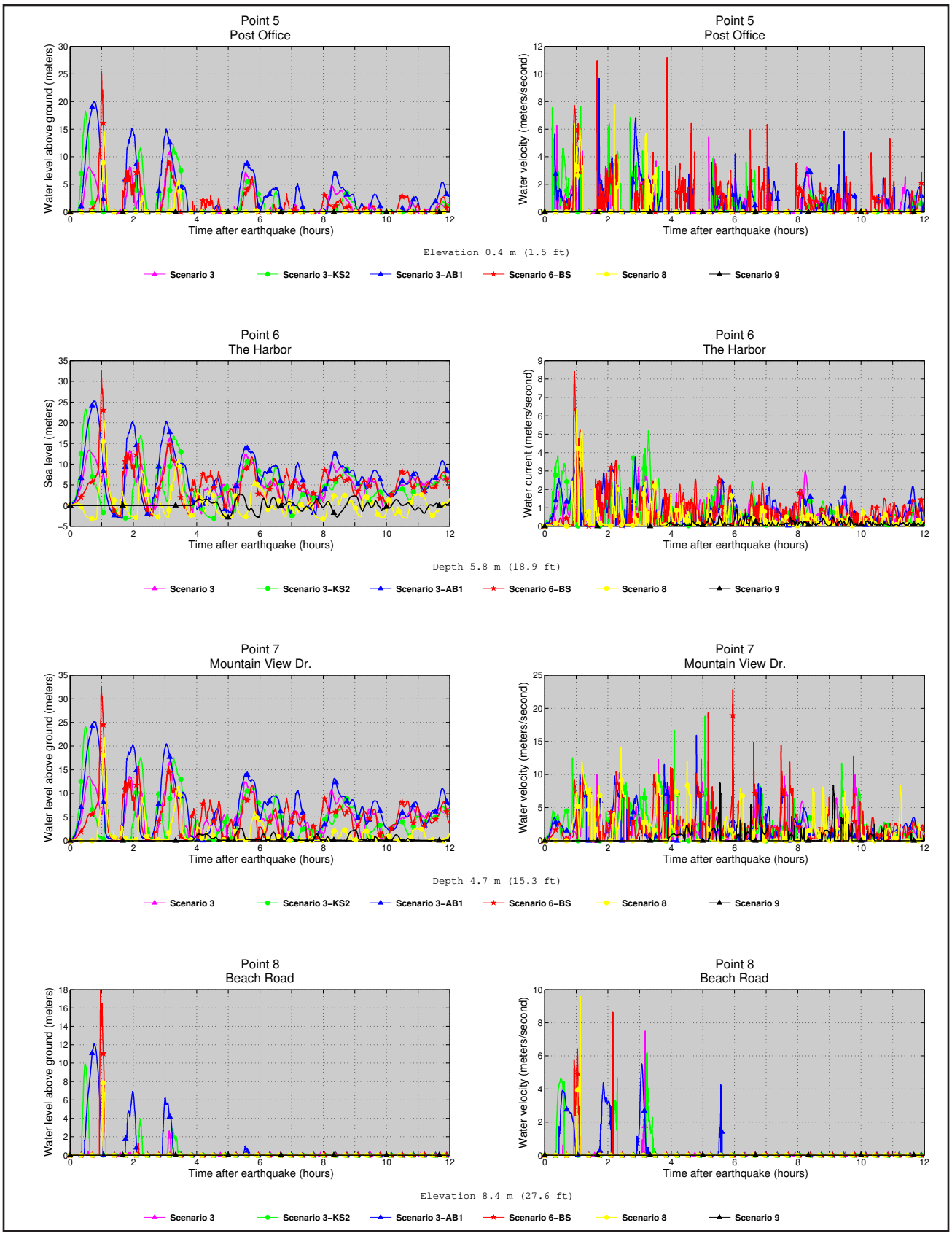

Figure C2, continued. Time series of water level (left column) and velocity (right column) for selected scenarios at locations shown in figure C1. Elevations of onshore locations and ocean depth at offshore locations are given based on the pre-earthquake MHHW datum.

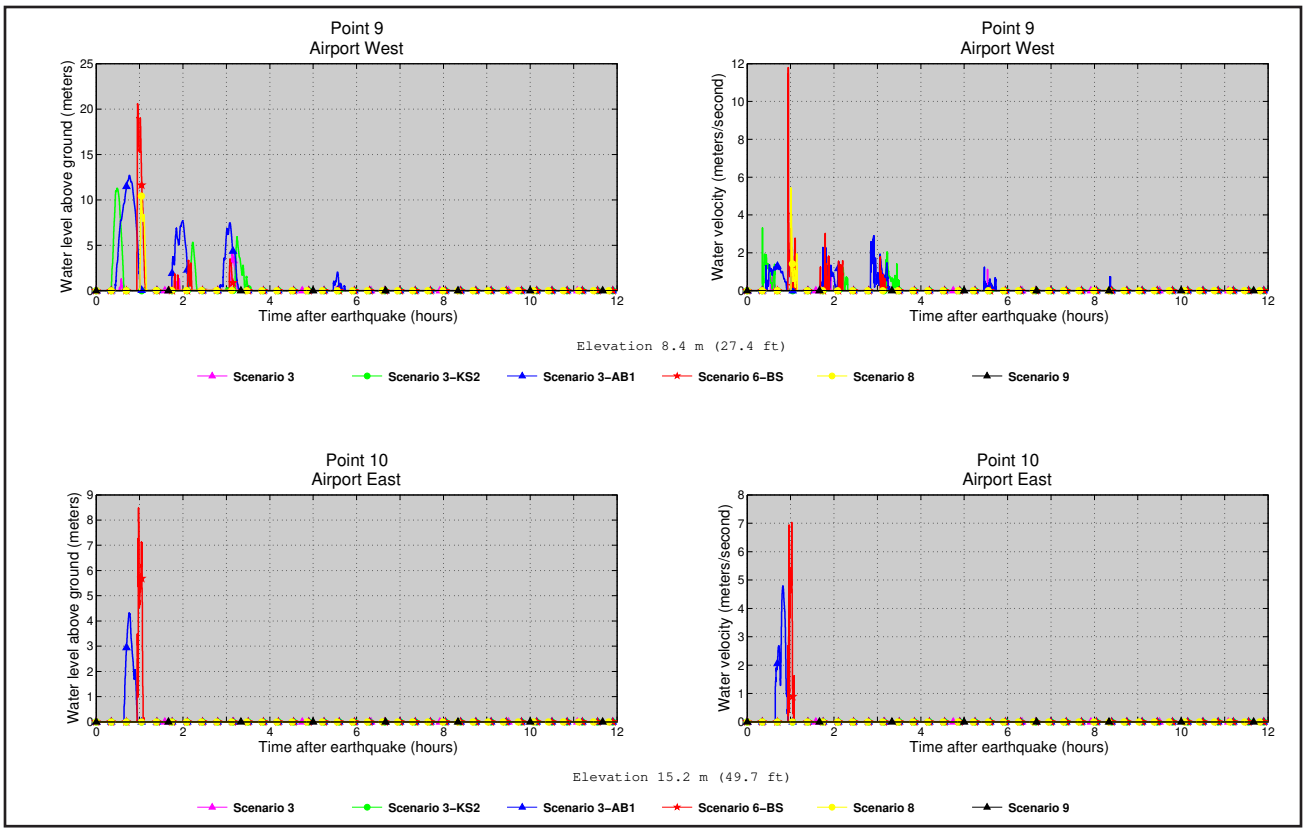

Figure C2, continued. Time series of water level (left column) and velocity (right column) for selected scenarios at locations shown in figure C1. Elevations of onshore locations and ocean depth at offshore locations are given based on the pre-earthquake MHHW datum.

Table C3. Maximum water velocities for all tsunami scenarios at time series points near Old Harbor, which are listed in table C1.

#	Label	Maximum water velocity (meters/second)																							
		Scenario																							
		1	2	3	4	5	6	7	8	9	10	11	12	13	14	15	16	17	18	19	20	21	22	23	24
1	Sitkalidak Strait	3.9	4.3	5.7	4.1	4.4	7.8	8.0	7.2	4.3	4.8	5.1	5.1	4.4	7.4	7.7	8.5	5.3	5.7	3.6	3.4	7.4	7.6	6.8	0.8
2	Sitkalidak Passage	5.3	7.0	6.3	7.0	8.1	9.1	8.8	7.4	5.4	6.5	5.4	6.9	7.3	7.8	8.6	7.3	5.4	7.7	5.9	6.8	7.7	7.9	9.9	3.5
3	Port Hobron	3.7	5.4	4.7	6.4	7.4	9.0	7.0	6.9	3.9	4.8	4.7	7.6	7.9	4.9	3.9	5.1	5.3	6.8	8.8	6.7	6.0	8.0	7.0	0.8
4	The Church	9.6	7.9	13.0	13.4	9.5	7.8	7.5	7.9	11.4	7.3	8.4	11.0	19.0	10.4	8.6	12.5	7.8	19.6	13.4	9.5	8.0	8.9	14.4	0.9
5	Post Office	5.1	6.8	6.3	9.4	7.6	9.7	11.2	7.1	6.5	6.3	7.1	17.7	26.0	11.8	16.9	11.2	5.2	7.8	5.4	12.7	5.4	14.3	10.6	0
6	The Harbor	4.7	3.1	3.2	3.9	5.2	3.8	3.9	4.5	4.4	3.1	6.7	4.5	4.3	3.7	4.1	8.4	3.3	6.3	2.7	2.9	2.8	3.4	7.6	0.9
7	Mountain View Dr.	16.5	18.3	12.3	17.3	18.8	15.9	18.4	15.7	16.3	18.2	18.9	17.8	19.3	20.3	16.0	22.8	14.9	14.0	15.6	10.5	12.9	21.8	18.2	8.7
8	Beach Road	1.7	7.9	7.5	1.8	6.2	5.5	5.8	5.9	1.9	8.9	7.3	6.7	7.9	3.7	5.1	8.6	0	9.6	0	0	5.5	5.1	6.0	0
9	Airport West	1.3	0.8	1.1	1.2	3.3	2.9	1.8	4.9	1.7	1.3	11.1	2.4	4.1	1.6	3.2	11.8	0	5.4	0	0	1.5	1.6	9.4	0
10	Airport East	0	0	0	0	0	4.8	7.8	0	0	0	0	0	0	0	0	7.0	0	0	0	0	0	0	0	0

Table D1. Longitude and latitude locations of time series points in Ouzinkie. The pre-earthquake onshore (S) and offshore (O) locations are specified in the third column. The minimum elevation (sixth column) above the post-earthquake MHHW datum is provided for onshore locations, while the minimum post-earthquake depth is provided for offshore locations. The horizontal datum used is World Geodetic System of 1984.

#	Label	S/O	Longitude (°W)	Latitude (°N)	Minimum elevation/ depth, m (ft)
1	Narrow Strait	O	-152.484722	57.907222	96.9 (317.9)
2	Ouzinkie Point	O	-152.518333	57.916111	-1.8 (5.9)
3	The Harbor	O	-152.495	57.920556	6.4 (21.0)
4	School	S	-152.5075	57.922222	18.5 (60.7)
5	1st Street	S	-152.505	57.920556	-0.6 (2.0)
6	2nd Street	S	-152.502222	57.921944	-4.1 (13.5)
7	The Church	S	-152.500278	57.923056	-0.5 (1.6)
8	3rd Street	S	-152.491389	57.921111	6.7 (22.0)
9	Post Office	S	-152.501667	57.922778	-3.0 (9.8)
10	The Terminal	S	-152.500833	57.920833	-0.1 (0.3)

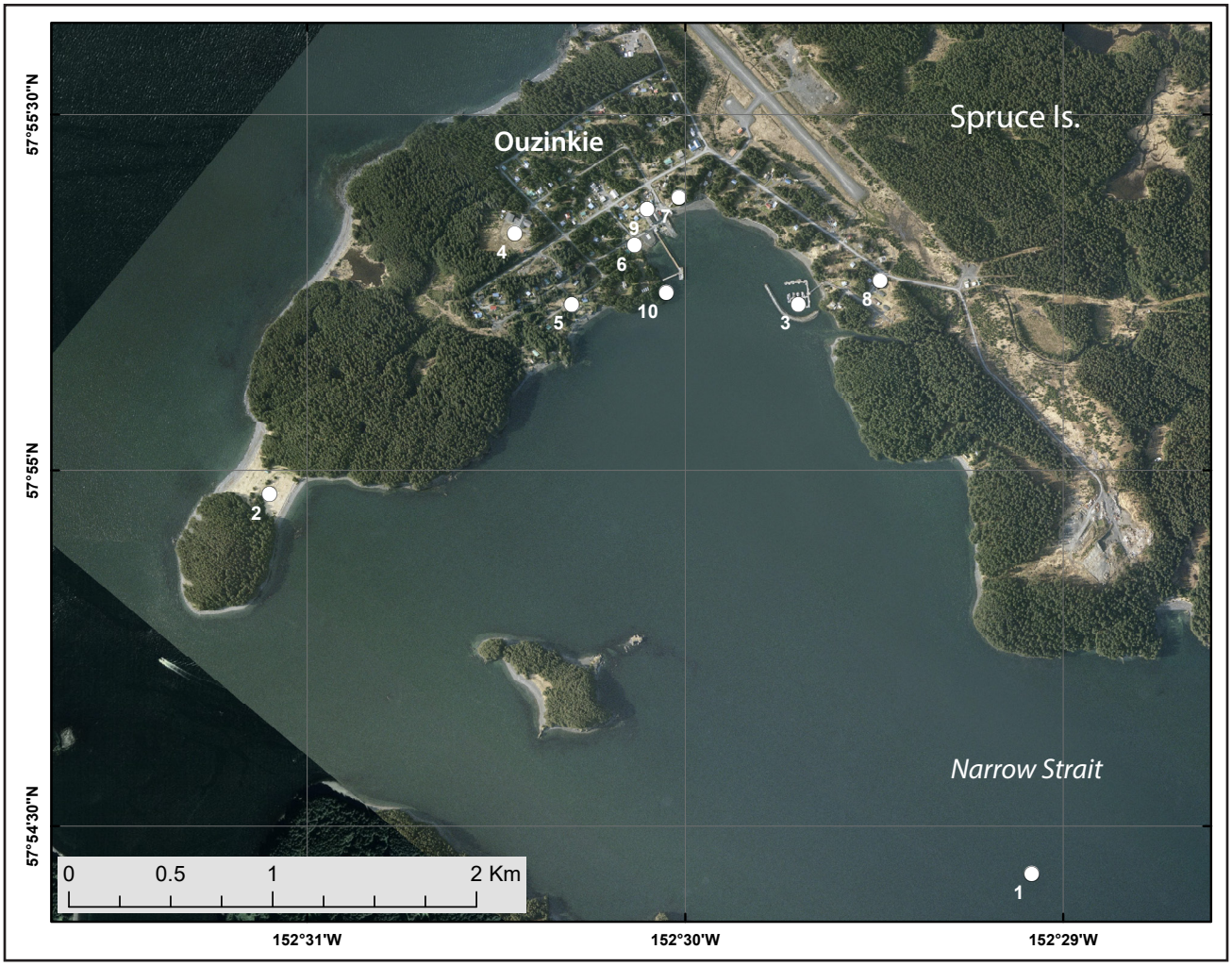

Figure D1. Locations of time series points in and around Ouzinkie. The longitude and latitude locations of the time series points are listed in table D1.

Table D2. Maximum water levels for all tsunami scenarios at time series points near Ouzinkie, which are listed in table D1. The maximum water depth above ground is provided for onshore (S) locations, whereas the maximum water level above the pre-earthquake MHHW is provided for offshore (O) locations.

#	Label	Maximum water depth above ground/sea level (meters)																							
		Scenario																							
		1	**2**	**3**	**4**	**5**	**6**	**7**	**8**	**9**	**10**	**11**	**12**	**13**	**14**	**15**	**16**	**17**	**18**	**19**	**20**	**21**	**22**	**23**	**24**
1	Narrow Strait	8.6	11.9	12.3	13.6	14.1	16.2	17.7	16.0	8.8	11.3	12.2	10.6	11.4	14.6	15.3	21.9	8.7	16.2	6.2	7.1	7.8	7.6	15.0	2.1
2	Ouzinkie Point	9.6	10.0	12.0	12.0	12.7	14.9	14.4	13.4	10.1	9.0	12.8	11.9	12.1	15.1	17.1	17.3	6.3	13.3	4.4	5.6	5.8	6.6	13.8	0.3
3	The Harbor	9.4	12.1	14.0	15.0	14.9	16.9	18.2	16.6	10.1	11.4	12.7	12.1	13.2	16.1	17.2	22.8	9.2	17.8	7.0	7.6	8.2	7.8	17.3	2.1
4	School	0	0	0	0	0	0	0	0	0	0	0	0	0	0	0	0	0	0	0	0	0	0	0	0
5	1st Street	2.7	5.3	7.3	8.3	8.0	10.1	11.2	9.7	3.4	4.6	6.9	5.9	6.5	9.4	11.0	15.8	2.4	11.1	0.2	0.8	1.4	1.0	10.4	0
6	2nd Street	6.9	8.8	11.0	12.1	11.8	13.7	14.8	13.5	7.5	8.3	9.7	9.9	10.2	13.0	14.4	19.6	6.4	14.8	3.9	4.3	5.1	4.8	14.5	0
7	The Church	3.2	5.2	7.4	8.4	8.1	10.0	11.2	9.9	3.8	4.6	6.0	6.2	6.6	9.4	10.7	16.2	2.7	11.2	0.2	0.7	1.4	1.1	10.8	0
8	3rd Street	0	0	0	1.2	1.1	2.9	4.2	2.4	0	0	0	0	0	2.1	3.2	8.7	0	3.6	0	0	0	0	3.2	0
9	Post Office	5.9	7.8	10.1	11.1	10.8	12.7	13.8	12.5	6.5	7.3	8.7	9.0	9.3	12.1	13.4	18.8	5.5	13.9	3.0	3.3	4.2	3.8	13.6	0
10	The Terminal	2.2	4.8	6.7	7.7	7.5	9.5	10.9	9.3	2.9	4.1	5.4	5.1	5.9	8.6	10.0	15.4	2.0	10.4	0	0.3	0.9	0.5	10.0	0

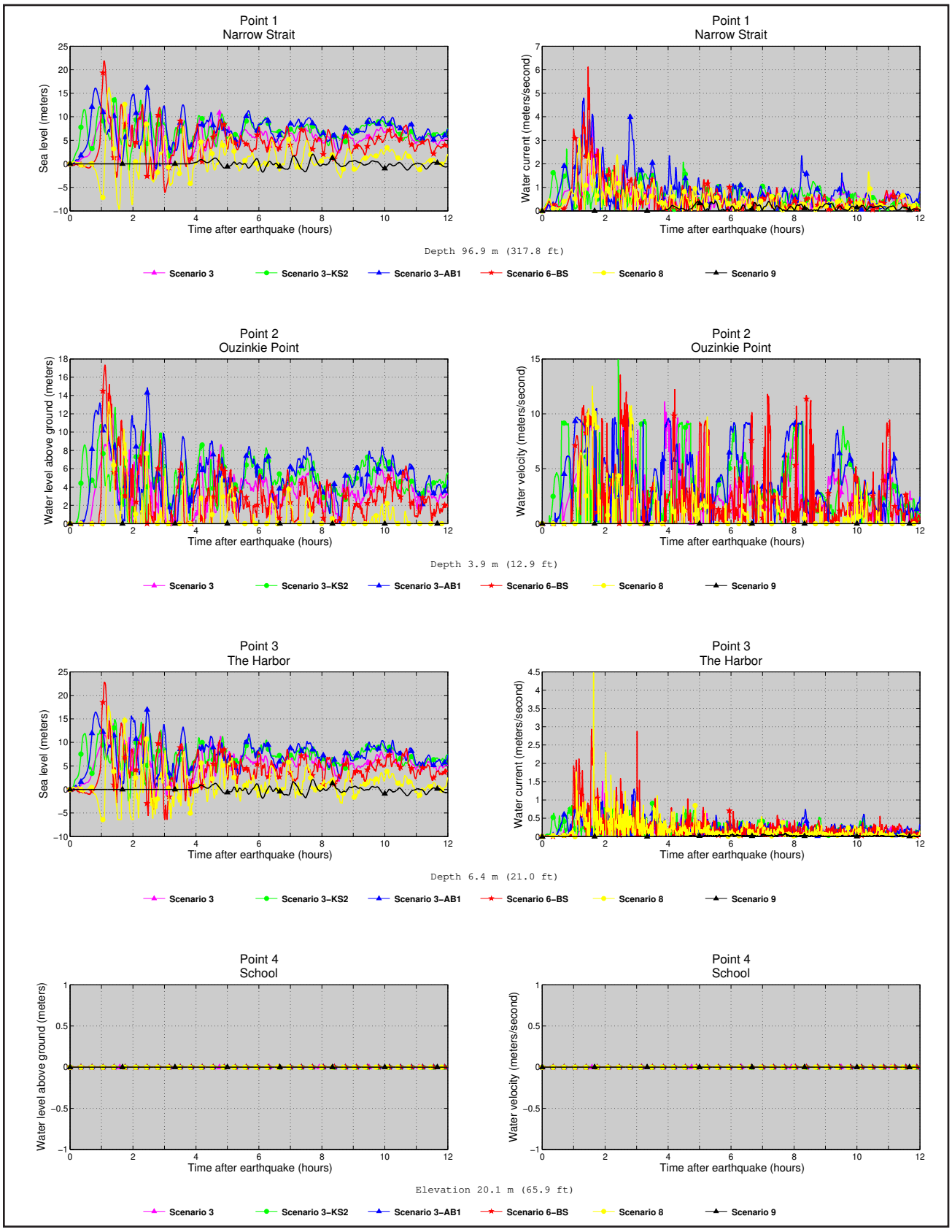

Figure D2. Time series of water level (left column) and velocity (right column) for selected scenarios at locations shown in figure D1. Elevations of onshore locations and ocean depth at offshore locations are given based on the pre-earthquake MHHW datum.

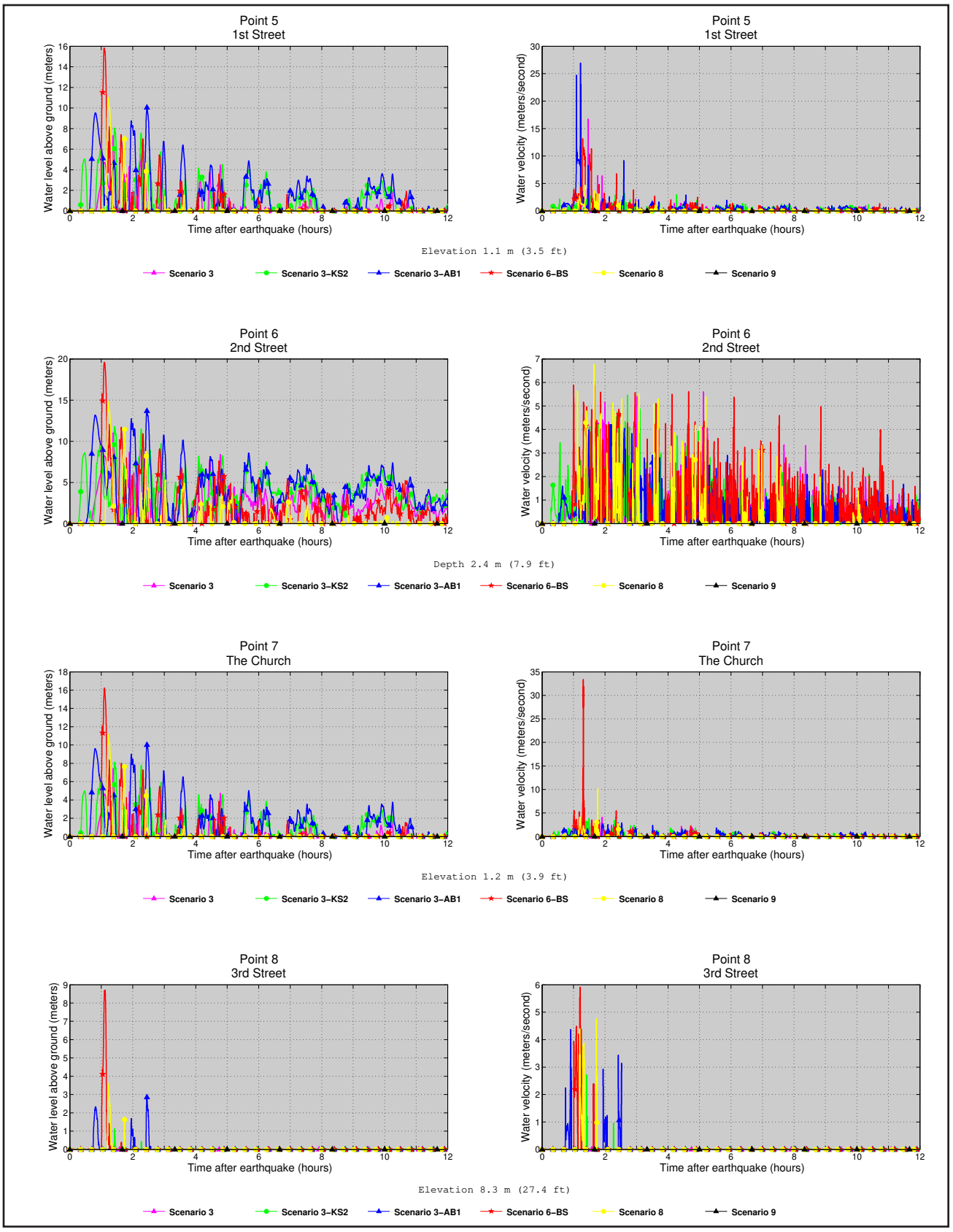

Figure D2, continued. Time series of water level (left column) and velocity (right column) for selected scenarios at locations shown in figure D1. Elevations of onshore locations and ocean depth at offshore locations are given based on the pre-earthquake MHHW datum.

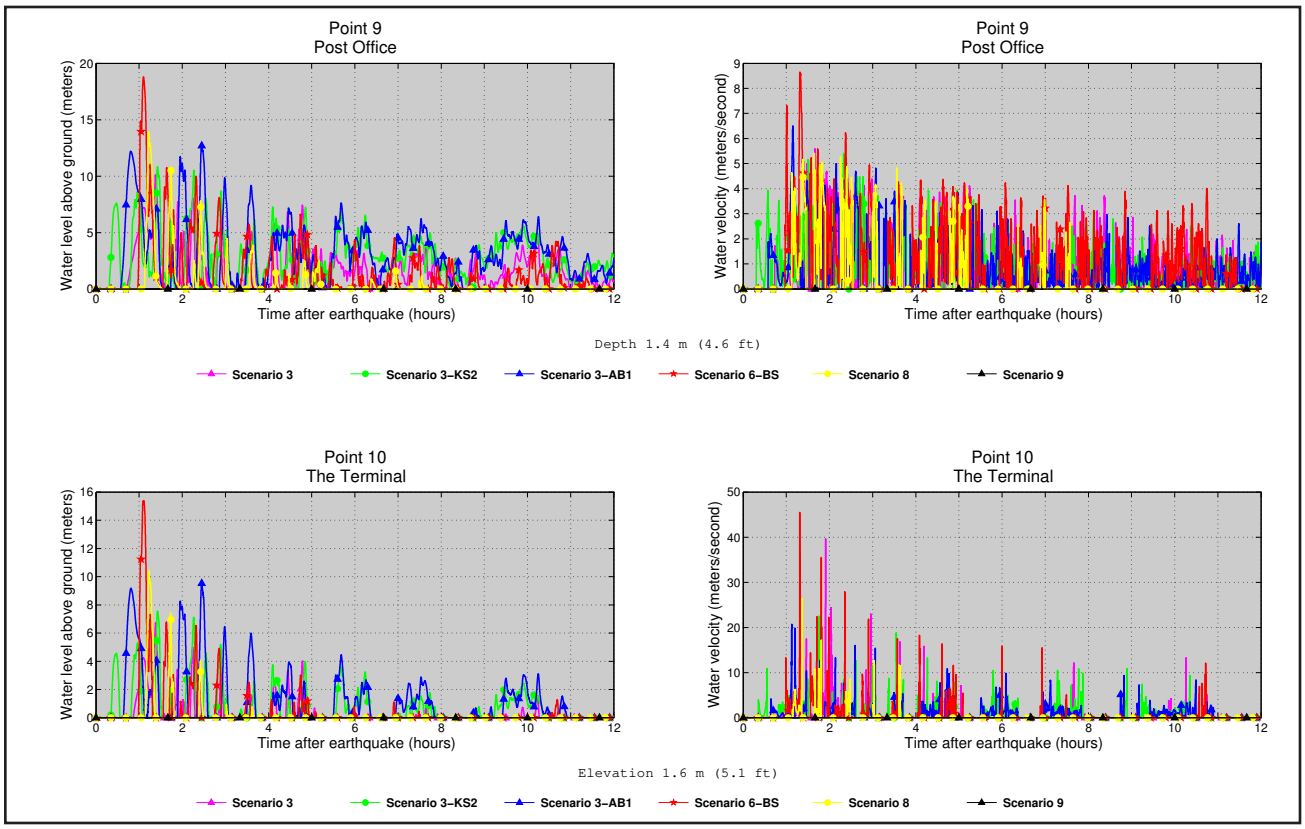

Figure D2, continued. Time series of water level (left column) and velocity (right column) for selected scenarios at locations shown in figure D1. Elevations of onshore locations and ocean depth at offshore locations are given based on the pre-earthquake MHHW datum.

Table D3. Maximum water velocities for all tsunami scenarios at time series points near Ouzinkie, which are listed in table D1.

#	Label	Maximum water velocity (meters/second)																							
		Scenario																							
		1	**2**	**3**	**4**	**5**	**6**	**7**	**8**	**9**	**10**	**11**	**12**	**13**	**14**	**15**	**16**	**17**	**18**	**19**	**20**	**21**	**22**	**23**	**24**
1	Narrow Strait	2.1	5.4	3.8	2.7	2.6	4.8	5.8	6.5	2.2	3.4	3.6	2.8	3.0	3.2	3.2	6.1	1.8	3.1	3.8	2.0	1.6	1.8	3.2	0.4
2	Ouzinkie Point	13.8	9.4	11.1	9.9	14.9	10.5	9.7	12.3	14.9	12.7	15.3	11.9	14.3	11.7	13.6	13.5	12.1	12.5	13.3	11.3	13.2	14.6	13.2	0.4
3	The Harbor	1.1	0.9	1.5	1.2	1.0	1.3	1.5	1.3	1.0	1.1	1.1	1.2	1.2	2.7	1.8	2.9	4.3	4.5	3.5	3.4	2.6	2.0	4.2	0.1
4	School	0	0	0	0	0	0	0	0	0	0	0	0	0	0	0	0	0	0	0	0	0	0	0	0
5	1st Street	9.3	4.7	16.7	2.9	3.2	26.9	28.7	14.5	6.8	7.1	17.9	11.8	13.0	9.7	18.7	13.1	1	4.7	0	0.5	2.3	0.9	6.7	0
6	2nd Street	5.3	4.9	5.9	4.9	5.5	4.3	5.1	7.5	5.6	5.7	5.7	7.5	5.9	6.2	6.8	5.9	5.2	6.8	5.2	5.3	5.7	5.5	8.5	0
7	The Church	1.8	1.5	4.1	4.1	3.8	2.9	3.3	64.3	1.9	1.9	2.9	3.2	3.0	4.1	4.5	33.3	1.0	10.2	0	0	1.1	0	5.9	0
8	3rd Street	0	0	0	2.9	2.7	4.4	4.0	4.7	0	0	0	0	0	3.5	3.7	5.9	0	4.8	0	0	0	0	4.1	0
9	Post Office	4.4	4.0	5.6	5.2	5.4	6.5	6.2	8.3	5.2	4.3	5.3	6.5	5.9	6.3	5.8	8.6	4.0	5.4	4.0	4.1	4.9	4.2	7.4	0
10	The Terminal	18.5	16.9	39.6	27.5	22.5	20.7	25.4	70.0	20.2	26.6	24.2	21.5	22.6	29.3	19.0	45.5	6.6	26.3	0	0	7.0	11.8	34.7	0

Table E1. Longitude and latitude locations of time series points in Port Lions. The pre-earthquake onshore (S) and offshore (O) locations are specified in the third column. The minimum elevation (sixth column) above the post-earthquake MHHW datum is provided for onshore locations, while the minimum post-earthquake depth is provided for offshore locations. The horizontal datum used is World Geodetic System of 1984.

#	Label	S/O	Longitude (°W)	Latitude (°N)	Minimum elevation/ depth, m (ft)
1	Kizhuyak Bay	O	-152.838611	57.849722	20.7 (67.9)
2	Port Wakefield	O	-152.860556	57.862222	7.8 (25.6)
3	The Harbor	O	-152.867778	57.871944	6.9 (22.6)
4	Kizhuyak Drive	S	-152.866389	57.862778	4.4 (14.4)
5	The Bridge	O	-152.876111	57.864444	2.5 (8.2)
6	Port Lions Lodge	S	-152.880556	57.865833	-3.3 (-10.8)
7	Post Office	S	-152.879722	57.867778	12.3 (40.4)
8	Birch Drive	S	-152.881944	57.865278	-2.2 (-7.2)
9	Airport West	S	-152.853611	57.884167	6.4 (21.0)
10	Airport East	S	-152.841111	57.885278	-2.4 (-7.9)

Figure E1. Locations of time series points in and around Port Lions. The longitude and latitude locations of the time series points are listed in table E1.

Table E2. Maximum water levels for all tsunami scenarios at time series points near Port Lions, which are listed in table E1. The maximum water depth above ground is provided for onshore (S) locations, whereas the maximum water level above the pre-earthquake MHHW is provided for offshore (O) locations.

#	Label	Maximum water depth above ground/sea level (meters)																						
		Scenario																						
		1	2	3	4	5	6	7	8	9	10	11	12	13	14	15	16	17	18	19	20	21	22	23	24
1	Kizhuyak Bay	12.8	18.1	19.0	17.6	17.8	22.9	22.2	25.6	13.2	18.2	17.2	15.9	15.2	16.7	19.6	25.3	7.3	20.7	12.4	10.4	10.4	10.4	20.0	2.5
2	Port Wakefield	14.9	18.0	19.1	17.7	18.3	22.9	22.5	25.3	15.0	18.0	19.8	18.4	16.4	17.7	20.9	24.5	8.2	23.0	14.2	12.6	11.9	12.4	21.5	2.7
3	The Harbor	13.8	17.6	19.2	17.8	19.0	22.1	22.1	25.0	14.4	17.7	18.7	15.1	14.2	18.2	21.8	25.8	8.6	20.3	12.1	11.5	9.3	11.3	17.9	2.3
4	Kizhuyak Drive	3.3	6.8	8.1	6.7	6.8	11.9	11.5	14.2	3.7	6.8	8.2	7.3	5.9	6.7	10.1	13.9	0	11.4	4.3	3.0	2.1	1.5	9.7	0
5	The Bridge	14.7	17.9	19.5	18.6	18.6	23.2	22.7	25.7	15.5	18.1	19.6	16.0	15.6	16.9	20.6	26.8	9.3	23.2	12.7	11.5	10.9	10.7	20.2	2.6
6	Port Lions Lodge	11.7	14.6	16.4	15.8	15.7	20.3	19.9	22.6	12.4	14.9	16.8	14.8	12.9	15.2	18.6	23.5	6.4	21.5	10.6	8.4	7.9	7.6	18.6	0
7	Post Office	0	0	0.7	0.2	0.7	4.6	4.1	7.0	0	0	1.2	1.5	0.1	0	2.8	8.2	0	6.5	0	0	0	0	3.4	0
8	Birch Drive	10.6	13.5	15.4	14.7	14.7	19.2	18.8	21.5	11.4	13.8	15.8	13.6	12.1	14.5	17.8	22.5	5.4	20.3	9.6	7.3	7.0	6.7	18.6	0
9	Airport West	1.0	3.9	5.8	5.2	3.6	10.2	9.8	11.6	2.2	4.1	6.7	1.8	1.8	6.6	7.8	15.3	0	9.1	0	0	0	0	7.2	0
10	Airport East	9.0	12.4	14.2	12.0	12.3	17.3	18.1	19.3	10.0	12.6	14.1	10.2	9.7	14.2	15.6	22.6	4.7	16.1	8.2	7.0	5.5	5.6	13.8	0

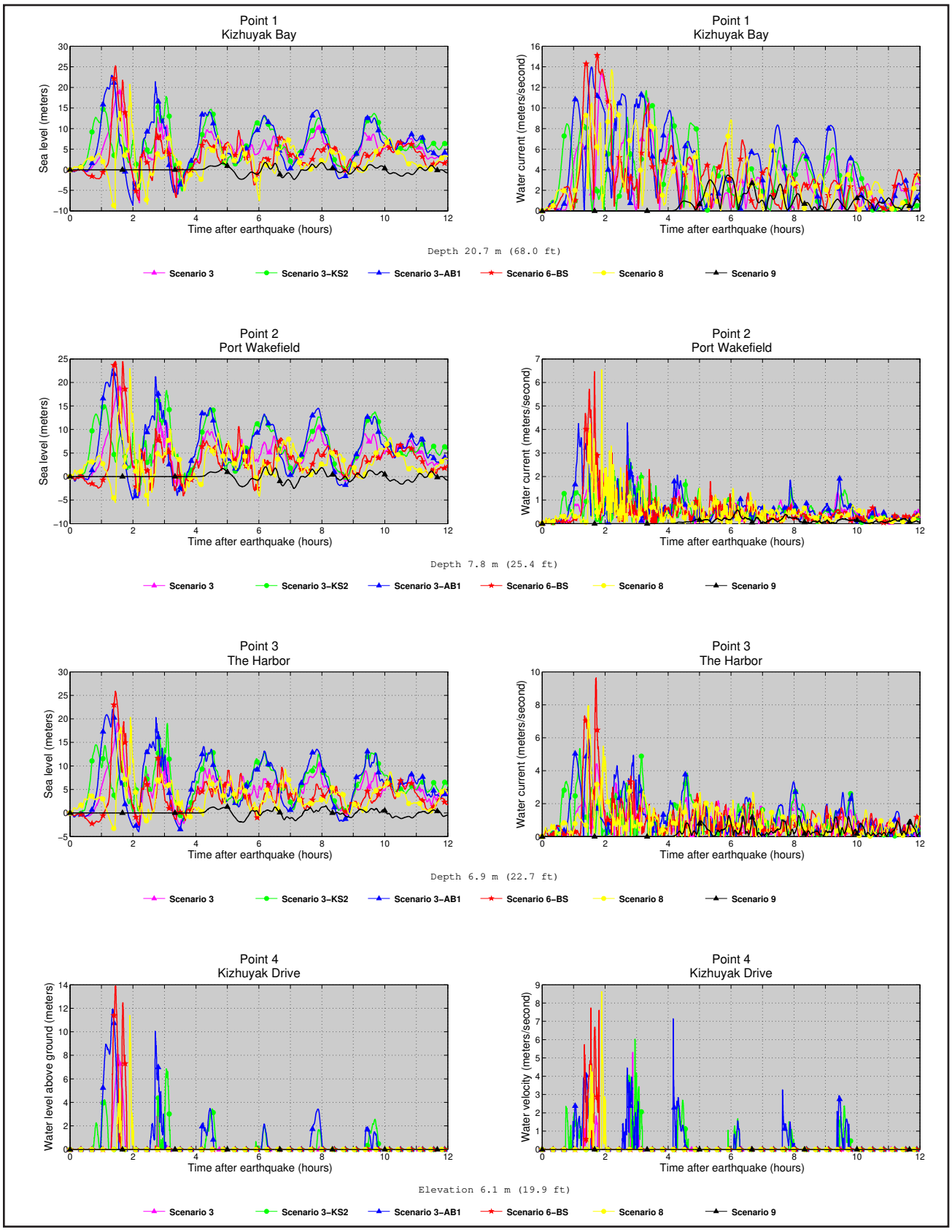

Figure E2. Time series of water level (left column) and velocity (right column) for selected scenarios at locations shown in figure E1. Elevations of onshore locations and ocean depth at offshore locations are given based on the pre-earthquake MHHW datum.

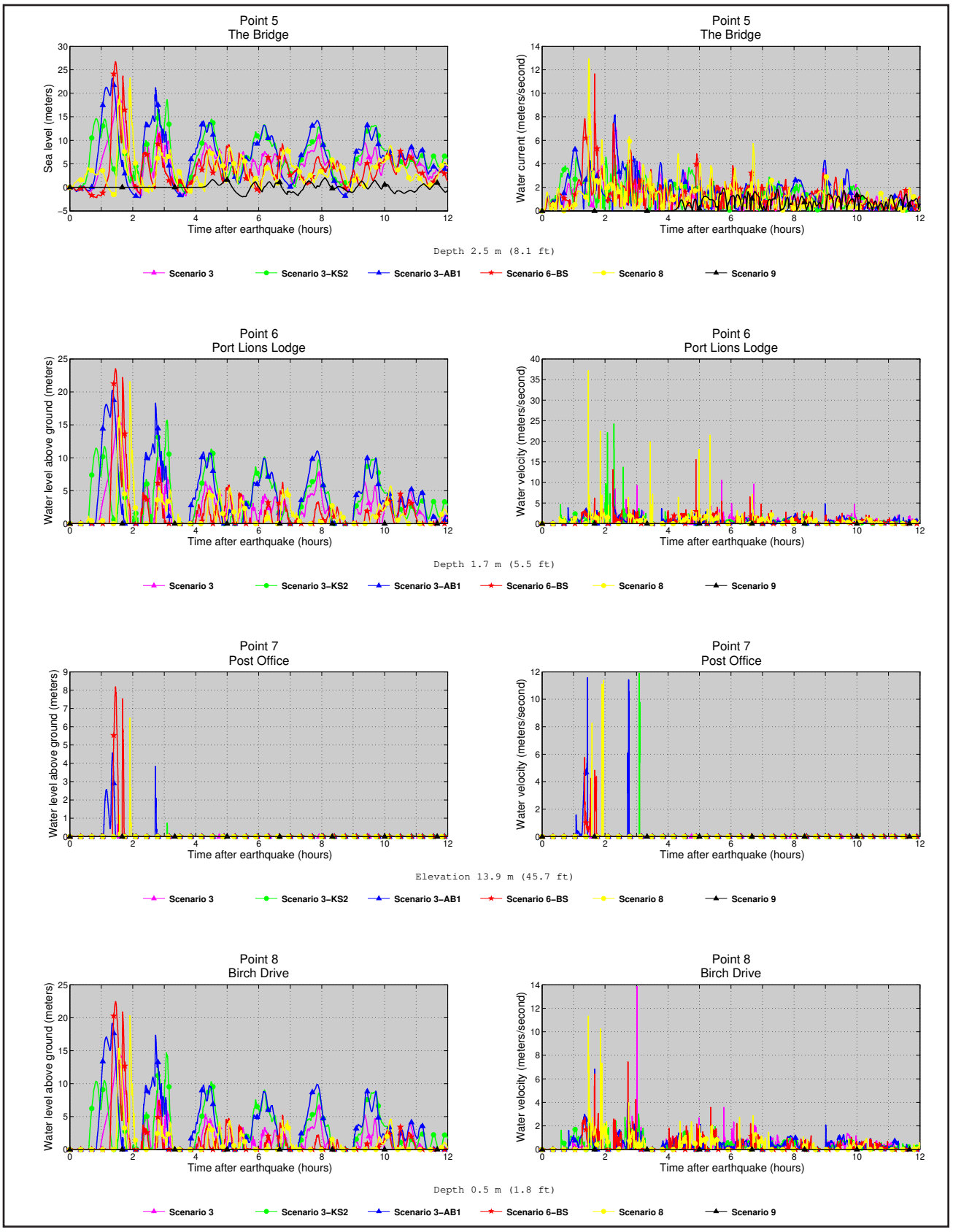

Figure E2, continued. Time series of water level (left column) and velocity (right column) for selected scenarios at locations shown in figure E1. Elevations of onshore locations and ocean depth at offshore locations are given based on the pre-earthquake MHHW datum.

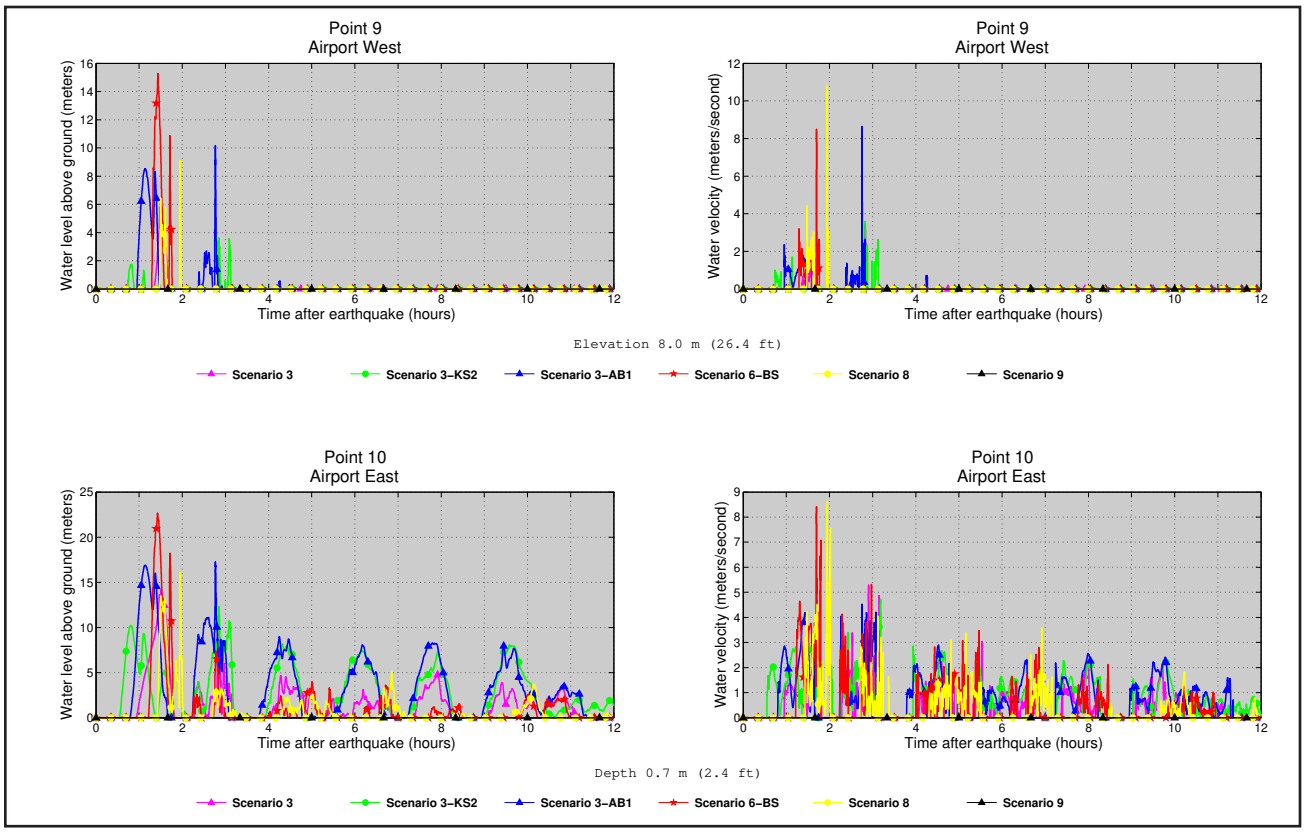

Figure E2, continued. Time series of water level (left column) and velocity (right column) for selected scenarios at locations shown in figure E1. Elevations of onshore locations and ocean depth at offshore locations are given based on the pre-earthquake MHHW datum.

Table E3. Maximum water velocities for all tsunami scenarios at time series points near Port Lions, which are listed in table E1.

#	Label	Maximum water velocity (meters/second)																							
		Scenario																							
		1	2	3	4	5	6	7	8	9	10	11	12	13	14	15	16	17	18	19	20	21	22	23	24
1	Kizhuyak Bay	11.1	12.1	13.3	10.7	11.7	14	13.2	15.5	11.1	12.7	12	12.8	12.8	12.7	14.4	15.1	11.3	13.7	12.8	12.1	7.5	8.0	11.9	3.8
2	Port Wakefield	2.3	2.6	2.8	3.1	2.7	4.3	4.7	3.5	2.2	2.8	4.3	6.7	5.3	4.2	3.4	6.5	2.1	6.5	5.1	5.0	2.4	2.7	6.6	0.6
3	The Harbor	3.8	4.1	4.4	4.8	5.3	6.0	6.0	5.5	4.1	4.3	5.7	6.6	6.4	3.9	4.2	9.6	2.5	7.9	5.4	5.6	2.8	3.3	8.0	1.3
4	Kizhuyak Drive	5.5	3.9	5.3	4.5	6.0	7.1	6.0	11.1	7.5	3.5	9.0	6.6	11.4	4.1	4.3	7.7	0	8.6	5.5	3.8	3.3	1.1	6.6	0
5	The Bridge	8.7	5.8	7.1	5.6	4.7	8.2	6.5	7.8	8.5	6.0	11.1	12.0	10.4	6.6	6.0	11.6	3.4	12.9	10.4	9.9	5.9	6.7	12.8	1.9
6	Port Lions Lodge	4.9	6.6	10.5	13.3	24.2	8.2	8.1	16.8	4.7	6.9	5.7	41.6	29.6	24.6	18.5	15.7	6.0	37.1	24.6	24.4	27.7	9.7	40.7	0
7	Post Office	0	0	4.0	0	11.9	11.6	10.3	9.5	0	0	15.5	11.8	0	0	14.0	5.7	0	11.4	0	0	0	0	16.4	0
8	Birch Drive	3.4	2.7	13.8	6.8	3.0	6.8	3.1	5.2	2.2	6.7	3.7	9.9	8.9	17.7	6.3	7.4	4.2	11.3	11.3	8.6	16.9	7.6	16.9	0
9	Airport West	2.0	3.4	3.5	4.0	3.6	8.6	5.2	6.9	1.7	2.5	3.9	3.3	2.0	4.0	3.2	8.5	0	10.8	0	0	0	0	6.4	0
10	Airport East	4.2	4.6	5.3	5.4	4.7	4.5	4.0	5.6	4.0	4.6	5.9	7.5	6.4	7.4	5.2	8.4	3.7	8.6	6.3	6.5	4.9	4.0	7.1	0